ISSN 0030-6096

OSAKA CITY MEDICAL JOURNAL

Vol. 65 No. 1

2019

PUBLISHED BY
OSAKA CITY MEDICAL ASSOCIATION
OSAKA JAPAN

Osaka City Medical Journal
Vol. 65, No. 1, June 2019

CONTENTS

Osaka City Med. J. Vol. 65, 1-8, 2019

Serum Myostatin Level in COPD Patients with and without Sarcopenia -Application for Biomarker of Sarcopenia Diagnosis-

Shinya Yoshida, Kazuhisa Asai, Naoki Ijiri, Yohkoh Kyomoto, Tamaki Kawamoto, Atsuko Okamoto, Kazuhiro Yamada, Tetsuya Watanabe, Yoshihiro Tochino, and Tomoya Kawaguchi

Department of Respiratory Medicine, Osaka City University Graduate School of Medicine

Abstract

Background

Chronic obstructive pulmonary disease (COPD) has significant extrapulmonary effects including weight loss, nutritional abnormalities, and skeletal muscle dysfunction. Sarcopenia is one of several comorbidities experienced by COPD patients, which may negatively affect quality of life and increase mortality. Previous studies have reported that exercise may reduce the severity of sarcopenia; however, the mechanism is only partially understood. We hypothesized that levels of irisin and myostatin, one of the myokines, are correlated with sarcopenia in COPD patients.

Methods

A total of 39 male COPD patients were enrolled, in addition to 30 male never-smokers as a control group. Pulmonary function testing was performed on all participants, while body-composition analysis was performed on the COPD patients to measure muscle mass and diagnose sarcopenia. Serum irisin and myostatin levels were measured using a commercially available enzyme-linked immunosorbent assay kit.

Results

The COPD patients were divided into a sarcopenia group (n=9) and a non-sarcopenia group (n=30). Serum myostatin levels were significantly lower in COPD patients with sarcopenia than in those without sarcopenia, while there was no significant difference in irisin levels among COPD patients with and without sarcopenia.

Conclusions

Serum myostatin level was correlated with muscle mass and is a potential biomarker for sarcopenia in COPD patients.

Key Words: Sarcopenia; Irisin; Myostatin; Myokine; COPD

Received August 30, 2018; accepted November 27, 2018.

Correspondence to: Kazuhisa Asai, MD.
Department of Respiratory Medicine, Osaka City University Graduate School of Medicine,
1-4-3 Asahimachi, Abeno-ku, Osaka 545-8585, Japan
Tel: +81-6-6645-3916; Fax: +81-6-6646-6160
E-mail: kazuasai@msic.med.osaka-cu.ac.jp

Introduction

Chronic obstructive pulmonary disease (COPD) is a common, preventable, and treatable disease that is characterized by persistent respiratory symptoms and airflow limitation due to airway and/or alveolar abnormalities usually caused by significant exposure to noxious particles or gases. COPD has significant extrapulmonary effects including weight loss, nutritional abnormalities, and skeletal muscle dysfunction. Skeletal muscle dysfunction is characterized by both sarcopenia and abnormal function of the remaining cells[1].

As the human body ages, skeletal muscle mass declines annually by 0.1% to 0.5% starting from 30 years old, with a dramatic acceleration after 65 years old. This gradual decrease in muscle mass is accompanied by a simultaneous reduction in strength. Excessive age-related loss of muscle mass and strength is often referred to as "primary sarcopenia"[2]. There is also a "secondary sarcopenia" related to disease. Sarcopenia is among the comorbidities present in COPD patients and may negatively impact quality of life. Therefore, early detection of sarcopenia can reduce the long-term care needs of this population, as well as improve quality of life and reduce morbidity and mortality[3]. Previous studies have reported that exercise may reduce the severity of sarcopenia; however, the mechanism is only partially understood.

Recently, myokines, such as irisin and myostatin, were discovered to be secreted from muscle tissue. Irisin is secreted by proteolytic cleavage of the membrane protein fibronectin type Ⅲ domain-containing protein 5 (FNDC5)[4]. Exercise triggers the cleavage of FNDC5 to secrete irisin into the bloodstream, which subsequently elevates energy expenditure in the subcutaneous adipose tissue through adipocyte browning[4]. The beneficial role of irisin in skeletal muscle metabolism has been described and it has been shown that irisin stimulates glucose uptake and lipid metabolism via activation of AMP-activated protein kinase[5,6].

On the other hand, myostatin, a member of the transforming growth factor-beta superfamily, has been established to be a negative regulator of skeletal muscle mass and is mainly expressed in skeletal muscles[7]. Myostatin inhibits satellite cell proliferation and differentiation in an autocrine and paracrine manner; conversely genetic deletion of myostatin leads to muscle hypertrophy in humans and mice[8]. While myostatin activation negatively regulates muscle growth, myostatin expression is downregulated after endurance and resistance exercise[9]. Myostatin is considered to be negatively correlated with muscle mass because it is a negative regulator of muscle growth. However a recent study reported that plasma myostatin levels were positively correlated with lean body mass[10].

The relationship between these myokines and muscle mass in COPD patients, however, has been unclear. We hypothesized that myostatin and irisin levels are correlated with sarcopenia in COPD patients. To address this hypothesis, we measured serum myostatin and irisin levels, and evaluated the relationships between these myokines and sarcopenia and muscle mass.

Methods

Subjects

Thirty-nine male COPD patients were recruited prospectively in the outpatient department of Osaka City University Hospital (Osaka, Japan) between April 2016 and December 2016. All COPD patients were stable outpatients and diagnosed with COPD according to the Global Initiative for Chronic Obstructive Lung Disease guidelines[11]. They had no history of malignant diseases, pulmonary comorbidities and oral corticosteroid therapy. We recruited male never-smokers older

than 70 years as controls from a group of healthy volunteers at Medcity21, medical examinations clinics between March 2016 and October 2017.

This study was approved by the Ethics Committee of Osaka City University Hospital (approval No. 3330), and all patients provided informed written consent for participation. All procedures were performed according to the guidelines of the Declaration of Helsinki.

Body composition analysis (BIA)

Body-composition analysis was performed in the COPD patients to measure BMI, muscle mass (MM), fat-free mass (FFM), FFM index (FFMI), and skeletal muscle mass index (SMI), using bioelectrical impedance analysis using the InBody 3.0 system analyzer (InBody, Seoul, South Korea). We didn't check their ingestion of food or drink before BIA. SMI is defined as appendicular skeletal muscle mass (ASM) divided by the square of height. ASM is calculated by summing the muscle mass of the four limbs. Sarcopenia was defined according to the Asian Working Group for Sarcopenia (AWGS) standard, with SMI <7 kg/m^2 and grip strength <26 kg.

Myokine measurements

For each subject, peripheral venous blood was drawn at the rest and serum samples were deep frozen and kept at -80℃ until the measurement. Serum irisin levels were measured using a commercially available enzyme-linked immunosorbent assay (ELISA) kit (Phoenix Pharmaceuticals, Burlingame, CA, USA) according to the manufacturer's protocol. Serum myostatin levels also were measured using an ELISA kit (R&D systems Inc., Minneapolis, USA) according to the manufacturer's protocol.

Statistical analysis

Data are expressed as mean±standard deviation unless otherwise indicated. Baseline differences were determined using Student's t test or the Mann-Whitney U test. Group of data that failed tests for normality and equal variance were analyzed by the nonparametric Kruskal-Wallis analysis of variance followed by Dunn's test. Associations between continuous variables were described by Spearman's correlation coefficients for variables that were not normally distributed. Statistical analyses were performed using JMP version 10.0.0 (SAS Institute, Cary, NC, USA) for Windows (Microsoft Corporation, Redmond, WA, USA). In all statistical analyses, $p<0.05$ was considered to be statistically significant.

Results

Patient characteristics

The characteristics of the 39 COPD patients and 30 healthy controls are summarized in Table 1. There were no significant differences in age or BMI between the COPD patients and healthy controls. As shown in Table 1, there was no significant difference in FVC and %FVC between the two groups. However, FEV_1 was significantly lower in COPD patients than in healthy controls (1.8±0.6 vs 2.7±0.4, respectively; $p<0.0001$) and FEV_1 (% predicted) was also significantly lower in COPD patients than in healthy controls (66.4±21.1 vs 97.3±14.6, respectively; $p<0.0001$).

COPD patients were divided in two groups, the sarcopenia group (n=9) or the non-sarcopenia (n=30) group in accordance with AWGS standards (Table 2). There was no significant difference in FVC, FEV_1, FEV_1/FVC or BMI between COPD patients with and without sarcopenia. However, MM, FFMI, and SMI were significantly lower in COPD patients with sarcopenia than in those without sarcopenia ($p<0.0005$).

Table 1. Characteristics of all participants

	COPD	healthy controls	p value
Subject No.	39	30	
Age (years)	74±8	74±3	NS
BMI (kg/m^2)	23.3±3.6	23.0±2.9	NS
FVC (L)	3.3±0.8	3.4±0.5	NS
%FVC (%)	100.2±16.9	98.8±13.7	NS
FEV_1 (L)	1.8±0.6	2.7±0.4	<0.0001
%FEV_1 (%)	66.4±21.1	97.3±14.6	<0.0001
FEV_1/FVC (%)	51.9±13.9	78.8±3.9	<0.0001

COPD, chronic obstructive pulmonary disease; BMI, body mass index; FVC, forced vital capacity; and FEV_1, forced expiratory volume in 1 second.

Table 2. Characteristics of COPD patients with and without sarcopenia

	non-sarcopenia	sarcopenia	p value
Subject No.	30	9	
GOLD stage Ⅰ, n	9	1	
GOLD stage Ⅱ, n	12	7	
GOLD stage Ⅲ, n	8	1	
GOLD stage Ⅳ, n	1	0	
FVC (L)	3.5±0.9	2.9±0.3	NS
%FVC (%)	101±18	97±10	NS
FEV_1 (L)	1.8±0.7	1.6±0.6	NS
%FEV_1	66±20	67±23	NS
FEV_1/FVC (%)	51±14	53±14	NS
Age (yr)	73±8	80±5	<0.05
BMI (Kg/m^2)	23.8±3.2	21.7±3.6	NS
MM	46.5±6.2	37.1±3.5	<0.001
FFMI	17.8±1.5	15.6±1.5	<0.0005
SMI (Kg/m^2)	7.3±0.8	6.1±0.6	<0.0005

COPD, chronic obstructive pulmonary disease; GOLD, Global Initiative for Chronic Obstructive Lung Disease; FVC, forced vital capacity; FEV_1, forced expiratory volume in 1 second; BMI, body mass index; MM, muscle mass; FFMI, fat free mass index; and SMI, skeletal muscle mass index.

Relationships between myokine levels and body composition

In COPD patients, serum irisin levels were positively correlated with FFMI ($r=0.36$, $p<0.05$) and SMI ($r=0.40$, $p<0.01$), but not significantly correlated with MM ($r=0.32$, $p>0.05$) (Fig. 1). However, serum myostatin levels were positively correlated with all body composition indices including MM ($r=0.44$, $p<0.005$), FFMI ($r=0.50$, $p<0.01$), and SMI ($r=0.54$, $p<0.005$) (Fig. 2).

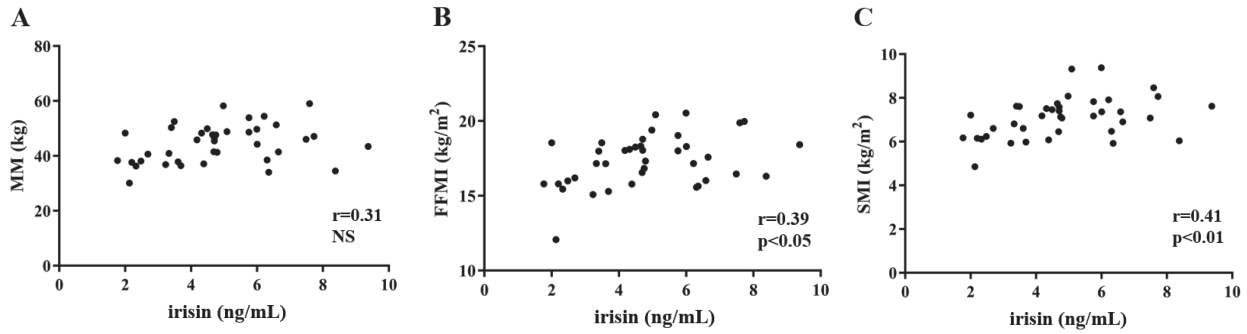

Figure 1. Correlations of serum irisin levels with MM, FFMI, and SMI. A, There was no significant correlation between serum irisin levels and MM. B and C, There were significant positive correlations between serum irisin levels and FFMI and SMI. MM, muscle mass; FFMI, fat free mass index; and SMI, skeletal muscle mass index.

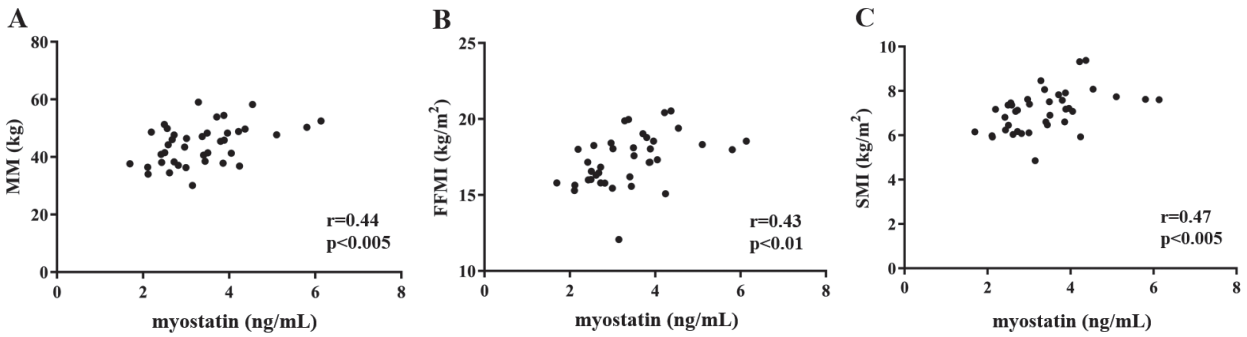

Figure 2. Correlations of serum myostatin levels with MM, FFMI, and SMI. A-C, There were significant positive correlations between serum myostatin levels and MM, FFMI, and SMI. MM, muscle mass; FFMI, fat free mass index; and SMI, skeletal muscle mass index.

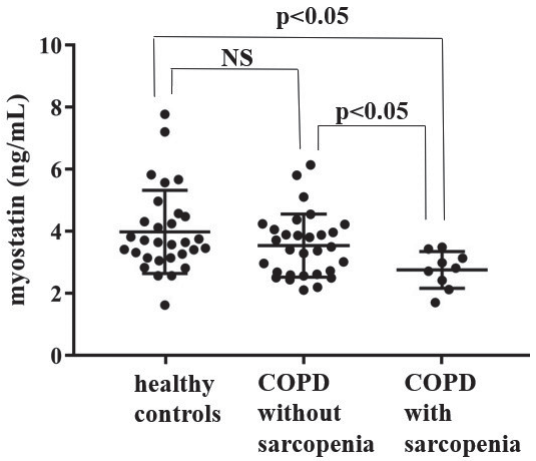

Figure 3. Comparison of serum myostatin levels between healthy controls and COPD patients with and without sarcopenia. There was a significant difference in serum myostatin levels between healthy controls and COPD patients with sarcopenia. COPD, chronic obstructive pulmonary disease.

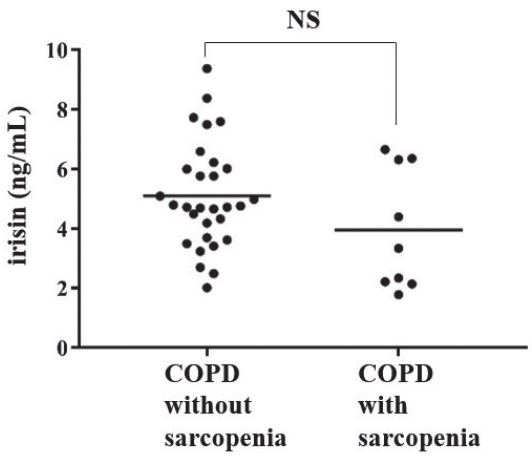

Figure 4. Comparison of serum irisin levels between COPD patients with and without sarcopenia. There was no significant difference in serum irisin levels between COPD with and without sarcopenia. COPD, chronic obstructive pulmonary disease.

Sarcopenia and myostatin levels

Serum myostatin levels in healthy controls were significantly higher than COPD patients with sarcopenia (4.01±0.25 ng/mL vs 2.76±0.20 ng/mL; $p<0.05$) but there was no significant difference in serum myostatin levels between healthy controls and those without sarcopenia. Serum myostatin levels were significantly lower in COPD patients with sarcopenia than in those without sarcopenia (2.76±0.20 ng/mL vs 3.53±0.19 ng/mL; $p<0.05$) (Fig. 3). There was no significant difference in serum irisin levels between COPD patients with sarcopenia and those without sarcopenia (3.94±0.68 ng/mL vs 5.10±0.33 ng/mL; $p>0.1$) (Fig. 4).

Discussion

In this study, we examined body composition and sarcopenia in COPD patients, and revealed that irisin and myostatin, one of the myokines, were positively correlated with muscle mass parameters including FFMI and SMI. Sarcopenia is a comorbidity in COPD, and is characterized by the loss of skeletal muscle mass and strength, which is associated with low exercise capacity, lower quality of life, and increased mortality[12,13].

The assessment of body composition measured using bioelectrical impedance analysis (BIA) or dual energy X-ray absorptiometry (DXA) are among the diagnostic methods for sarcopenia. BIA measures the resistance to flow of an electrical current as it passes through the body and is reflective of body composition. DXA calculates body density and body composition by irradiating the body with two X-ray beams. Early detection of sarcopenia in COPD patients is important. However, in many clinics and hospitals, body composition cannot be measured due to a lack of these devices; thus early detection of sarcopenia is difficult. Alternatively, we focused on myokine levels, such as irisin and myostatin, to be potential biomarkers of sarcopenia.

Myostatin is mainly produced by skeletal muscles and served as a negative regulator of muscle growth and it is released into plasma in a form of precursor protein, which can be cleaved into mature myostatin by bone morphogenetic-1/tolloid family of metalloproteases. Some studies have reported that postnatal inhibition of myostatin unequivocally increased skeletal muscle mass in adults and older mammals[14,15]. Another study reported that weekly injection of a neutralizing antibody to myostatin for 4 weeks significantly increased the relative weights of individual muscles by up to 17% in aged mice and improved indices of muscle performance and whole-body metabolism[16]. The other study reported that blocking myostatin might be a therapeutic target to combat sarcopenia and inhibiting myostatin-activin A signaling is therefore a highly promising therapeutic strategy to combat muscle loss in older people[17]. Therefore, myostatin was considered to be a negative regulator of muscle growth.

However, a recent study demonstrated a positive correlation between plasma myostatin levels and lean body mass[11]. Our study also revealed a positive correlation between serum myostatin levels and muscle mass. We speculate that hypertrophied muscle may secrete more myostatin as negative feedback to inhibit excessive muscle hypertrophy. Our study demonstrated that myostatin levels were significantly lower in COPD patients with sarcopenia than in those without sarcopenia. This result suggests that myostatin may be a potential biomarker for sarcopenia in COPD patients.

Previous studies have also reported that serum C1q, C-terminal agrin fragment, and p53 codon 72 polymorphism may be also be potential biomarkers of sarcopenia[18-20]. On the other hand, there was no significant difference in serum irisin levels between COPD patients with and without sarcopenia.

Considering the different results between myostatin and irisin, we speculated that myostatin would be mainly correlated with muscle mass but irisin would be correlated with muscle mass and other metabolic disorder such as diabetes mellitus. As a result, serum irisin levels might be influenced by not only muscle mass but also other metabolic factors.

In conclusion, myostatin is a potential biomarker of sarcopenia in COPD patients. However, there were some limitations to this study, among which include its single-center, cross-sectional design and limited sample size; therefore, causal relationships could not be determined. Second, this study enrolled only male COPD patients; therefore, it also remains unknown whether these results apply to female COPD patients. Third, twenty-four out of thirty-nine COPD patients overlapped with those in the previous report[21] which our group reported. Fourth, we didn't estimate the difference in amount of muscle mass between COPD patient and healthy controls because we didn't measure body composition in healthy controls.

Further studies are needed to better understand the pathophysiology of sarcopenia in COPD and to determine other potential biomarkers.

Acknowledgments

All authors have no COI to declare regarding the present study.

We acknowledge Tatsuo Kimura and Shinya Fukumoto (Medcity 21, medical examinations clinics) for providing serum samples and clinical data of never-smokers enrolled in this study.

References

1. Munhoz da Rocha Lemos Costa T, Costa FM, Jonasson TH, et al. Body composition and sarcopenia in patients with chronic obstructive pulmonary disease. Endocrine 2018;60:95-102.
2. Liguori I, Russo G, Aran L, et al. Sarcopenia: assessment of disease burden and strategies to improve outcomes. Clin Interv Aging 2018;13:913-927.
3. Chang JS, Kim TH, Nguyen TT, et al. Circulating irisin levels as a predictive biomarker for sarcopenia: a cross-sectional community-based study. Geriatr Gerontol Int 2017;17:2266-2273.
4. Boström P, Wu J, Jedrychowski MP, et al. A PGC1-α-dependent myokine that drives brown-fat-like development of white fat and thermogenesis. Nature 2012;481:463-468.
5. Huh JY, Dincer F, Mesfum E, et al. Irisin stimulates muscle growth-related genes and regulates adipocyte differentiation and metabolism in humans. Int J Obes (Lond) 2014;38:1538-1544.
6. Lee HJ, Lee JO, Kim N, et al. Irisin, a novel myokine, regulates glucose uptake in skeletal muscle cells via AMPK. Mol Endocrinol 2015;29:873-881.
7. McNally EM. Powerful genes--myostatin regulation of human muscle mass. N Engl J Med 2004;350:2642-2644.
8. Huh JY. The role of exercise-induced myokines in regulating metabolism. Arch Pharm Res 2018;41:14-29.
9. Allen DL, Hittel DS, McPherron AC. Expression and function of myostatin in obesity, diabetes, and exercise adaptation. Med Sci Sports Exerc 2011;43:1828-1835.
10. Wu LF, Zhu DC, Wang BH, et al. Relative abundance of mature myostatin rather than total myostatin is negatively associated with bone mineral density in Chinese. J Cell Mol Med 2018;22:1329-1336.
11. Vogelmeier CF, Criner GJ, Martinez FJ, et al. Global strategy for the diagnosis, management, and prevention of chronic obstructive lung disease 2017 report. GOLD executive summary. Am J Respir Crit Care Med 2017;195:557-582.
12. Tunsupon P, Lal A, Abo Khamis M, et al. Comorbidities in patients with chronic obstructive pulmonary disease and pulmonary rehabilitation outcomes. J Cardiopulm Rehabil Prev 2017;37:283-289.
13. Polkey MI, Moxham J. Attacking the disease spiral in chronic obstructive pulmonary disease. Clin Med (Lond) 2006;6:190-196.
14. Whittemore LA, Song K, Li X, et al. Inhibition of myostatin in adult mice increases skeletal muscle mass and strength. Biochem Biophys Res Commun 2003;300:965-971.
15. LeBrasseur NK, Schelhorn TM, Bernardo BL, et al. Myostatin inhibition enhances the effects of exercise on

performance and metabolic outcomes in aged mice. J Gerontol A Biol Sci Med Sci 2009;64:940-948.
16. White TA, LeBrasseur NK. Myostatin and sarcopenia: opportunities and challenges - a mini-review. Gerontology 2014;60:289-293.
17. Cohen S, Nathan JA, Goldberg AL. Muscle wasting in disease: molecular mechanisms and promising therapies. Nat Rev Drug Discov 2015;14:58-74.
18. Watanabe S, Sato K, Hasegawa N, et al. Serum C1q as a novel biomarker of sarcopenia in older adults. FASEB J 2015;29:1003-1010.
19. Drey M, Sieber CC, Bauer JM, et al. C-terminal Agrin Fragment as a potential marker for sarcopenia caused by degeneration of the neuromuscular junction. Exp Gerontol 2013;48:76-80.
20. Di Renzo L, Gratteri S, Sarlo F, et al. Individually tailored screening of susceptibility to sarcopenia using p53 codon 72 polymorphism, phenotypes, and conventional risk factors. Dis Markers 2014;2014:743634.
21. Sugiyama Y, Asai K, Yamada K, et al. Decreased levels of irisin, a skeletal muscle cell-derived myokine, are related to emphysema associated with chronic obstructive pulmonary disease. Int J Chron Obstruct Pulmon Dis 2017;12:765-772.

Osaka City Med. J. Vol. 65, 9-17, 2019

Decreased Level of Phosphatase and Tensin Homolog Deleted from Chromosome 10 (PTEN), a Negative Regulator of Phosphoinositide 3-kinase (PI3K)/Serine-threonine Protein Kinase (Akt) Pathway, is Related to Chronic Obstructive Pulmonary Disease

Tamaki Kawamoto, Kazuhisa Asai, Kazuhiro Yamada, Shinya Yoshida, Atsuko Okamoto, Kanako Sato, Naoki Ijiri, Tetsuya Watanabe, and Tomoya Kawaguchi

Department of Respiratory Medicine, Osaka City University Graduate School of Medicine

Abstract

Background

Cigarette smoking causes persistent airway inflammation and is considered to be the major cause of chronic obstructive pulmonary disease (COPD). The activation of phosphoinositide 3-kinase (PI3K)/serine-threonine protein kinase (Akt) pathway is known to have an important role in COPD pathogenesis. Phosphatase and tensin homolog deleted from chromosome 10 (PTEN) is a negative regulator of the PI3K/Akt pathway and is the gene most significantly associated with COPD. However, the role of PTEN in COPD pathogenesis remains unclear.

Methods

Bronchial epithelial cells were obtained by bronchial brushing technique from patients with COPD, healthy smokers, and healthy non-smokers. PTEN and PI3Kδ expression in bronchial epithelial cells were examined by real-time polymerase chain reaction (PCR) and western blotting. Moreover, we investigated the correlation of PTEN and PI3KCD (encoding PI3Kδ) with pulmonary function and clinical parameters.

Results

Forty-nine COPD patients, 31 healthy smokers, and 22 healthy non-smokers were enrolled in this study. In COPD patients, PTEN expression was significantly decreased in bronchial epithelial cells and negatively correlated with pack-year ($r=-0.40$, $p<0.001$). PTEN mRNA expression was significantly correlated with the parameters of obstructive impairment, such as $\%FEV_1$ ($r=0.26$ $p<0.01$), FEV_1/FVC, ($r=0.20$, $p=0.04$) and %diffusing capacity of the lung for carbon monoxide (DLco) ($r=0.34$, $p<0.01$). There was no significant difference in PI3Kδ mRNA levels between each group.

Conclusions

PTEN expression in COPD patients was significantly lower than that in healthy non-smokers,

Received August 30, 2018; accepted November 27, 2018.
Correspondence to: Kazuhisa Asai, MD, PhD.
Department of Respiratory Medicine, Osaka City University Graduate School of Medicine,
1-4-3 Asahimachi, Abeno-ku, Osaka, 545-8585, Japan
Tel: +81-6-6645-3821; Fax: +81-6-6636-0439
E-mail: kazuasai@med.osaka-cu.ac.jp

suggesting that decrease of PTEN expression might be related to pathogenesis of COPD. Furthermore, the decrease in PTEN expression was correlated with obstructive impairment of COPD. PTEN might be a possible therapeutic target for COPD.

Key Words: Chronic obstructive pulmonary disease (COPD); phosphatase and tensin homolog deleted from chromosome 10 (PTEN); phosphoinositide 3-kinase (PI3K)/serine-threonine protein kinase (Akt) pathway

Introduction

Chronic obstructive pulmonary disease (COPD) is a global health problem. The World Health Organization estimated that more than 3 million people died from COPD in 2005 which corresponds to 5% of all deaths globally, and COPD will be the third leading cause of death by 2030[1]. COPD is characterized by progressive irreversible airflow limitation and chronic inflammation of the airways[2]. Cigarette smoke is the major risk factor of COPD[3-5]. Oxidative stress caused by cigarette smoke damages lipids, proteins, and DNA and induces inflammatory reactions in the lung[6-8]. Even if cigarette smoke exposure is stopped, the disease may still progress due to ageing and persistence of inflammation[9,10]. *In vitro* studies have shown that oxidative stress by hydrogen peroxide (H_2O_2) activates phosphoinositide 3-kinase (PI3K) and serine/threonine protein kinase (Akt)[11,12]. A recent study suggested that persistent activation of Akt is implicated in the pathogenesis of COPD[13]. Akt is activated by phosphatidylinositol-3,4,5-triphosphate (PIP3). PIP3 is converted to phosphatidylinositol-4,5 bisphosphate (PIP2) through PI3K, which is encoded by the PI3Kδ gene in humans.

Phosphatase and tensin homolog deleted from chromosome 10 (PTEN) was originally isolated as a tumor suppressor gene and is known to be a negative regulator of PI3K. PTEN converts PIP3 back to PIP2, antagonizing PI3K action; thus, the activation of PTEN regulates Akt signaling pathway negatively[14-16]. PTEN is reported to be the most significantly associated gene with COPD[17]. Moreover, previous study has demonstrated that the protein expression levels of PTEN are significantly decreased in the lung tissue of emphysematous mice exposed to cigarette smoke[18]. Another study has shown that PTEN protein is decreased in lung homogenate of COPD patients[19]. PTEN may be related to the pathogenesis of COPD, however, in humans, there are few reports that reveal the levels of PTEN in COPD patients. A recent study on human bronchial biopsies of COPD patients has demonstrated an increased inflammatory gene and protein expression and structural alterations in bronchial epithelial cells, which suggests that these cells may be the key effector in the pathogenesis of COPD[20].

Therefore, we hypothesized that impaired expression of PTEN in human bronchial epithelial cells would be a possible cause of COPD. To address this hypothesis, PTEN and PI3Kδ expression in human bronchial epithelial cells were measured by real-time polymerase chain reaction (PCR) and western blotting. Moreover, we examined the correlation of PTEN and PI3Kδ with pulmonary functions and clinical parameters.

Methods

Subjects

COPD patients, healthy smokers, and healthy non-smokers were enrolled in this study. COPD was diagnosed according to the Global Initiative for Chronic Obstructive Lung Disease (GOLD) guidelines[21]. Healthy smokers were current or former smokers with more than 10 pack-year history

who had no clinically significant medical disorders. All healthy non-smokers were never smokers who had no clinically significant medical disorders. These subjects had no acute exacerbation and pneumonia for at least 2 weeks. All the subjects underwent pulmonary function test by spirometry (Chestac-25F, Chest Co., Tokyo, Japan). The diffusing capacity of the lung for carbon monoxide (DLco) was measured at least twice by the single-breath method. Bronchoscopy was performed in all subjects to diagnose small nodules or the examination of bloody sputum at Osaka City University. During bronchoscopic procedure, bronchial epithelial cells were obtained from the normal side by bronchial brushing. This study was approved by the ethics committee of Osaka City University Hospital (approval number 1819), and all subjects gave written informed consent for their participation.

Real-time PCR

Total RNA was extracted from bronchial epithelial cells using TRIzol (Life Technologies Japan, Tokyo, Japan). After quantification, 1 μg of RNA was reverse transcribed into complementary DNA with a SuperScript VILO cDNA Synthesis Kit® (Thermo Fisher Scientific, Carlsbad, CA, USA). Quantitative real-time PCR was performed using an Applied Biosystems 7500 Real-Time PCR System (Life Technologies Japan, Tokyo, Japan) with TaqMan Gene Expression Assays (Thermo Fisher Scientific) for PTEN (Hs02621230_s1), PI3Kδ (Hs00192399_m1) and glycer-aldehyde 3-phosphate dehydrogenase (GAPDH) (Hs99999905_m1).

Western blot analysis

Brushed bronchial epithelial cells were suspended in 4 mL of phosphate buffered saline (PBS) and centrifuged at 1500×g at 4℃ for 10 minutes. Supernatant was discarded, and pellet was dissolved in 100 μL of cell lysis buffer (Cell Signaling Technology, Danvers, MA, USA). BCA Protein Assay Kit (Pierce, Waltham, MA, USA) was used for protein quantification. Proteins for each sample were separated by sodium dodecyl sulfate polyacrylamide gel electrophoresis and transferred onto polyvinylidene difluoride (PVDF) membrane by western blotting using Mini-PROTEAN® TGX™ Precast Protein Gels (4561023, Bio-Rad, Hercules, California, USA). Membranes were incubated with anti-PTEN (accession number: P60484) rabbit IgG antibody (ab32199, Abcam, 1:2000 dilution) or anti-GAPDH (accession number: P04406) antibody (ab128915, Abcam, 1:10000 dilution) overnight at 4℃, and further incubated with horseradish peroxidase (HRP) conjugated goat anti-rabbit IgG secondary antibody (sc-2004, Santa Cruz Biotechnology) for 2 hours at room temperature. The densitometry analysis was performed to measure protein level in PTEN and GAPDH using LAS4000 (Fuji Imaging, Tokyo, Japan).

Statistical analysis

GraphPad Prism version 7.04 (GraphPad Software, San Diego, CA, USA) was used for Statistical analysis. To compare two groups, Student's t-test and for more than three groups, one-way analysis of variance (ANOVA) with Tukey-Kramer post hoc test was performed. The significance of correlation was analyzed by Spearman's rank correlation coefficients. In all statistical analyses, p-values <0.05 were considered significant.

Results

Subject characteristics

Forty-nine COPD patients, 31 healthy smokers, and 22 healthy non-smokers were enrolled in this study. The characteristics of the subjects and parameters of pulmonary function test are shown in

Table 1. COPD patients were in GOLD stage Ⅰ-Ⅳ (25/16/7/1). There was a significant difference in term of sex ratio between the three groups, for instance, in case of COPD, the proportion of males was higher than females. However, in terms of age and body mass index (BMI) there was no significant difference between the three groups. %FEV_1 values were significantly lower in COPD patients compared to healthy non-smokers ($p<0.001$).

PTEN and PI3Kδ expression in COPD patients

PTEN mRNA levels were significantly decreased in COPD patients ($p<0.001$) and healthy smokers ($p=0.004$) compared to healthy non-smokers (Fig. 1A). On the other hand, there was no significant difference in PI3Kδ mRNA level between the three groups (Fig. 1B). Moreover, PTEN protein level in COPD patients was significantly lower than that of healthy non-smokers ($p=0.013$) (Figs. 2A and 2B).

Table 1. Subjects characteristics

	Healthy non-smoker	Healthy smoker	COPD	p-value
Subjects No.	22	31	49	
Sex (male/female)	6/16	26/5	42/7	$p<0.001$
Age (year) *	67.1 (62.6-71.5)	67.6 (64.0-71.2)	69.4 (67.7-71.2)	N.S.
BMI (kg/m^2) *	22.1 (20.8-23.5)	21.5 (20.1-23.0)	20.9 (19.9-22.0)	N.S.
Smoking history (Pack-Year) *	0	48.8 ** (38.5-59.1)	60.4 ** (52.8-68.0)	$p<0.001$
FEV_1 (% predicted) *	130.7 (120-142)	122 (112-132)	86 ** (76.3-96.3)	$p<0.001$

*:mean (95% confidence interval) **:$p<0.05$ compared with healthy non-smoker.

COPD, chronic obstructive pulmonary disease; BMI, body mass index; and FEV_1, forced expiratory volume in one second.

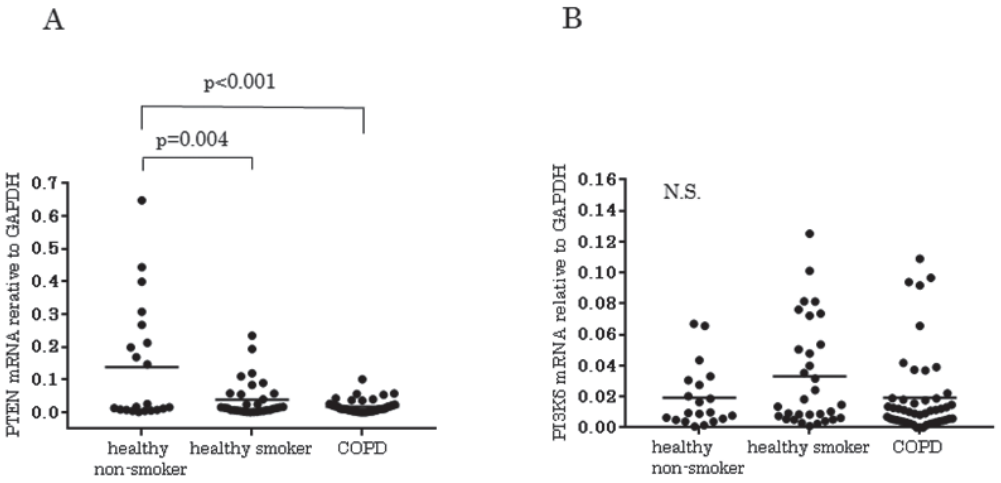

Figure 1. PTEN and PI3Kδ mRNA expression in study subjects. A, PTEN mRNA levels were significantly decreased in COPD patients and healthy smokers compared to healthy non-smokers. Each bar represents the mean value. B, There was no significant difference in PI3Kδ mRNA level between the three groups. Each bar represents the mean value. COPD, chronic obstructive pulmonary disease; PTEN, phosphatase and tensin homolog deleted from chromosome 10; PI3K, phosphoinositide 3-kinase; GAPDH, glyceraldehyde 3-phosphate dehydrogenase; and N.S., not significant.

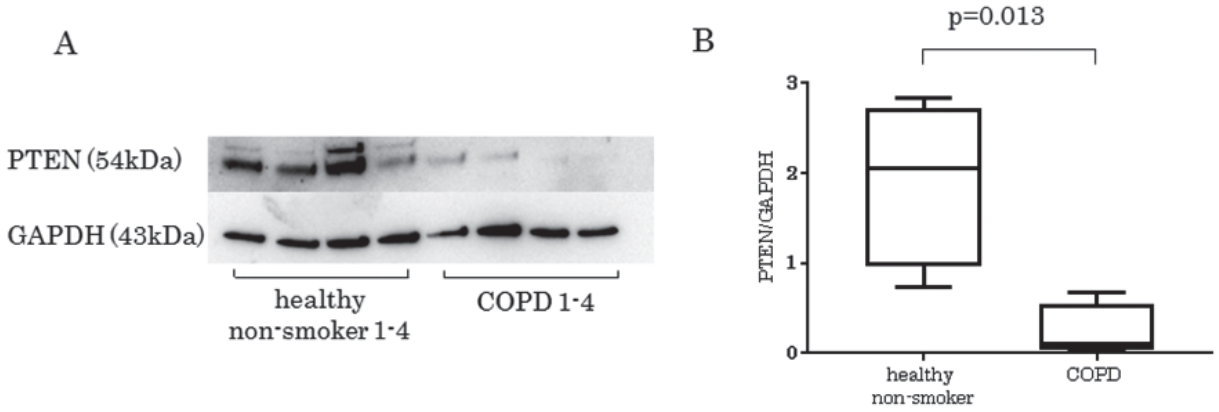

Figure 2. A and B, Western blotting analysis of PTEN in COPD patients and healthy non-smokers. PTEN protein level in COPD patients (n=4) was significantly lower (0.2±0.3) than that of healthy non-smokers (n=4) (1.9±0.9). Statistical analyses were performed using the Student's t-test. Values are means±standard deviation. COPD, chronic obstructive pulmonary disease; PTEN, phosphatase and tensin homolog deleted from chromosome 10; and GAPDH, glycer¬aldehyde 3-phosphate dehydrogenase.

Correlation between PTEN mRNA level and clinical parameters

There was a negative correlation between PTEN mRNA levels and pack-year (Fig. 3; $r=-0.40$, $p<0.001$). However, there was no correlation of PTEN mRNA levels with age and BMI (data not shown). There were significant positive correlations between PTEN mRNA levels and $\%FEV_1$ ($r=0.26$, $p<0.01$), FEV_1/FVC ($r=0.20$, $p=0.04$), and %DLco ($r=0.34$, $p<0.01$) (Figs. 4A-4C). In contrast, PI3Kδ mRNA levels were not significantly correlated with any parameters of pulmonary function test (Figs. 5A-5C).

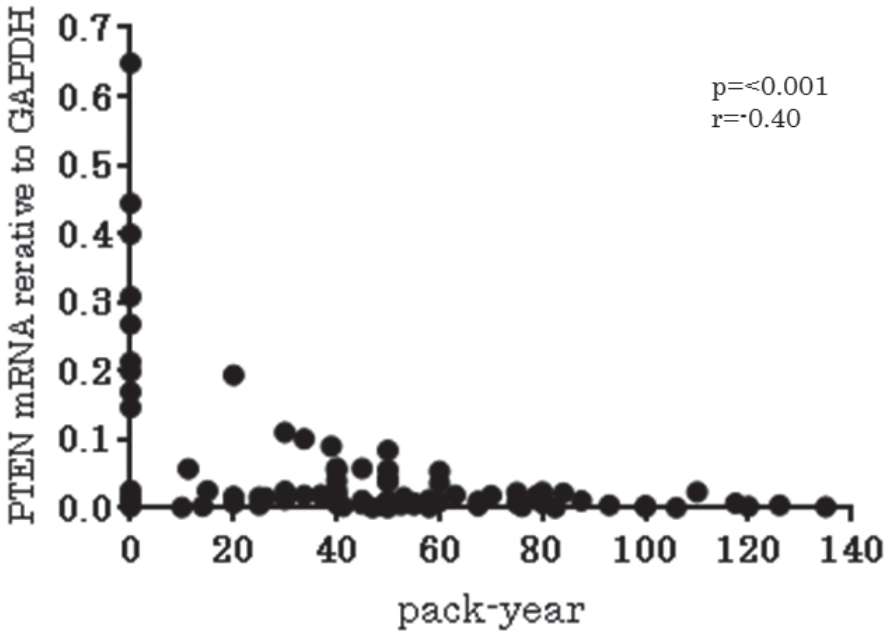

Figure 3. Relationship between PTEN mRNA expression and pack year. There was a significant correlation between PTEN mRNA levels and pack year. PTEN, phosphatase and tensin homolog deleted from chromosome 10; and GAPDH, glyceraldehyde 3-phosphate dehydrogenase.

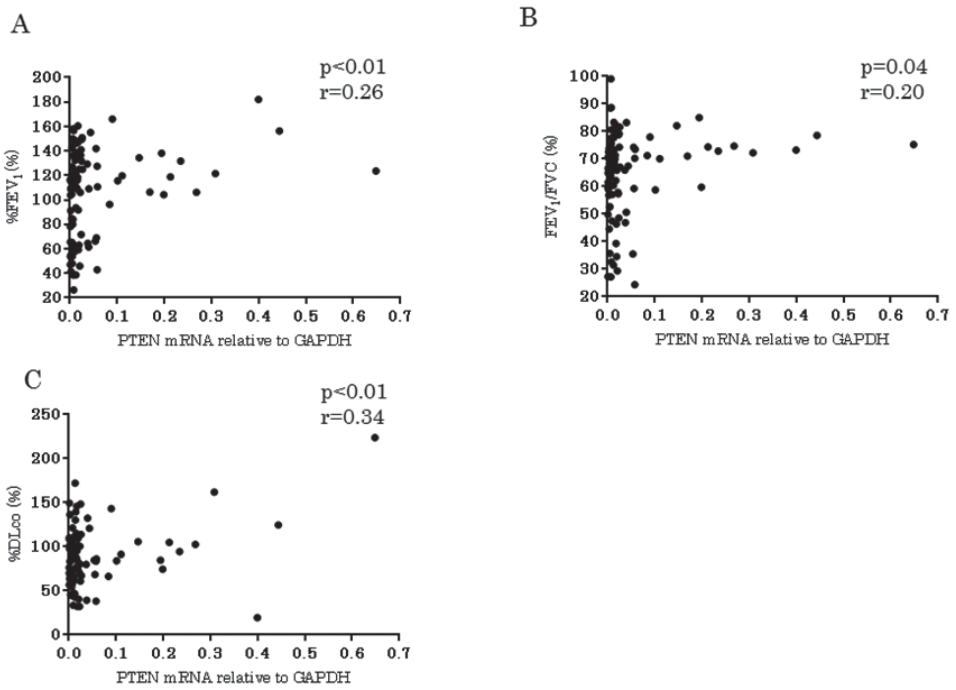

Figure 4. Correlations of PTEN mRNA levels with pulmonary function test values. A: $\%FEV_1$, B: FEV_1/FVC, and C: %DLco. There were significant positive correlations between PTEN mRNA levels and $\%FEV_1$, FEV_1/FVC, and %DLco. PTEN, phosphatase and tensin homolog deleted from chromosome 10; GAPDH, glyceraldehyde 3-phosphate dehydrogenase; FEV_1, forced expiratory volume in one second; FVC, forced vital capacity; and DLco, diffusing capacity of carbon monoxide.

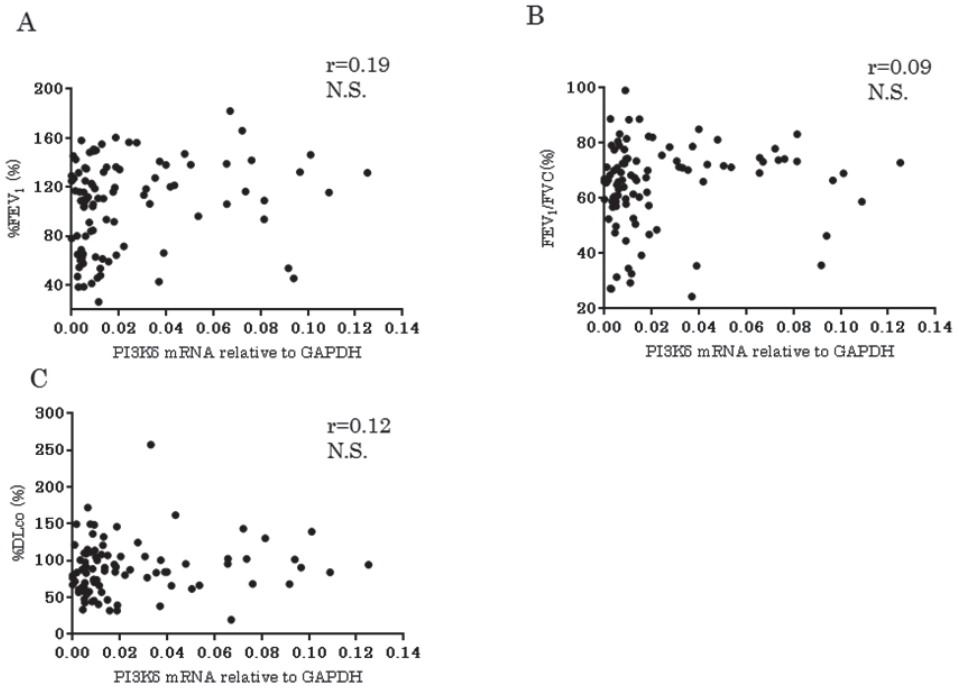

Figure 5. Correlations of PI3Kδ mRNA levels with pulmonary function test values. A: $\%FEV_1$, B: FEV_1/FVC, and C: %DLco. No significant correlations were observed between PI3Kδ mRNA levels and $\%FEV_1$, FEV_1/FVC, and %DLco. PI3K, phosphoinositide 3-kinase; GAPDH, glyceraldehyde 3-phosphate dehydrogenase; FEV_1, forced expiratory volume in one second; FVC, forced vital capacity; DLco, diffusing capacity of carbon monoxide; and N.S., not significant.

Discussion

In the present study, we found that PTEN expression was significantly decreased in human bronchial epithelial cells of COPD patients, and it was related to pack-year and pulmonary functions.

Previous studies have reported that most inflammatory cells related to COPD were controlled by class I PI3Ks[22,23]. There are four class I PI3K isoforms in mammals (p110α, p110β, p110γ, and p110δ), named after their respective p110 catalytic subunits. Among these isoforms, PI3Kδ (p110δ) distinctly correlates with inflammation[24,25]. Additionally, we examined the mRNA level of PI3Kδ in the bronchial epithelial cells, however, we found no significant difference between groups. A recent study indicates that persistent activation of Akt is strongly implicated in the etiology of COPD[11]. PI3K/Akt pathway is mainly regulated by PI3K and PTEN. PI3K phosphorylates PIP2 to PIP3 and activates the PI3K/Akt signaling pathway. In contrast, PTEN negatively regulates PI3K signaling by dephosphorylating PIP3 to PIP2[15,16]. The failure of these regulation mechanisms might be involved in the progression of pathogenesis of COPD.

In an emphysematous mouse model, it was observed that there was notably increased phosphorylated-Akt (p-Akt) expression and decreased PTEN expression in the lung tissue[18]. In humans, it has been reported that PTEN was the most significantly associated gene with COPD, and two PTEN single nucleotide polymorphism (SNP)s (rs701848, rs1903858) were observed to be associated with COPD risk among heavy smokers[17]. To our knowledge, there are few reports regarding regulation of PI3K/Akt signaling by PTEN in COPD patients. Our results indicated that in COPD patients, persistent activation of Akt signaling pathway is caused by decreased PTEN expression rather than increased PI3Kδ expression. However, the mechanism underlying the decreased expression of PTEN in COPD is still unknown.

We presumed that smoking might be related to PTEN expression, and thus, examined the relationship between PTEN mRNA levels and pack-year. We confirmed that there was a negative correlation between PTEN mRNA levels and pack-year. Although we had considered the possibility that the decrease in PTEN expression was possibly affected by aging, there was no correlation between PTEN mRNA levels and age in our study. Decreased expression of PTEN was reported in lung homogenates of COPD patients. PTEN expression was decreased following cigarette smoke extract (CSE) stimulation in BEAS-2B cells[19]. Recent studies have reported that oxidative stress decreases PTEN expression[26], and Nuclear factor erythroid 2-related factor 2 (Nrf2) is the main regulator of antioxidant response[27]. We previously reported that Nrf2 expression was significantly decreased in bronchial epithelial cells in COPD patients, and Nrf2 had a protective role against CSE-induced apoptosis[28]. Cigarette smoke contains reactive oxygen species (ROS) that can cause oxidative stress[29]. This oxidative stress might have decreased PTEN expression in COPD patients.

We examined the correlation of PTEN and PI3Kδ with pulmonary functions. We found significant positive correlations between PTEN mRNA levels and the parameters of obstructive impairment, such as %FEV_1, FEV_1/FVC, and %DLco. Yanagisawa et al reported that PTEN protein levels were significantly decreased in the peripheral lung of COPD patients. There was a significant positive correlation between the PTEN protein levels and FEV_1/FVC or %FEV_1, indicating that the PTEN levels were decreased significantly as COPD progresses[19]. These results were consistent with our results.

In COPD, neutrophils play an important role in chronic inflammation[30]. The number of neutrophils, the level of IL-6 and IL-8 in sputum or broncho-alveolar lavage fluid of COPD patients

were reported to be negatively correlated with severities of air flow limitation[31-35]. Akt activation has been implicated in neutrophil migration and polarization[36,37]. PTEN has been shown to control inflammation by suppressing PI3K/Akt pathway[38]. These results suggest that PTEN is related to the pathogenesis of COPD through chronic neutrophilic inflammation. PTEN may be a possible therapeutic target for COPD.

Our study has some limitations. First, the study sample size was small. Second, we acquired bronchial epithelial cells from approximately the 4th branch, not the alveolar region because of technical reasons. Third, there was a significant difference in the sex ratio between each group. Since smokers and COPD patients were mostly men, it was difficult to align the sex ratio. However, to the best of our knowledge, there was no report that PTEN expression was affected by gender. Despite these limitations, we could evaluate the level of PTEN in COPD patients and provide a first step to understand the etiology of COPD.

In conclusion, in COPD patients, PTEN expression was significantly decreased in bronchial epithelial cells. Furthermore, we found significant positive correlations between PTEN mRNA levels and the parameters of obstructive impairment. Our study suggests that the decrease of PTEN expression might be related to pathogenesis of COPD and PTEN might be a possible therapeutic target for COPD. Further research is needed to confirm our findings.

Acknowledgments

All authors have no COI to declare regarding the present study.

This work was supported by grants from the Japan Society for the Promotion of Science (JSPS) Kakenhi grant 15K09185.

References

1. World Health Organization. Burden of COPD. Available from:http://www.who.int/respiratory/copd/burden/en/
2. Vogelmeier CF, Criner GJ, Martinez FJ, et al. Global Strategy for the Diagnosis, Management, and Prevention of Chronic Obstructive Lung Disease 2017 Report: GOLD Executive Summary. Arch Bronconeumol 2017; 53:128-149.
3. Hogg JC, Timens W. The pathology of chronic obstructive pulmonary disease. Annu Rev Pathol 2009;4:435-459.
4. The Surgeon General's 1989 Report on Reducing the Health Consequences of Smoking: 25 Years of Progress. MMWR Suppl 1989;38:1-32.
5. Lapperre TS, Postma DS, Gosman MM, et al. Relation between duration of smoking cessation and bronchial inflammation in COPD. Thorax 2006;61:115-121.
6. Zinellu E, Zinellu A, Fois AG, et al. Circulating biomarkers of oxidative stress in chronic obstructive pulmonary disease: a systematic review. Respir Res 2016;17:150.
7. Rahman I. The role of oxidative stress in the pathogenesis of COPD: implications for therapy. Treat Respir Med 2005;4:175-200.
8. van Eeden SF, Sin DD. Oxidative stress in chronic obstructive pulmonary disease: a lung and systemic process. Can Respir J 2013;20:27-29.
9. Donohue JF. Ageing, smoking and oxidative stress. Thorax 2006;61:461-462.
10. Rutgers SR, Postma DS, ten Hacken NH, et al. Ongoing airway inflammation in patients with COPD who do not currently smoke. Thorax 2000;55:12-18.
11. To Y, Ito K, Kizawa Y, et al. Targeting phosphoinositide-3-kinase-delta with theophylline reverses corticosteroid insensitivity in chronic obstructive pulmonary disease. Am J Respir Crit Care Med 2010; 182:897-904.
12. Mercado N, Ito K, Barnes PJ. Accelerated ageing of the lung in COPD: new concepts. Thorax 2015;70:482-489.
13. Bozinovski S, Vlahos R, Hansen M,et al. Akt in the pathogenesis of COPD. Int J Chron Obstruct Pulmon Dis 2006;1:31-38.

14. Manning BD, Cantley LC. AKT/PKB signaling: navigating downstream. Cell 2007;129:1261-1274.
15. Stambolic V, Suzuki A, de la Pompa JL, et al. Negative regulation of PKB/Akt-dependent cell survival by the tumor suppressor PTEN. Cell 1998;95:29-39.
16. Maehama T, Dixon JE. The tumor suppressor, PTEN/MMAC1, dephosphorylates the lipid second messenger, phosphatidylinositol 3,4,5-trisphosphate. J Biol Chem 1998;273:13375-13378.
17. Hosgood HD 3rd, Menashe I, He X, et al. PTEN identified as important risk factor of chronic obstructive pulmonary disease. Respir Med 2009;103:1866-1870.
18. Lu J, Xie L, Liu C, et al. PTEN/PI3k/AKT regulates macrophage polarization in emphysematous mice. Scand J Immunol 2017;85:395-405.
19. Yanagisawa S, Baker JR, Vuppusetty C, et al. Decreased phosphatase PTEN amplifies PI3K signaling and enhances proinflammatory cytokine release in COPD. Am J Physiol Lung Cell Mol Physiol 2017;313:L230-L239.
20. Gao W, Li L, Wang Y, et al. Bronchial epithelial cells: the key effector cells in the pathogenesis of chronic obstructive pulmonary disease? Respirology 2015;20:722-729.
21. Global Strategy for the Diagnosis, Management and Prevention of COPD. Global Initiative for Chronic Obstructive Lung Disease (GOLD) 2015. Available from: http://www.goldcopd.org/ .
22. Sriskantharajah S, Hamblin N, Worsley S, et al. Targeting phosphoinositide 3-kinase delta for the treatment of respiratory diseases. Ann N Y Acad Sci 2013;1280:35-39.
23. Marwick JA, Chung KF, Adcock IM. Phosphatidylinositol 3-kinase isoforms as targets in respiratory disease. Ther Adv Respir Dis 2010;4:19-34.
24. Kok K, Geering B, Vanhaesebroeck B. Regulation of phosphoinositide 3-kinase expression in health and disease. Trends Biochem Sci 2009;34:115-127.
25. Ito K, Caramori G, Adcock IM. Therapeutic potential of phosphatidylinositol 3-kinase inhibitors in inflammatory respiratory disease. J Pharmacol Exp Ther 2007;321:1-8.
26. Kim SJ, Jung HJ, Lim CJ. Reactive oxygen species-dependent down-regulation of tumor suppressor genes PTEN, USP28, DRAM, TIGAR, and CYLD under oxidative stress. Biochem Genet 2013;51:901-915.
27. Kensler TW, Wakabayashi N, Biswal S. Cell survival responses to environmental stresses via the Keap1-Nrf2-ARE pathway. Annu Rev Pharmacol Toxicol 2007;47:89-116.
28. Yamada K, Asai K, Nagayasu F, et al. Impaired nuclear factor erythroid 2-related factor 2 expression increases apoptosis of airway epithelial cells in patients with chronic obstructive pulmonary disease due to cigarette smoking. BMC Pulm Med 2016;16:27.
29. Church DF, Pryor WA. Free-radical chemistry of cigarette smoke and its toxicological implications. Environ Health Perspect 1985;64:111-126.
30. Hoenderdos K, Condliffe A. The neutrophil in chronic obstructive pulmonary disease. Am J Respir Cell Mol Biol 2013;48:531-539.
31. Hacievliyagil SS, Gunen H, Mutlu LC, et al. Association between cytokines in induced sputum and severity of chronic obstructive pulmonary disease. Respir Med 2006;100:846-854.
32. Yamamoto C, Yoneda T, Yoshikawa M, et al. Airway inflammation in COPD assessed by sputum levels of interleukin-8. Chest 1997;112:505-510.
33. Di Stefano A, Capelli A, Lusuardi M, et al. Severity of airflow limitation is associated with severity of airway inflammation in smokers. Am J Respir Crit Care Med 1998;158:1277-1285.
34. Stänescu D, Sanna A, Veriter C, et al. Airways obstruction, chronic expectoration, and rapid decline of FEV1 in smokers are associated with increased levels of sputum neutrophils. Thorax 1996;51:267-271.
35. Soler N, Ewig S, Torres A, et al. Airway inflammation and bronchial microbial patterns in patients with stable chronic obstructive pulmonary disease. Eur Respir J 1999;14:1015-1022.
36. Billadeau DD. PTEN gives neutrophils direction Nat Immunol. United States, 2008:716-718.
37. Zou W, Chu X, Cai C, et al. AKT-mediated regulation of polarization in differentiated human neutrophil-like HL-60 cells. Inflamm Res 2012;61:853-862.
38. Yamada KM, Araki M. Tumor suppressor PTEN: modulator of cell signaling, growth, migration and apoptosis. J Cell Sci 2001;114:2375-2382.

Osaka City Med. J. Vol. 65, 19-29, 2019

Focal Atrophy of the Dorsal Brainstem Correlates with Hallucinations in Patients with Dementia with Lewy Bodies

Tadashi Ohtomo[1)], Yasunori Matsuda[1)], Kentaro Uchida[1)], Jumpei Maruta[1)], and Koki Inoue[1,2)]

Departments of Neuropsychiatry[1)] and Center for Brain Science[2)], Osaka City University Graduate School of Medicine

Abstract

Background

Visual hallucinations, the characteristic symptom of dementia with Lewy bodies (DLB), and their underlying mechanisms have not been researched extensively and their pathophysiology remains unknown. Because the quality of hallucinations in patients with DLB and peduncular hallucinosis (PH) is similar, we investigated the relationship between focal atrophy of the dorsal brainstem and hallucinations in patients with DLB.

Methods

Brain magnetic resonance imaging was conducted in 24 DLB patients and data were analyzed with the voxel-based specific regional analysis system for Alzheimer's disease (VSRAD) advance 2 software, which assesses the degree of focal atrophy of dorsal brainstem gray matter (GM) and white matter (WM). Patients were divided into two groups in three different ways: GM atrophy, WM atrophy, and relative atrophic degree of either GM or WM. The degree of hallucinations was estimated using the Neuropsychiatric Inventory (NPI). Then, the VSRAD results and NPI scores were analyzed.

Results

The mean NPI total score and hallucination score were significantly lower in the group with WM atrophy ($p<0.01$), whereas there were no significant differences between the groups divided on the basis of the degree of GM atrophy. There was also a significant inverse correlation between the degree of WM atrophy and the NPI hallucinations score ($p<0.01$).

Conclusions

Our findings suggest that focal atrophy of the dorsal brainstem GM with relatively spared WM in patients with DLB might cause visual hallucinations similar to PH. Further longitudinal studies could elucidate the pathophysiology of hallucinations in patients with DLB.

Key Words: Dementia with Lewy bodies; Visual hallucinations; Peduncular hallucinosis; Brainstem atrophy; MRI

Received August 30, 2018; accepted November 27, 2018.

Correspondence to: Tadashi Ohtomo, MD, MFA.
Department of Neuropsychiatry, Osaka City University Graduate School of Medicine,
1-4-3 Asahimachi, Abeno-ku, Osaka 545-8585, Japan
Tel: +81-6-6645-3821; Fax: +81-6-6636-0439
E-mail: dayouli@gmail.com

Introduction

Dementia with Lewy bodies (DLB) is the second most common cause of neurodegenerative dementia after Alzheimer disease (AD)[1]. Complex or formed visual hallucinations (VH) are a core feature of DLB[2,3]; these are also reported in patients with Parkinson's disease (PD)[4]. VH in DLB are typically described as non-threatening images of people, animals, or objects that persist for seconds to minutes. The images may be vivid, colorful, and detailed; for example, the people and animals may be smaller than normal size "Lilliputian", and dressed in colorful costumes. Patients are usually aware of the images' hallucinatory nature. However, night-time hallucinations can be accompanied by confusion where patients tend to interact with their VH and wandering behavior and agitation are common[5-7]. The phenomenology of VH in DLB has been described in detail; however, its pathomechanism has not been researched extensively.

Several morphological changes in the specific brain regions associated with VH in DLB have been reported, including changes in the right inferior frontal gyrus[8], pedunculopontine nucleus[9], superior parietal gyrus and precuneus[10], and right anterior insula[11]. Many studies report that the morphological changes are gray matter (GM) atrophy, yet some argue that they are DLB with other neurodegenerative diseases such as PD[9] and AD[11]. At present, consensus on this issue has yet to be reached. This dispute might be due to difference in duration of the disease and different methods of evaluating focal brain atrophy and VH.

Peduncular hallucinosis (PH) is a syndrome of hallucinations and brainstem symptoms that was first reported in 1922 by the French neurologist Lhermitte. His case report described a 72-year-old female who experienced strange VH that occurred late in the day, particularly at dusk. Although the patient knew the images were not real, she would sometimes try to touch them. Her symptoms suggested a focal infarct involving the midbrain and pons (left ptosis, total external ophthalmoplegia, lateral pulsion when walking, right dysmetria, intention tremor, and a Babinski sign). The hallucinations in the reported case were associated with insomnia and daytime somnolence[12]. In PH, the images are vivid with colorful people, animals, or scenes. PH and VH in DLB have distinctive common features. Hayashi reported that a patient recovering from immune-mediated brainstem encephalitis was able to draw colorful, vivid pictures of his hallucinations[13].

The quality of the VH in DLB closely resembles that of PH: complex, vivid, detailed, and usually occur at dusk, as described above. The duration of hallucinations, however, is one of the differences. Whereas PH usually lasts several days to weeks[14], VH in DLB last longer. Janzen indicated similarities in the phenomenology of VH in PD and PH[9]. We hypothesized that VH in DLB might involve a dorsal brainstem lesion similar to PH, particularly focal atrophy, and therefore investigated their relationship using the Neuropsychiatric Inventory (NPI) and voxel-based specific regional analysis system for Alzheimer's disease (VSRAD) advance 2 software, which evaluates dorsal brainstem atrophy.

Methods

Patients

Twenty-four patients (12 men, 12 women) who were diagnosed with probable DLB through clinical examinations, including brain magnetic resonance imaging (MRI) and NPI, were recruited from the outpatient clinic of the Department of Neuropsychiatry in the Osaka City University Hospital between July 2013 and January 2018. Diagnoses were assisted by ^{123}iodine-metaiodobenzylguanidine

(MIBG) myocardial scintigraphy (4 cases), dopamine transporter (DAT) imaging (11 cases) or both (1 case). The mean age of the patients was 81.0±6.1 years. The clinical diagnosis of DLB was based on the third consensus report of the DLB consortium[2]. The patients who were suspected of AD's or cerebrovascular dementia's complications were excluded by clinical interviews and examinations including brain imaging mentioned above. Other causes of dementia and cognitive impairment, including thyroid dysfunction, venereal diseases (including neural syphilis), and vitamin B_{12} or folate deficiency, were excluded by laboratory investigations. This study was reviewed and approved by the Human Subject Review Committee at Osaka City University, and informed consent was obtained from each patient and a representative from his or her family after a detailed explanation of this study was given.

Functional and neuropsychological assessment

Each patient underwent a clinical assessment before the MRI procedure. To assess the presence of cognitive impairment, the Mini-Mental State Examination (MMSE)[15] and Revised Hasegawa Dementia Scale (HDS-R: from 0 to 30, with 0 being the most severe)[16] were used. The HDS-R has been used exclusively in East Asian countries as a screening test for dementia. The severity of the hallucinations was rated using the Japanese version of the NPI which assesses 10 sub-domains of behavioral functioning, namely, delusions, hallucinations, agitation/aggression, dysphoria, anxiety, euphoria, apathy, disinhibition, irritability/lability, and aberrant motor activity. Each sub-domain examines both frequency and severity and the score is obtained by multiplying these scores. The frequency rating is from 0 to 4, and the severity rating is from 0 to 3. The total NPI score is the sum of the domain scores (from 0 to 120)[17,18].

MRI procedure

All subjects underwent an MRI study using a 1.5T Vision Plus imager (Avanto, SIEMENS, German). Axial, coronal, and sagittal T1-weighted sequence images and axial T2-weighted sequence images were obtained for diagnosis. For VSRAD analysis, 3-D T1-weighted sequence imaging was used [field of view (FOV), 230 mm; time of repeat (TR), 1900 ms; time to echo (TE), 3.14 ms; flip angle, 25° ; and phase resolution, 256, 1.00-mm slice thickness].

Imaging analysis

All MRI data were analyzed with VSRAD advance 2® (Eisai, Japan) software based on voxel-based morphometry (VBM), an automated method for analysis of brain MRI images that statistically evaluates atrophy at the voxel level. This software program, which runs on Windows for VBM analysis with Statistical Parametrical Mapping (SPM) and the Diffeomorphic Anatomical Registration Through Exponentiated Lie algebra (DARTEL), was developed to differentiate DLB and AD. 3D-T1-weighted whole brain images were spatially normalized with a 12-parameter affine transformation to the SPM template so as to correct for differences in brain size. These linearly transformed images were nonlinearly transformed and then modulated to the customized template for DARTEL, followed by smoothing using an 8-mm full width at half maximum (FWHM) kernel. The GM and white matter (WM) image of a patient was compared with the mean and standard deviation (SD) of GM images of healthy volunteers using voxel-by-voxel analysis. Finally, the z score was acquired {z score=[(control mean)-(individual value)]/control SD}. These z score maps were displayed by overlay on tomographic sections and surface renderings of the standardized brain. The target volume of interest (VOI) included the entire region of the entorhinal cortex, hippocampus, amygdala, and dorsal brainstem (Fig. 1). The validity of the VSRAD software has already been

reported elsewhere[19]. In the present study, we used the averaged positive z score in the GM and WM of the dorsal brainstem. The higher the z score, the more severe the atrophy in the target VOI. Using VSRAD advance 2, the dorsal brainstem GM and WM z scores are automatically calculated. The patients were divided into two groups in three different ways: GM atrophy, WM atrophy, and relative atrophic degree of either GM or WM (subtracted value of GM from WM). We adopted the mean z score of GM and WM, which were 0.491 and 0.611 respectively, as the criteria for the first and second grouping, and the subtraction value of zero (z score of GM and WM are equal) as the criterion for the third.

Statistical analysis

Statistical analysis was performed with SPSS for Windows 23.0 (SPSS Japan, Tokyo, Japan). We

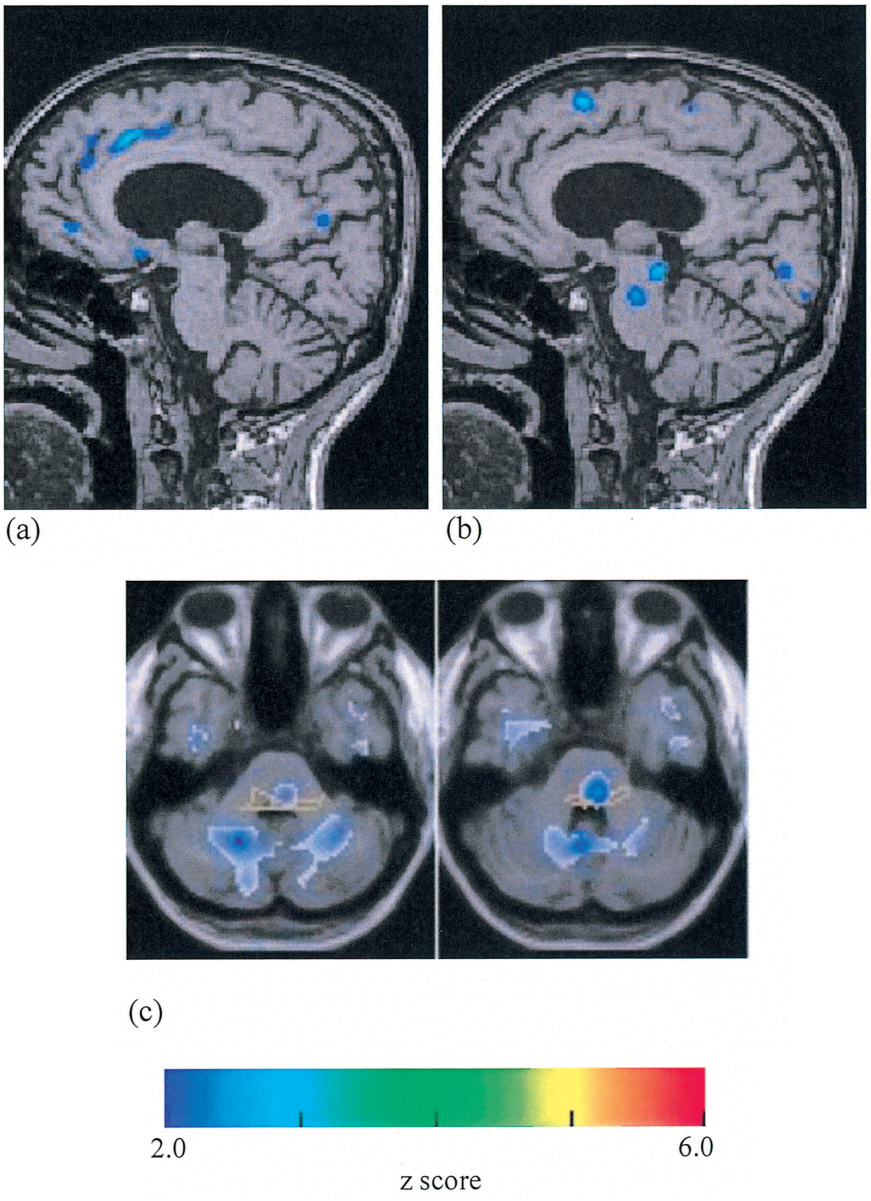

Figure 1. GM atrophy map (a) and WM atrophy map (b) of an octogenarian man with DLB. Colored areas indicating higher z score are overlaid on tomographic sections of the patient's MRI. The target VOI in the dorsal brainstem is demarcated with the yellow line in axial planes of standardized MRI template (c). GM, gray matter; WM, white matter; DLB, dementia with Lewy bodies; MRI, magnetic resonance imaging; and VOI, volume of interest.

compared the clinical characteristics and VSRAD parameters between the two groups with the Mann-Whitney' s U-test or Student' s t-test according to the normality in distribution. Categorical variables such as sex were analyzed using the chi-square test. The normality in distribution was examined using the Shapiro-Wilk test. The following statistical examinations were also used: Mann-Whitney' s U-test for duration of disease and the NPI scores, chi-square test for sex distribution, and Student' s t-test for all other analyses. In addition, we assessed the correlation between z score and NPI score

Table 1. Demographic and clinical characteristics of the GMA and GMNA, WMA and WMNA groups, or GM≧WM and WM≧GM atrophy groups

1a. Categorized on the basis of the degree of GM atrophy

	Total (n=24)	GMA group (n=10)	GMNA group (n=14)	p value
Male/Female	12/12	4/6	8/6	0.527/0.593#
Age (years, mean±SD)	81.01±6.09	80.15±6.06	81.62±6.50	0.580
Onset age (years)	77.76±5.63	77.83±6.39	77.71±5.50	0.963
Duration of DLB (years)	3.25±3.07	2.33±2.18	3.91±3.61	0.230
Education (years)	10.90±2.78	9.75±2.66	11.82±2.79	0.122
HDS-R total score	17.88±6.14	18.80±6.70	17.21±6.12	0.553
MMSE total score	19.67±4.89	19.90±4.93	19.50±5.21	0.852

1b. Categorized on the basis of the degree of WM atrophy

	Total (n=24)	WMA group (n=9)	WMNA group (n=15)	p value
Male/Female	12/12	5/4	7/8	0.739/0.796#
Age (years, mean±SD)	81.01±6.09	83.92±5.44	79.27±6.17	0.076
Onset age (years)	77.76±5.63	80.86±4.25	75.90±5.84	0.037 *
Duration of DLB (years)	3.25±3.07	3.06±2.52	3.37±3.54	0.818
Education (years)	10.90±2.78	10.71±2.63	11.08±3.09	0.795
HDS-R total score	17.88±6.14	18.89±6.77	17.27±6.11	0.551
MMSE total score	19.67±4.89	20.44±5.13	19.20±5.03	0.566

1c. Categorized on the basis of the value of subtraction (WM-GM)

	Total (n=24)	GM≧WM group (n=11)	WM≧GM group (n=13)	p value
Male/Female	12/12	4/7	8/5	0.366/0.405#
Age (years, mean±SD)	81.01±6.09	78.34±6.63	83.27±5.06	0.051
Onset age (years)	77.76±5.63	75.85±6.33	79.37±4.89	0.138
Duration of DLB (years)	3.25±3.07	2.49±2.16	3.90±3.74	0.262
Education (years)	10.90±2.78	10.13±2.75	11.55±2.91	0.298
HDS-R total score	17.88±6.14	18.18±6.21	17.62±6.56	0.831
MMSE total score	19.67±4.89	19.82±4.62	19.54±5.47	0.895

#p value of GMA/GMNA, WMA/WMNA or GM≧WM/WM≧GM group; *$p<0.05$.

GMA group, patients with gray matter atrophy; GMNA group, patients without gray matter atrophy; WMA group, patients with white matter atrophy; WMNA group, patients without white matter atrophy; GM≧WM group, patients with relatively severe gray matter atrophy; WM≧GM group, patients with relatively severe white matter atrophy; GM, gray matter; WM, white matter; DLB, dementia with Lewy bodies; HDS-R, the Revised Hasegawa Dementia Scale; and MMSE, Mini-Mental State Examination.

using the Spearman rank correlation coefficient. All statistical tests were two-tailed, with significance at $p<0.05$.

Results

Table 1 shows the demographic features of the patients with DLB categorized on the basis of the degree of dorsal brainstem atrophy of GM (Table 1a), of WM (Table 1b), or of GM subtracted from WM (Table 1c). There were no significant differences in the age, onset age, duration of dementia, HDS-R total score, or MMSE total score between the groups, except for onset age of the WMA (WM atrophy) and WMNA (without WM atrophy) groups.

The NPI subscales showed no significant differences (data not shown) except for hallucinations score. When the patients were divided using degree of WM atrophy, the NPI total and hallucinations scores of the WMNA group were significantly higher than those of the WMA group (Table 2b), whereas there was no significant difference among the groups divided on the basis of the degree of GM atrophy (Table 2a). In the groups divided using the subtraction (WM-GM) value, the hallucinations score of the GM≧WM (GM atrophy was relatively severe and WM was relatively spared) group was higher (Table 2c). In the hallucinations subscale of NPI, acoustic, optic, and

Table 2. Differences in NPI score between the GMA and GMNA, WMA and WMNA groups, or GM≧WM and WM≧GM atrophy groups

2a. Categorized on the basis of the degree of GM atrophy

	GMA group (n=10)	GMNA group (n=14)	p value
Delusion (mean±SD)	2.70±3.69	3.86±3.18	0.291
Hallucination	5.00±3.58	3.14±3.66	0.197
Total score	16.60±14.56	17.29±11.46	0.639

2b. Categorized on the basis of the degree of WM atrophy

	WMA group (n=9)	WMNA group (n=15)	p value
Delusion (mean±SD)	2.11±2.42	4.00±3.81	0.341
Hallucination	1.11±1.59	5.60±3.65	0.004**
Total score	8.78±6.14	21.93±13.29	0.007**

2c. Categorized on the basis of the value of subtraction (WM-GM)

	GM≧WM group (n=11)	WM≧GM group (n=13)	p value
Delusion (mean±SD)	3.45±3.70	3.31±3.22	1.000
Hallucination	6.36±3.57	1.85±2.38	0.004**
Total score	19.73±15.29	14.69±9.77	0.582

NPI, Neuropsychiatric Inventory; GMA group, patients with gray matter atrophy; GMNA group, patients without gray matter atrophy; WMA group, patients with white matter atrophy; WMNA group, patients without white matter atrophy; GM≧WM group, patients with relatively severe gray matter atrophy; WM≧GM group, patients with relatively severe white matter atrophy; GM, gray matter; and WM, white matter. **$p<0.01$.

Table 3. Correlation of dorsal brainstem atrophy and NPI score

	GM z score		WM z score		(WM-GM) value	
	coefficient (ρ)	p value	coefficient (ρ)	p value	coefficient (ρ)	p value
Delusion	−0.145	0.498	−0.124	0.562	−0.039	0.856
Hallucination	0.350	0.094	−0.521	0.009**	−0.603	0.002**
Total score	−0.102	0.636	−0.394	0.057	−0.312	0.138

NPI, Neuropsychiatric Inventory; GM, gray matter; and WM, white matter. **p<0.01.

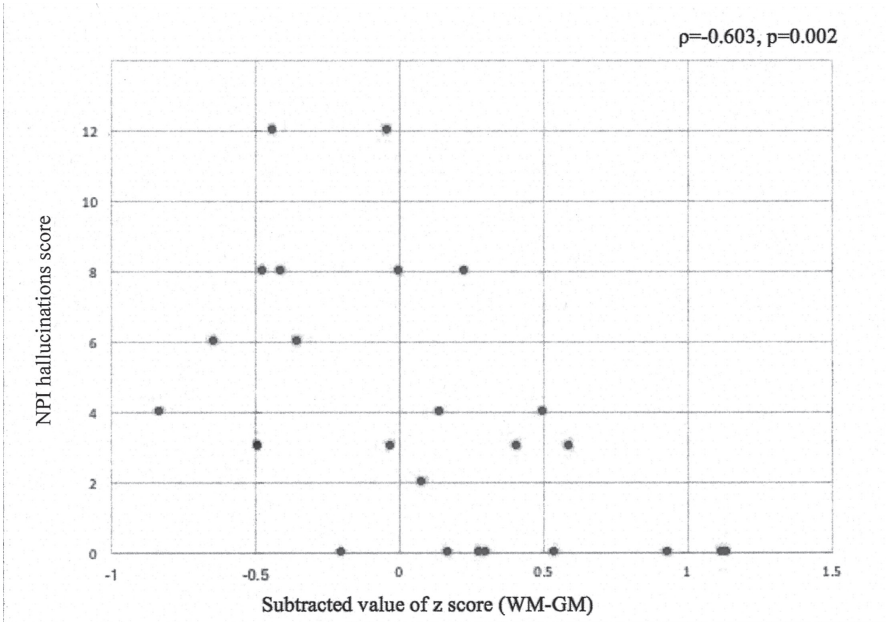

Figure 2. Correlation of the NPI hallucinations score and subtracted value of z score (WM z score-GM z score). Smaller value indicates GM atrophy is relatively severe, and vice versa. NPI, Neuropsychiatric Inventory; WM, white matter; and GM, gray matter.

olfactory hallucinations were rated together. Thus, we retrospectively checked the medical records and confirmed that the main hallucinatory symptom of these patients was VH.

Correlation between the degree of atrophy in the dorsal brainstem and NPI score was examined. Significant inverse correlations were observed in the WM atrophy and NPI hallucination scores ($\rho = -0.521$, $p = 0.009$) and also in the WM-GM value and NPI hallucination score ($\rho = -0.603$, $p = 0.002$) (Table 3 and Fig. 2).

Discussion

We examined VH and dorsal brainstem atrophy in patients with DLB using VSRAD advance 2 software which automatically assesses the degree of atrophy. The results of the present study suggest that the correlation between brainstem GM atrophy and hallucinations is not obvious while WM atrophy inversely correlates. Because the GM of the dorsal brainstem, especially that of the midbrain, showed significant atrophy in the patients with DLB[20], we speculate that impaired nuclei with comparatively spared axons might cause disturbances in perception. In other words, degenerating nerve cell bodies with a spared neural network provokes hallucinations. This idea

seems to be consistent with previous studies arguing that the lesions related to PH are heterogeneously distributed, whereas the lesions show specific network anti-correlation with the extrastriae visual cortex[21].

Our findings suggest that focal atrophy of brainstem GM with relatively spared corresponding WM in patients with DLB might cause symptoms similar to PH. In the literature, the culprit lesion of PH includes infarction[22-26], hemorrhage[27], hematoma[24], inflammation[13], and tumor[28-30]. There are also a few reports of PH as a side effect of cardiac or cerebral angiography[26,31]. We speculate that dorsal brainstem GM atrophy with relatively retained WM might have a similar pathophysiology to that of brainstem infarction, hemorrhage, hematoma, inflammation, and tumor.

In terms of the pathomechanism of PH, Lhermitte proposed the hypothesis that a hallucination reflects a consequence of derangement in the sleep-wake cycle[12,14]. His contemporary neurologist, van Bogaert, on the other hand, proposed that hallucinations were a state of ego dissolution with loss of ability to distinguish external reality from imagination[14,23,32]. In recent years, there are few literatures present pathophysiological models to explain PH. These models suppose that a loss of brainstem control of the cortex is the primary factor of PH[33]. Middleton and Strick's model emphasizes function of substantia nigra pars reticularis (SNpr) which has inhibitory effect to infero-temporal cortex through thalamus. It has been previously shown that artificial stimulation at infero-temporal cortex induces VH in humans[34]. A lesion at SNpr removes suppression of the thalamus and as a consequence leads to abnormal excitation of infero-temporal cortex accompanied by VH[35]. Manford and Andermann' s model focuses on dorsolateral geniculate nucleus (dLGN) which is under brainstem control and act as a center for brainstem modulation of inputs from the retina to the visual cortex. It is shown that dLGN receives many inputs from various neurons including pedunculopontine tegmental nucleus (PPTN) which is the main component of the reticular activating system[36]. Given that a loss of brainstem control of the cortex is the cause of PH, one of possible interpretations of our results might be as follows: impaired nuclei (GM) cause unfiltered or disordered signals and spared axons (WM) transmit to neural network. Consequently, the signal leads confusion and over-activity in the cortex, in other words, a loss of control of the cortex. And if axons are atrophic and their functions are lost, the disturbance to the neural network is relived.

However, the issue of the etiology of PH is still controversial today. Further detailed investigations are needed to examine brainstem lesions of patients with PH. Morphological studies of brain used to focus on GM and tend to neglect WM. Our study indicates WM have profound influence on the brain functioning. The authors hope that future study regarding not only GM but also WM might deepen our understanding of underlying mechanism of hallucinations.

VSRAD advance 2 may be useful for objective assessment of atrophy at the dorsal brain stem in patients with dementia and hallucinations. The software was originally designed to evaluate medial temporal lobe atrophy in order to diagnose AD. Later, the VOI was extended so that the dorsal "brainstem", namely, the midbrain and pons, was included, because it was revealed that the medial temporal lobe was relatively retained and the dorsal midbrain and pons were more atrophic in patients with DLB[20,37,38]. Although the value of [(z score of dorsal brainstem atrophy)/(z score of medial temporal atrophy)] is the index for AD-DLB differentiation, we adopted the raw z score of dorsal brainstem atrophy as the index because we were not focused on the relationship with medial temporal atrophy but on the extent of focal atrophy itself.

There are some limitations in the present study. First, the number of participants was relatively

small (24 patients) and we should consider this as a pilot study. For further investigation and longitudinal study, more patients should be recruited. Second, diagnoses of DLB was not pathologically confirmed but relied on clinical diagnoses alone; therefore, the possibility of overestimation cannot be excluded. Third, the influence of medication was not taken into consideration. We used the data and information at the first visit of each participant, and most patients did not take anti-dementia medication. The influence of other medication, however, is undeniable. Fourth, although visual disturbances are reported as one of the hypothesized causes of VH in PD and DLB[39,40], our patients did not undergo ophthalmological testing. On the other hand, despite the occurrence of visual abnormalities, ocular pathology does not seem to distinguish the patients who hallucinate from those who did not[41]. However, ophthalmological examination results should be taken into consideration in future studies. Fifth, although VSRAD enable us to assess atrophy objectively, the target VOI is fixed and it is not possible to tell which region is atrophic within the VOI. In further investigations, morphological change should be examined with other method which is able to intentionally set VOI. The regions to examine preferably include the occipital lobe that is thought to be related VH, brainstem or neighboring nuclei such as SNpr, PPTN and dLGN, and projecting fibers between these structures.

Finally, our result leads to the further presumption that hallucinatory symptoms may alleviate as WM atrophy progresses with the natural process of neural degeneration. These results are consistent with Braak' s hypothesis indicating that physical contact between susceptible regions may play a key role and that α-synuclein inclusions developed from the olfactory bulbs to the neocortex via the medulla oblongata and midbrain[42]. In terms of our participants' background, the WM atrophy group tended to be older, although this difference was not significant (Table 1b and 1c), and onset age of the WM atrophy group was statistically higher (Table 1b). Therefore, VH in DLB seems to be relieved by the passage of time. It is also consistent with the common clinical course of VH in DLB. Hallucinations usually do not exacerbate, but gradually alleviate over time. Although we tend to assume that the remission of VH is the effect of medical treatment, including drug therapy, it might partially be the natural course of DLB.

Acknowledgments

All authors have no COI to declare regarding the present study.

The authors would like to thank R. Tagawa for valuable discussions. We also thank H. Ohtomo for his help in reading French articles. Finally, we are grateful to the referees for useful comments.

References

1. Galasko D, Hansen LA, Katzman R, et al. Clinical-neuropathological correlations in Alzheimer's disease and related dementias. Arch Neurol 1994;51:888-895.
2. McKeith IG, Dickson DW, Lowe J, et al. Diagnosis and management of dementia with Lewy bodies: third report of the DLB Consortium. Neurology 2005;65:1863-1872.
3. McKeith IG, Boeve BF, Dickson DW, et al. Diagnosis and management of dementia with Lewy bodies: fourth consensus report of the DLB Consortium. Neurology 2017;89:88-100.
4. Fénelon G, Mahieux F, Huon R, et al. Hallucinations in Parkinson's disease: prevalence, phenomenology and risk factors. Brain 2000;123:733-745.
5. Iseki E, Marui W, Nihashi N, et al. Psychiatric symptoms typical of patients with dementia with Lewy bodies - similarity to those of levodopa-induced psychosis. Acta Neuropsychiatr 2002;14:237-241.
6. Nagahama Y, Okina T, Suzuki N, et al. Classification of psychotic symptoms in dementia with Lewy bodies. Am J Geriatr Psychiatry 2007;15:961-967.

7. Onofrj M, Taylor JP, Monaco D, et al. Visual hallucinations in PD and Lewy body dementias: old and new hypotheses. Behav Neurol 2013;27:479-493.
8. Sanchez-Castaneda C, Rene R, Ramirez-Ruiz B, et al. Frontal and associative visual areas related to visual hallucinations in dementia with Lewy bodies and Parkinson' s disease with dementia. Mov Disord 2010; 25:615-622.
9. Janzen J, van 't Ent D, Lemstra AW, et al. The pedunculopontine nucleus is related to visual hallucinations in Parkinson's disease: preliminary results of a voxel-based morphometry study. J Neurol 2012;259:147-154.
10. Delli Pizzi S, Franciotti R, Tartaro A, et al. Structural alteration of the dorsal visual network in DLB patients with visual hallucinations: a cortical thickness MRI study. PLoS One 2014;9:e86624.
11. Blanc F, Noblet V, Philippi N, et al. Right anterior insula: core region of hallucinations in cognitive neurodegenerative diseases. PLoS One 2014;9:e114774.
12. Lhermitte J. Syndrome de la calotte du pédoncule cérébral. Les troubles psycho-sensoriels dans les lésions du mésocéphale. Rev Neurol 1922;38:1359-1365.
13. Hayashi Y, Yoshikura N, Kimura A, et al. Peduncular hallucinations in brainstem encephalitis drawn by a patient. Neurology 2012;79;1625.
14. Risser AH, Powell FC. Lhermitte's peduncular hallucinosis. In: 45th Annual Meeting of the American Academy of Neurology, New York; 1993.
15. Folstein MF, Folstein SE, McHugh PR. ''Mini-mental state''. A practical method for grading the cognitive state of patients for the clinician. J Psychiatr Res 1975;12:189-198.
16. Kim KW, Lee DY, Jhoo JH, et al. Diagnostic accuracy of mini-mental status examination and revised Hasegawa dementia scale for Alzheimer's disease. Dement Geriatr Cogn Disord 2005;19:324-330.
17. Cummings JL, Mega M, Gray K, et al. The Neuropsychiatric Inventory: comprehensive assessment of psychopathology in dementia. Neurology 1994;44:2308-2314.
18. Hirono N, Mori E, Ikejiri Y, et al. Japanese version of the Neuropsychiatric Inventory-a scoring system for neuropsychiatric disturbance in dementia patients. No To Shinkei 1997;49:266-271. (In Japanese)
19. Matsuda H, Mizumura S, Nemoto K, et al. Automatic voxel-based morphometry of structural MRI by SPM8 plus diffeomorphic anatomic registration through exponentiated Lie algebra improves the diagnosis of probable Alzheimer disease. AJNR Am J Neuroradiol 2012;33:1109-1114.
20. Whitwell JL, Weigand SD, Shiung MM, et al. Focal atrophy in dementia with Lewy bodies on MRI: a distinct pattern from Alzheimer' s disease. Brain 2007;130:708-719.
21. Boes AD, Prasad S, Liu H, et al. Network localization of neurological symptoms from focal brain lesions. Brain 2015;138:3061-3075.
22. McKee AC, Levine DN, Kowall NW, et al. Peduncular hallucinosis associated with isolated infarction of the substantia nigra pars reticulata. Ann Neurol 1990;27:500-504.
23. Kölmel HW. Peduncular hallucinations. J Neurol 1991;238:457-459.
24. Benke T. Peduncular hallucinosis: a syndrome of impaired reality monitoring. J Neurol 2006;253:1561-1571.
25. Penney L, Galarneau D. Peduncular hallucinosis: a case report. Ochsner J 2014;14:450-452.
26. Notas K, Tegos T, Orologas A. A case of peduncular hallucinosis due to a pontine infarction: a rare complication of coronary angiography. Hippokratia 2015;19:268-269.
27. Harada Y, Ishimitsu H, Miyata I, et al. Peduncular hallucinosis associated with ruptured basilar-superior cerebellar artery aneurysm: case report. Neurol Med Chir (Tokyo) 1991;31:526-528.
28. Dunn DW, Weisberg LA, Nadell J. Peduncular hallucinations caused by brainstem compression. Neurology 1983; 33:1360-1361.
29. Nadvi SS, Ramdial PK. Transient peduncular hallucinations secondary to brain stem compression by a cerebellar pilocytic astrocytoma. Br J Neurosurg 1998;12:579-581.
30. Biswas SN, Biswas S, Chakraborty PP. Peduncular hallucinosis as first presentation of juvenile pilocytic astrocytoma. Indian J Pediatr 2016;83:736-737.
31. Rozanski J. Peduncular hallucinosis following vertebral angiography. Neurology 1952;2:341-349.
32. van Bogaert L. L' hallucinose pédonculaire. Rev Neurol 1927;47:608-617.
33. Müri RM. Thalamic and brainstem regulatory systems - why disturbances external to the visual system can cause hallucinations. In: Collerton D, Mosimann UP, Perry E, editors. The neuroscience of visual hallucinations. West Sussex: John Wiley & Sons; 2015. pp. 255-279.
34. Penfield W, Perot T. The brain's record of auditory and visual experience. a final summary and discussion. Brain 1963;86:595-696.
35. Middleton FA, Strick PL. The temporal lobe is a target of output from the basal ganglia. Proc Natl Acad Sci U S A. 1996;93:8683-8687.
36. Manford M, Andermann F. Complex visual hallucinations. Clinical and neurobiological insights. Brain 1998;

121:1819-1840.
37. Kantarci K, Ferman TJ, Boeve BF, et al. Focal atrophy on MRI and neuropathologic classification of dementia with Lewy bodies. Neurology 2012;79:553-560.
38. Nakatsuka T, Imabayashi E, Matsuda H, et al. Discrimination of dementia with Lewy bodies from Alzheimer's disease using voxel-based morphometry of white matter by statistical parametric mapping 8 plus diffeomorphic anatomic registration through exponentiated Lie algebra. Neuroradiology 2013;55:559-566.
39. Maurage CA, Ruchoux MM, de Vos R, et al. Retinal involvement in dementia with Lewy bodies: a clue to hallucinations. Ann Neurol 2003;54:542-547.
40. Matsui H, Udaka F, Tamura A, et al. The relation between visual hallucinations and visual evoked potential in Parkinson' s disease. Clin Neuropharmacol 2005;28:79-82.
41. Gallagher DA, Parkkinen L, O'Sullivan SS, et al. Testing an aetiological model of visual hallucinations in Parkinson's disease. Brain 2011;134:3299-3309.
42. Braak H, Del Tredici K. Nervous system pathology in sporadic Parkinson disease. Neurology 2008;70:1916-1925.

Osaka City Med. J. Vol. 65, 31-40, 2019

Age-specific Differences in Insulin dose of Japanese Patients with Type 1 Diabetes of Various Ages

Yuko Hotta[1)], Tomoyuki Kawamura[1)], Naoko Nishikawa[1)], Kayako Hashimura[1,2)], Yoneo Kashihara[1,3)], Tomomi Hashimoto[1,4)], Masakazu Hirose[1,5)], Takashi Higashide[1,4)], Haruo Shintaku[1)], and Takashi Hamazaki[1)]

Department of Pediatrics[1)], Osaka City University Graduate School of Medicine; Hashimura Clinic[2)]; Watamachi Kids Clinic[3)]; Hug Hug Kids Clinic[4)]; and D Medical Clinic Osaka[5)]

Abstract

Background

Few studies have investigated changes in insulin dose of Japanese patients with type 1 diabetes with regard to patients' age. Therefore, this study aimed to investigate it of the patients who were using insulin pump to help adjust each patient' s insulin setting.

Methods

This study included 35 Japanese patients with type 1 diabetes aged <45 years who used Minimed 620G®, a type of insulin pump. Data on pump settings were retrospectively evaluated using the Carelink® system, which analyze data of insulin pump and continuous glucose monitor. We evaluated total daily insulin dose per body weight, total daily basal insulin dose per total daily dose, the patterns of basal insulin rate at each hour, carbohydrate ratio, and correction factor. We also compared carbohydrate ratio or correction factor of our data with the number calculated by the 300 rule (carbohydrate ratio=300/total daily insulin dose) or 1800 rule (correction factor=1800/total daily insulin dose).

Results

Age-specific tendency of insulin settings were turned out. One of the most remarkable results was that some preschool children needed a lower carbohydrate ratio than that calculated by the 300 rule and a higher correction factor than that calculated by the 1800 rule.

Conclusions

Our data might help determine the initial insulin settings and adjust it for Japanese patients with type 1 diabetes. Whereas, the rules which had been already reported cannot be applied to some patients especially preschool children, and it is important that the insulin settings were individually adjusted watching the blood glucose level.

Key Words: Type 1 diabetes; Insulin pump; Carbohydrate ratio; Correction factor

Received September 3, 2018; accepted November 27, 2018.

Correspondence to: Tomoyuki Kawamura, MD.
Department of Pediatrics, Osaka City University Graduate School of Medicine,
1-4-3 Asahimachi, Abeno-ku, Osaka, 545-8585, Japan
Tel: +81-6-6645-3816; Fax: +81-6-6636-8737
E-mail: kawam@med.osaka-cu.ac.jp

Introduction

Insulin pump is an insulin infusion device mainly used by type 1 diabetes patients. In the insulin pump therapy, insulin pumps deliver rapid- or short-acting insulin 24 hours a day through a catheter placed under the skin. The insulin doses are categorized as basal and bolus insulin.

Basal insulin is continuously delivered over 24 hours and maintains blood glucose levels in the normal range between meals and overnight. Different amounts of insulin can be programmed at different times (basal rate) of the day and night.

When patients eat, they use the insulin pump to administer additional insulin doses, called bolus, to cover the carbohydrate content in each meal or snack; this is known as carb bolus. Patients also take a bolus to treat high blood glucose levels, which is known as correction bolus. If patients have high blood glucose levels before eating, correction or supplemental bolus of insulin is required to reduce the levels to their target range[1,2].

Carbohydrate counting calculates the number of bolus insulin units required with respect to food intake. Carbohydrate ratio (CR) calculates how many grams of carbohydrate one unit of insulin will cover for in a meal. Correction factor (CF) calculates how much decrease in blood sugar level (mg/dL) will one unit of insulin lead to at hyperglycemia. The effects of carbohydrate counting for adjusting insulin doses have been reported[3,4]. In Japan, carbohydrate counting has recently become popular. Some rules, such as the 500 rule and 1800 rule, have been reported to calculate CR and CF of patients. In the 500 rule, CR is calculated by dividing 500 by the total daily dose (TDD) of insulin. Some researchers reported that the 300 or 400 rule was better than the 500 rule[5,6]. Furthermore, in the 1800 rule, CF is calculated by dividing 1800 by TDD, and some researchers have recommended the 1700 rule for CF[7].

Insulin doses of type 1 diabetes patients change as their age. To understand the trend of insulin dose of type 1 diabetes patients with respect to age is useful for adjusting each patient's insulin settings. Although some studies have reported on the number of insulin units required by patients[3,5,6,8], but few studies have investigated the insulin dose for type 1 diabetes Japanese children and adolescents. Kuroda et al and Nakamura et al respectively reported that basal insulin requirement was around 30% of TDD in Japanese patients and it was lower rate than Western past reports[8,9], but the subjects were adult. There was a possibility that not only age-specific differences but also racial differences in insulin settings. It was necessary to investigate Japanese children and adolescents.

This study aimed to investigate age-specific differences in basal rate, CR, and CF of Japanese patients with type 1 diabetes and assess whether it was consistent with the above rules to help determine and adjust insulin settings for each patient.

Methods

The subjects of this study were type 1 diabetes patients who were using Minimed 620G®, a insulin pump with continuous glucose monitor (CGM). The CGM is a revolutionary technology developed in the last two decades that continuously measures glucose levels in subcutaneous tissues via an inserted sensor. Patients with diabetes and medical staffs need to be able to adjust insulin and/or drug regimens. The sensor augmented pump (SAP) is an insulin pump that displays CGM data. Minimed 620G® is the first SAP which could be used in Japan since 2015. Using SAP, patients can adjust their insulin dose according to CGM data, and doctors can analyze CGM data using the

Carelink® system, the system analyzing data of insulin pump and continuous glucose monitor, and more accurately adjust insulin doses than before[10]. On the other hand, it is possible to use Minimed 620G® without CGM, and some patients in this study sometimes used the pump without CGM.

Type 1 diabetes was diagnosed according to the criteria for acute onset type 1 diabetes proposed by the Japanese Diabetes Society[11]. Minimed 620G® were introduced to the type 1 diabetes patients at the Department of Pediatrics of Osaka City University Hospital who were judged that Minimed 620G® were indicated by the doctor and who themselves wanted them. There were 87 Japanese patients with type 1 diabetes aged <45 years who had visited the hospital and had used Minimed 620G® for >2 months in March of 2017. We excluded the patients as follows from the 87 patients; (1) 2 patients with advanced diabetic chronic complications, (2) 3 pregnant women, (3) 1 patient with myositis taking steroid therapy, (4) 1 patient with short stature taking growth hormone therapy, (5) 8 patients whose blood C-peptide levels were >0.6 ng/mL, (6) 4 patients who were not using bolus calculator, the system of insulin pump which calculates unit of bolus by inputting the blood glucose level and the amount of carbohydrate they were going to eat if CR and CF were registered in advance.

The data of the remaining 68 patients during January and March 2017 were examined, but the data of 33 patients were missing for some reason, such as self-discontinuation of visiting the hospital, computer trouble, and so on.

Finally, 35 subjects were enrolled (male/female: 8/27, aged 4.4-41.8 years). Blood C-peptide levels were undetectable in 24 patients and were 0.02-0.31 ng/mL in the other 11 patients. All patients used rapid-acting insulin. Two patients in the preadolescent group used long-acting insulin via the pen delivery system (one used glargine U300 and the other used degludec) to administer basal insulin so as to avoid wearing the insulin pump during sports activity.

The patients were classified into the following four groups by age: preschool (<6 years, n=8),

Table 1. Characteristics of the subjects

	Preschool	Preadolescent	Adolescent	Adults
	n=8	n=14	n=8	n=5
Sex (male/female)	4/4	3/11	1/7	0/5
Age (years)	6.2	10.8	14.8	34.9
	(4.4-6.7)	(7.2-12.6)	(13.4-20.8)	(33.4-41.8)
HbA1c (%)	8.6	8.0	8.0	7.3
	(7.1-9.2)	(6.7-8.9)	(6.0-9.1)	(6.9-7.8)
T1DM duration (years)	2.9	5.0	10.5	26.1
	(1.5-4.7)	(2.0-8.5)	(1.8-15.7)	(16.8-29.3)
Number of patients whose	4 (50.0%)	4 (28.6%)	2 (25.0%)	1 (20.0%)
CPR were detected	(0.05, 0.07, 0.1, 0.25)	(0.02, 0.13, 0.25, 0.28)	(0.02, 0.31)	(0.18)
BMI-SDS	0.8	0.2	0.7	
	(−1.1-1.6)	(−1.0-0.9)	(−0.1-2.3)	
BMI (kg/m^2)				26.2
				(21.5-29.1)

The data were shown as a median (range). The C-peptide (CPR) was occasional serum C-peptide (ng/mL). TIDM, type 1 diabetes; CPR, C-peptide; BMI, body mass index; and BMI-SDS, BMI standard deviation score.

preadolescent (7-12 years, n=14), adolescent (13-20 years, n=8), and adults (33-41 years, n=5). No patients aged 21-32 years used the Minimed 620G®.

Patients themselves adjusted their insulin settings daily according to continuous glucose monitor (CGM) and self-monitoring of blood glucose (SMBG) data. They visited the hospital once each month, where their CGM data and pump records were checked by doctors using the Carelink® system, and their insulin settings were adjusted. Basal insulin dose was adjusted so that the patient's blood glucose level was not changed when food was not consumed. CR was adjusted so that blood glucose levels 4 hours after consuming a meal returned to pre-meal blood glucose levels when hyperglycemia was not observed before meals. CF was adjusted to reduce high blood glucose levels to target blood glucose levels 4 hours after the bolus injection when no food was consumed. In this study, insulin doses were retrospectively evaluated using the Carelink® system from January to March 2017. The study was approved by Ethics Committee of Osaka City University (authorization number: 3743).

We evaluated the median total daily doses (TDD/kg), the median percentage of total daily basal insulin dose to total daily dose (TBD/TDD), the basal insulin rate at each hour, CR, and CF. We also evaluated those were different by age. We calculated CR×TDD to evaluate whether 500 rule (CR =500/TDD) or 300 rule (CR=300/TDD) that had been recommended were applicable. Similarly, we calculated CF×TDD to evaluated whether 1800 rule (CF=1800/TDD) or 1700 rule (CF=1700/TDD).

The results were analyzed by single regression analysis, distributed analysis by iterative measurement, and the Kruskal-Wallis test using IBM SPSS Statistics, version 24. The Kruskal-Wallis test was used to compare among groups, and the distributed analysis by iterative measurement was used when considering difference in time. P values <0.05 were considered significant.

Results

Thirty-five subjects were enrolled in this study. The proportion of female was higher in preschool, adolescent, and adult. Median HbA1c of preschool group was higher than other groups. We thought that this meant the difficulty of blood glucose control in patients of that age, and it was also characteristic of this age. Some reports have reported that HbA1c in this population is higher than other ages[12,13]. Therefore, we thought that this group of subjects in our study were not a special group (Table 1).

The median total daily doses (TDDs) per body weight were 0.79 (0.56-0.91), 1.00 (0.58-1.71), 0.93 (0.72-1.21), and 0.65 (0.60-1.16) unit/kg in the preschool, preadolescent, adolescent, and adult groups, respectively, described as median (range). The median TDDs seemed to increase with age until preadolescence or adolescence age, after which they appeared to decrease, although not significantly (Fig. 1).

The median percentage of total daily basal insulin dose (TBD) to TDD (TBD/TDD) was 32.8% (18.2%-55.3%) (Fig. 2). Two patients in the preadolescent group who used long-acting insulin were excluded from this analysis. It was evaluated by single regression analysis and no age-specific differences were observed (p=0.948). There was no significant relationship between TBD/TDD and sex (p=0.48) or TDD (p=0.682). Patients of preschool, preadolescent, and adolescent groups were evaluated using the body mass index standard deviation score (BMI-SDS), whereas those of adult group were evaluated based on BMI, and TBD/TDD was not associated with BMI or BMI-SDS.

The patterns of basal insulin rate at each hour appeared to be different among the groups. We evaluated the basal ratio of every hour (%) to total basal dose (Fig. 3). Children and adolescents

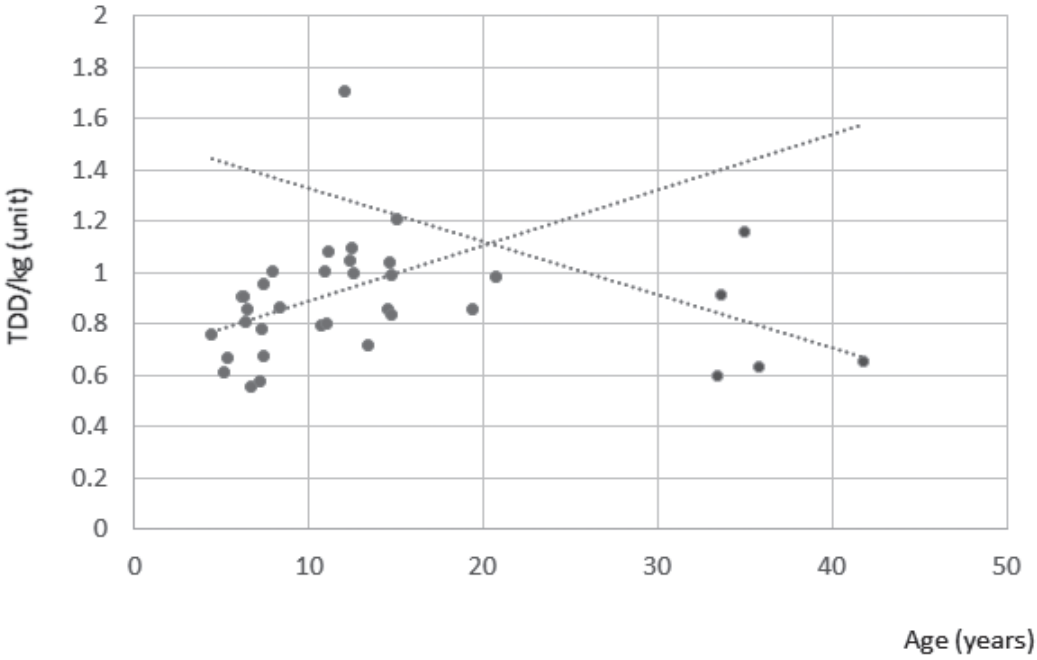

Figure 1. Relationship between age and TDD/kg. The broken line shows an approximate line. TDD, total daily dose.

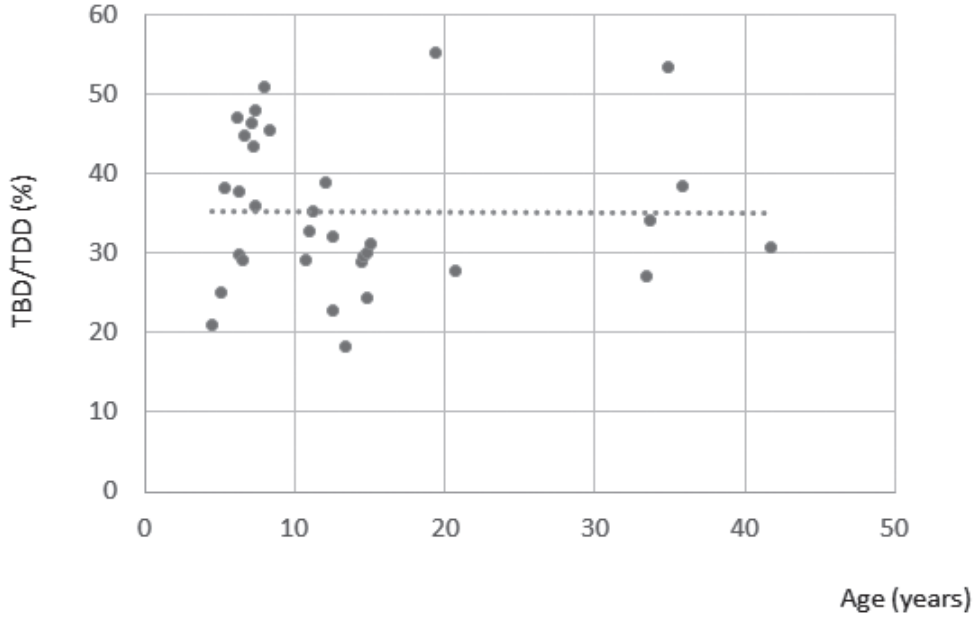

Figure 2. Relationship between age and TBD/TDD. The broken line shows an approximate line. TBD, total daily basal insulin dose; and TDD, total daily dose.

seemed to require higher basal insulin rates during 03:00-08:00, but not significantly in this study. In preschool and preadolescent children, the basal rate seemed to be higher in the morning and evening and lower in the daytime. These patterns were not related to whether C-peptide levels of the patients was positive or negative.

The median CRs were 16.7 (11.1-25.0), 14.3 (5.0-50.0), 7.0 (5.9-8.3), and 7.7 (3.6-10.0) g/unit in

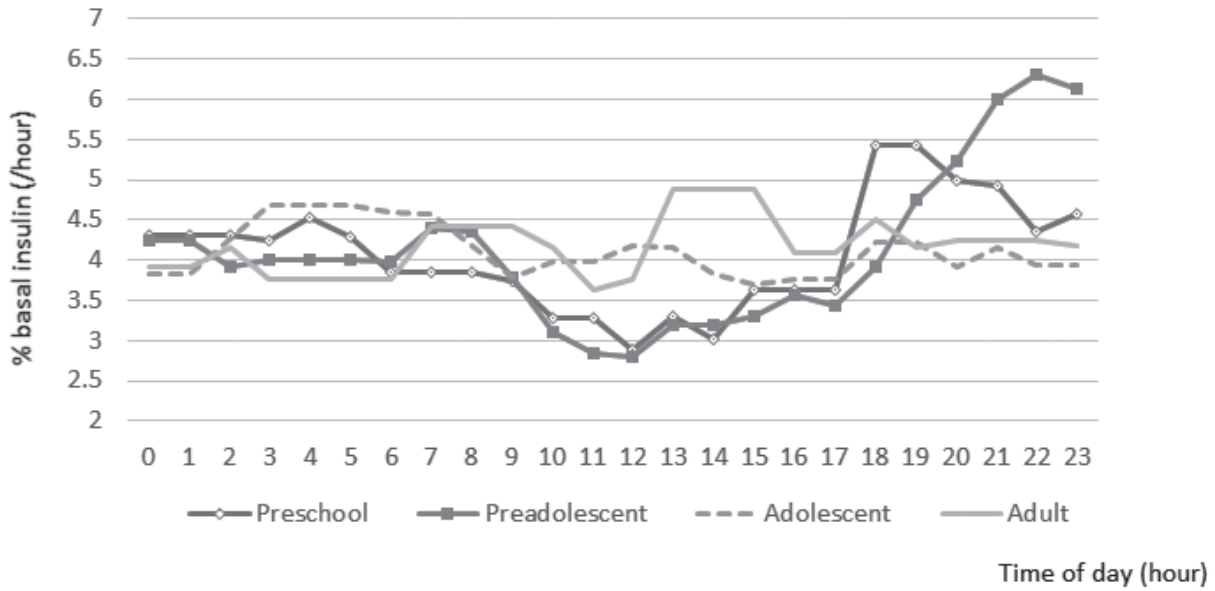

Figure 3. Basal infusion rate of the time zone in different groups. The data was shown the percentage of basal infusion dose every hour in total basal dose among groups.

Table 2. Carbohydrate ratio and correction factor

		Breakfast	Lunch	Dinner	Total
Preschool	CR	14.3(11.1-30.3)	16.7 (11.1-25.0)	14.3 (11.1-25.0)	16.7(11.1-25.0)
	CF	135 (100-300)	135 (100-400)	130 (100-300)	135 (100-400)
Preadolescent	CR	11.3 (5.0-30.3)	13.4 (5.0-33.3)	14.7 (5.0-50.0)	14.3 (5.0-50.0)
	CF	60 (30-300)	55 (30-300)	55 (30-300)	55 (30-300)
Adolescent	CR	6.7 (5.9-8.3)	6.0 (5.0-7.7)	6.3 (5.0-8.0)	7.0 (5.9-8.3)
	CF	40 (30-60)	50 (30-60)	40 (250-60)	50 (30-60)
Adult	CR	7.7 (4.9-9.1)	7.7 (2.9-10.0)	7.7 (3.1-10.0)	7.7 (3.6-10.0)
	CF	42.5 (20-50)	42.5 (20-50)	42.5 (20-50)	42.5 (20-50)

The data were shown as a median (range). CR and CF were picked up from Carelink® system, the system analyzing data of insulin pump and continuous glucose monitor, after they were adjusted. CR, carbohydrate ratio; and CF, correction factor.

the preschool, preadolescent, adolescent, and adult groups, respectively (Table 2). Fourteen patients (40.0%) required lower CR for breakfast than for lunch or dinner. In particular, 50.0% and 57.1% of patients in the preschool and preadolescent groups, respectively, required lower CR for breakfast than that for lunch or dinner (This result was not included in the table or figure). CRs of six patients (75.0%) in the preschool group were lower than those calculated by the 300 rule (Fig. 4). We calculated the constant, by the formula of CR×TDD in our data to compare that to 300-500 rules which were proposed in previous reports. As the results, for breakfast, 218.6 (142.9-534.8) in preschool, 365.6 (282.5-790.9) in preadolescents, 368.2 (248.5-392.0) in adolescents, and 328.5 (300.0-382.1) in adults. For lunch, 234.3 (146.7-532.5) in preschool, 427.4 (334.0-557.5) in preadolescents, 358.6 (290.2-404.6) in adolescents, 328.5 (228.9-402.0) in adults. For dinner, 234.3 (146.7-441.3) in preschool, 413.3 (226.0-680.0) in preadolescents, 331.8 (276.7-375.7) in adolescents, 314.7 (250.3-402.0) in adults. To

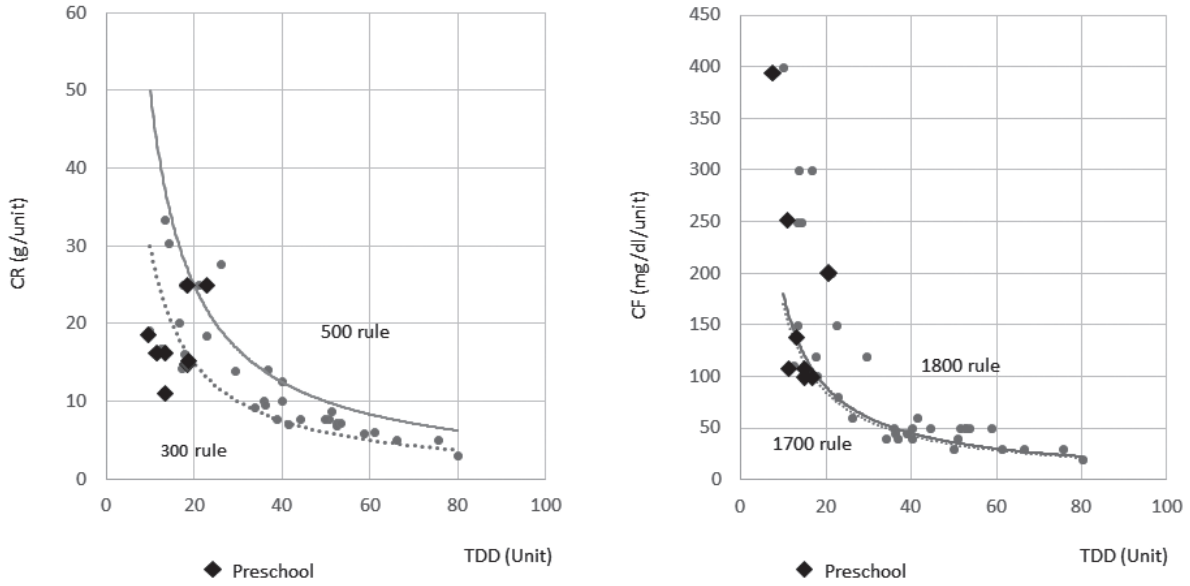

Figure 4. Relationship between TDD and CR or CF. The solid line of the 500 rule and the broken line of the 300 rule were shown to be compared with the patient's CR. The solid line of the 1800 rule and the broken line of the 1700 rule were shown to be compared with the patient's CF. CR or CF of all patients except preschool children were plotted as dots and CR or CF of preschool children were especially plotted as diamond marks. TDD, total daily dose; CR, carbohydrate ratio; and CF, correction factor.

summarize, at this study, the constant of many patients, CR×TDD was 300-450 in except preschool children and 200-250 in preschool children especially at morning.

The median CFs were 135 (100-400), 55 (30-300), 50 (30-60), and 42.5 (20-50) mg/dL/unit in the preschool, preadolescent, adolescent, and adult groups, respectively (Table 2). In many patients, CFs did not differ with respect to the time of day. Many patients needed higher CF than those calculated by the 1800 or 1700 rule (Fig. 4). CFs of eight patients in the preschool and preadolescent groups were higher than 3000 divided by TDD; however, the relationship between CF and age remained unclear. We calculated the constant, by the formula of CF×TDD in our data to compare that to 1700-1800 rules which were proposed in previous reports. As results, CFs were 2034 (1376-4260), 2148 (1356-5010), 2355 (1494-2940), and 1617 (1602-2675) in the preschool, preadolescent, adolescent, and adult groups, respectively.

Discussion

In this study, changes in insulin doses of Japanese patients with type 1 diabetes with respect to age were investigated.

We observed that median TDDs seemed to increase with age until preadolescence or adolescence age, after which they appeared to decrease, although not significantly among all groups. Lau et al reported that TDD/kg was 0.65 (0.61-0.70) in preschool group, 0.74 (0.62-0.83) in preadolescent, and 0.88 (0.74-1.00) in adolescent, as mean±SD[14]. Danne et al reported that 0.71±1.31 in preschool group, 0.73±0.16 in preadolescent group, and 0.83±0.19 in adolescent group[15]. They both reported that TDD increased with age until adolescence age, which is similar to our study results.

The median TBD/TDD was 32.8% (18.2%-55.3%). The median TBD/TDD was previously recommended to be approximately 50% of TDD in Western countries[16]. King et al recently proposed

a new formula for calculating TBD: 0.4×TDD=TBD[17]. The reason why a lower TBD value was recommended than previously used may be because the use of CGM became popular and basal dose could be more accurately adjusted. Kuroda et al reported that TBD was under 30% of the TDD in Japanese patients with type 1 diabetes[8], and Nakamura et al reported that TBD to be 27.3%±6.0% of TDD[6]. Generally, TBD/TDD was lower in Japanese data than in Western data. Hashimoto et al reported that in type 1 diabetes patients aged ≧14 years, TBD/body weight may be associated with fat energy ratio of the meal[18]. In our study, fat energy ratio of the meal was not assessed; however, compared with Western food, Japanese food generally contains large amounts of carbohydrate, possibly resulting in Japanese patients requiring less basal insulin dose[18].

However, TBD/TDD in our study was a little higher than that reported by Kuroda et al[8] and Nakamura et al[6] in Japanese patients. There are several reasons for this discrepancy. One is the difference in the ages of the subjects included in the studies. The subjects in their studies were adults, whereas most of the subjects in our study were children and adolescents. Another reason could be that our data were obtained from outpatients, whereas their data were obtained from inpatients, and basal insulin settings can be more accurately adjusted in admitted settings.

In Japan compared with in Western country, TDD/kg was similar and TBD/TDD was less, so the insulin dose of bolus was inferred to be higher. It might be also related to the higher carbohydrates in Japanese meals.

Basal insulin patterns at each hour appeared to be different among the groups. We evaluated basal ratio of every hour to total basal dose. Children and adolescents seemed to need higher basal insulin rates during 03:00-08:00. In preschool and preadolescent children, the basal rates seemed to be higher in the morning and evening and lower in the daytime. The patterns of the basal rate according to time observed in our study were similar to those observed in previous studies[14,19,20]. The tendency of increasing insulin requirements in the early morning was most prominent in adolescents, possibly because of the secretion pattern of growth hormone or cortisol early in the morning, known as the dawn phenomenon[21]. The higher basal rates in the evening were observed in preschool children, and preadolescent children; these findings are consistent with those previously reported[14,19,20]. Although the mechanism underlying this phenomenon was unclear, one reason could be the increase in growth hormone secretion[22,23].

Fourteen patients (40.0%) had smaller CRs for breakfast than for lunch or dinner. Especially, 50.0% and 57.1% of patients in the preschool and preadolescent groups, respectively, had smaller CRs for breakfast than for lunch or dinner, possibly because of cortisol secretion pattern in the morning, which increases insulin resistance in the morning[24].

Kuroda et al reported that the CR was estimated by the 300 rule at breakfast or by the 400 rule at lunch or dinner[5], whereas Nakamura et al reported that the CR was estimated by the 300 rule at breakfast, 500 rule at lunch, and 400 rule at dinner[6]. In our study, the calculated constant for CR was 300-450 in all groups, except the preschool group, and 200-250 in the preschool group, especially in the morning. However, the reason why young children required smaller CRs for meal than other age children was unclear. Their TDDs were related to their body weight. However, the nutritional requirements did not linearly relate to the body weight of young children[25]. The discrepancy that TDD was related to the body weight of young children, whereas energy requirement was not, may explain the reason why their CRs were not calculated by the 300 rule, which is adaptable for older patients.

Regarding median CFs, there was no difference with regard to the time of the day in many patients. Furthermore, there was no correlation between CFs and age or TDD. The CFs of preschool children varied more widely. The CFs of some preschool and preadolescent children were higher than 3000 divided by TDD. The reason of this was unclear, but one possibility was that younger children might have higher insulin sensitivity. The fact that TDD/kg of younger children was lower than older patients might be also associated with their higher insulin sensitivity.

This study had some limitations. First, in this study, a meal omission test was not conducted for adjusting basal insulin. This study was a retrospective study, and it was difficult for children to omit meal. Meal omission tests were not conducted in some previous studies whose subjects were children and adolescents[14,15]. Second, we could not determine whether the calculated CRs and CFs were correct. Therefore, further studies should assess the accuracy of our results.

In this study, we assessed whether the rules, which have been already reported for the calculation of CR and CF, could be applied to children and adolescents with type 1 diabetes or not. As a result, those rules were not suitable to some patients especially preschool children. The rules used only TDD of the subjects. However, age and TDD among the subjects showed a complex relationship as shown in Figure 1. The complex relationship between age and TDD might be a reason why the rules could not be applied to our subjects.

In conclusion, this study revealed the age-related differences in insulin dose and settings for pump therapy. We believe that our data might be helpful in determining the initial insulin settings and adjusting it for Japanese patients with type 1 diabetes. On the other hand, the rules which have been already reported cannot be applied to some patients especially preschool children, and it is important that the insulin settings were individually adjusted watching the changes of blood glucose level.

Acknowledgments

All authors have no COI to declare regarding the present study.

References

1. Subramanian S, Baidal D, Skyler JS, et al. The Management of Type 1 Diabetes. In Endotext. Edited by De Groot LJ, Chrousos G, Dungan K, et al. MDText.com, Inc.; 2000.
2. Matejko B, Kukulka A, Kiec-Wilk B, et al. Basal insulin dose in adults with type 1 diabetes mellitus on insulin pumps in real-life clinical practice: a single-center experience. Adv Med 2018;2018:1473160.
3. Göksen D, Atik Altinok Y, Ozen S, et al. Effects of carbohydrate counting method on metabolic control in children with type 1 diabetes mellitus. J Clin Res Pediatr Endocrinol 2014;6:74-78.
4. Yamada E, Okada S, Nakajima Y, et al. Effect of carbohydrate counting using bolus calculators on glycemic control in type 1 diabetes patients during continuous subcutaneous insulin infusion. J Diabetes Investig 2017; 8:496-500.
5. Kuroda A, Yasuda T, Takahara M, et al. Carbohydrate-to-insulin ratio is estimated from 300-400 divided by total daily insulin dose in type 1 diabetes patients who use the insulin pump. Diabetes Technol Ther 2012; 14:1077-1080.
6. Nakamura T, Hirota Y, Hashimoto N, et al. Diurnal variation of carbohydrate insulin ratio in adult type 1 diabetic patients treated with continuous subcutaneous insulin infusion. J Diabetes Investig 2014;5:48-50.
7. Davidson PC, Hebblewhite HR, Steed RD, et al. Analysis of guidelines for basal-bolus insulin dosing: basal insulin, correction factor, and carbohydrate-to-insulin ratio. Endocr Pract 2008;14:1095-1101.
8. Kuroda A, Kaneto H, Yasuda T, et al. Basal insulin requirement is ~30% of the total daily insulin dose in type 1 diabetic patients who use the insulin pump. Diabetes Care 2011;34:1089-1090.
9. King AB, Armstrong DU. A prospective evaluation of insulin dosing recommendations in patients with type 1 diabetes at near normal glucose control: basal dosing. J Diabetes Sci Technol 2007;1:36-41.
10. de Bock M, Cooper M, Retterath A, et al. Continuous glucose monitoring adherence: lessons from a clinical

trial to predict outpatient behavior. J Diabetes Sci Technol 2016;10:627-632.
11. Kawasaki E, Maruyama T, Imagawa A, et al. Diagnostic criteria for acute-onset type 1 diabetes mellitus (2012): Report of the Committee of Japan Diabetes Society on the Research of Fulminant and Acute-onset Type 1 Diabetes Mellitus. J Diabetes Investig 2014;5:115-118.
12. Urakami T, Suzuki J, Yoshida A, et al. Association between sex, age, insulin regimens and glycemic control in children and adolescents with type 1 diabetes. Clin Pediatr Endocrinol 2010;19:1-6.
13. Pinhas-Hamiel O, Hamiel U, Boyko V, et al. Trajectories of HbA1c levels in children and youth with type 1 diabetes. PLoS One 2014;9:e109109.
14. Lau YN, Korula S, Chan AK, et al. Analysis of insulin pump settings in children and adolescents with type 1 diabetes mellitus. Pediatr Diabetes 2016;17:319-326.
15. Danne T, Battelino T, Kordonouri O, et al. A cross-sectional international survey of continuous subcutaneous insulin infusion in 377 children and adolescents with type 1 diabetes mellitus from 10 countries. Pediatr Diabetes 2005;6:193-198.
16. Walsh J, Roberts R, Bailey T, et al. Guidelines for insulin dosing in continuous subcutaneous insulin infusion using new formulas from a retrospective study of individuals with optimal glucose levels. J Diabetes Sci Technol 2010;4:1174-1181.
17. King AB. Continuous glucose monitoring-guided insulin dosing in pump-treated patients with type 1 diabetes: a clinical guide. J Diabetes Sci Technol 2012;6:191-203.
18. Hashimoto T, Kawamura T, Kashihara Y, et al. Factors associated with basal insulin dose in Japanese children and young adult type 1 diabetics. J Diabetes Investig 2012;3:276-282.
19. Conrad SC, McGrath MT, Gitelman SE, et al. Transition from multiple daily injections to continuous subcutaneous insulin infusion in type 1 diabetes mellitus. J Pediatr 2002;140:235-240.
20. Nicolajsen T, Samuelsson A, Hanas R, et al. Insulin doses before and one year after pump start: children have a reversed dawn phenomenon. J Diabetes Sci Technol 2012;6:589-594.
21. Weitzman ED. Biologic rhythms and hormone secretion patterns. Hosp Pract 1976;11:79-86.
22. Rabbone I, Bobbio A, Berger K, et al. Age-related differences in metabolic response to continuous subcutaneous insulin infusion in pre-pubertal and pubertal children with Type 1 diabetes mellitus. J Endocrinol Invest 2007; 30:477-483.
23. Rose SR, Municchi G, Barnes KM, et al. Spontaneous growth hormone secretion increases during puberty in normal girls and boys. J Clin Endocrinol Metab 1991;73:428-435.
24. Weitzman ED, Fukushima D, Nogeire C, et al. Twenty-four hour pattern of the episodic secretion of cortisol in normal subjects. J Clin Endocrinol Metab 1971;33:14-22.
25. German Nutrition Society (DGE). New Reference Values for Energy Intake. Ann Nutr Metab 2015;66:219-223.

Osaka City Med. J. Vol. 65, 41-54, 2019

Clinical Aspects and Genetic Analysis of Pediatric Neurofibromatosis Type 1 with Neurological Complications

Kenji Fujita[1)], Kanako Yamashita[1)], Takao Hoshina[1)], Norikatsu Hikita[1)], Taro Shimono[2)], Kazuyoshi Fukai[3,4)], Toshiki Takenouchi[5)], Tomoko Uehara[6)], Kenjiro Kosaki[6)], Hideyuki Saya[7)], Takashi Hamazaki[1)], and Toshiyuki Seto[1)]

Departments of Pediatrics[1)], Diagnostic and Interventional Radiology[2)], and Dermatology[3)], Osaka City University Graduate School of Medicine; Department of Dermatology[4)], Osaka City General Hospital; and Departments of Pediatrics[5)], Center for Medical Genetics[6)], and Institute for Advanced Medical Research[7)], Keio University School of Medicine

Abstract

Background

Neurofibromatosis type 1 (NF1) is an autosomal dominant disease causing multiple café-au-lait spots and various systemic signs. NF1 patients often need to be examined complications because of tumorigenesis. Here, with a focus on neurological complications, we studied the clinical features of the disease in patients in the Department of Pediatrics, Osaka City University Hospital, Japan, and the relationship between these features and patient genotype.

Methods

The subjects were 81 patients aged 0 to 44 (average 11.3, median 10.3) years who had visited our department; they were evaluated retrospectively by examination of their electronic medical records. We examined family history and characteristic physical findings of NF1, and we assessed patient development and brain and spine MRIs. In six patients with moderate to severe neurological complications we also analyzed the NF1 gene.

Results

A total of 45 patients were categorized as having definite NF1 and 24 patients as having suspected NF1, according to National Institutes of Health criteria. 56 patients had neurological complications and 12 had optic glioma, pilocytic astrocytoma, schwannoma, or severe plexiform neurofibroma. In the six patients subjected to genetic analysis we found pathogenic mutations in the *NF1*, one of which was undefined. Novel mutations were identified in four patients in three families.

Conclusions

We conclude that NF1 patients should be examined by MRI and genetic analysis during follow-up;

Received September 3 2018; accepted November 27, 2018.
Correspondence to: Toshiyuki Seto, MD, PhD.
Department of Pediatrics, Osaka City University Graduate School of Medicine,
1-4-3 Asahimachi, Abeno-ku, Osaka 545-8585, Japan
Tel: +81-6-6645-3816; Fax: +81-6-6636-8737
E-mail: setot@med.osaka-cu.ac.jp

this is especially true for those with suspected moderate to severe neurological complications. We need to accumulate more genotypic information on Japanese patients with NF1 to elucidate the genotype-phenotype relationship.

Key Words: Genetic testing; Mutation; Neurofibromatosis 1; Optic nerve glioma; Pediatric

Introduction

Neurofibromatosis type 1 (NF1) is a genetic disease that is inherited in an autosomal dominant pattern[1-4] and has a reported birth incidence of 1:2000-3000[1,2,5]. The initial signs are usually multiple café-au-lait spots (mCaLs). Most patients are referred from domestic public health centers to our Department of Pediatrics or Department of Dermatology at Osaka City University Hospital, Japan, because of the discovery of mCaLs during infancy. Other signs can be skin-fold freckling, neurofibroma, Lisch nodules, scoliosis, enlargement of the subdural cavity, optic glioma, low-grade astrocytoma, pilocytic astrocytoma, plexiform neurofibroma, intellectual disability, and neurodevelopmental disorders[1,2,6]. A clinical diagnosis of NF1 is usually arrived at by applying National Institutes of Health (NIH) criteria (Table 1)[7]. However, obvious neurofibroma, skin-fold freckling, and scoliosis usually become apparent after puberty, so the existence of characteristic neurological signs is important for NF1 diagnosis in some children before the diagnosis can be confirmed according to NIH criteria. Almost half of all NF1 patients have no family history because their mutations have arisen *de novo*[6,8,9], so in young children with a suspected diagnosis of NF1 it is important to look for neurological signs such as developmental delay. We propose that patients and their parents should undergo neuroradiological studies and other examinations at presentation, but because infants and young children can be difficult to evaluate they may need to be admitted to hospital to receive such studies and further follow-up studies under sedation. Ophthalmologic examination is also difficult without complete sedation.

Eventually, neurological signs in childhood become increasingly important from the perspective of not only the diagnosis of NF1 but also the necessary follow-up of neurological complications. Neuroradiological examinations sometimes reveal characteristic findings in the brains of children with NF1. Unidentified bright objects (UBOs) have been identified as high-intensity lesions in T2-

Table 1. NIH diagnostic criteria for neurofibromatosis type 1

Two or more of the following clinical features must be present
Six or more café-au-lait macules of more than 5 mm greatest diameter in prepubertal individuals, and more than 15 mm in greatest diameter in postpubertal individuals
Two or more neurofibromas of any type, or one plexiform neurofibroma
Freckling in the axillary or inguinal region
Optic glioma
Two or more iris hamartomas (Lisch nodules)
A distinctive bony lesion, such as sphenoid dysplasia, or medullary narrowing and cortical thickening of the long bone cortex, with or without pseudoarthrosis
A first-degree relative (parent, sibling, or offspring) with NF1 based on the above criteria

NIH, National Institutes of Health; and NF1, neurofibromatosis type 1.

weighted images and fluid-attenuated inversion recovery images during brain MRI in children with NF1[10,11]. Although most UBOs are regarded as benign tumors (hamartomas or low-grade astrocytomas), rarely, malignant brain tumors are found during the clinical course of the disease[10,12]. Optic glioma (also known as optic pathway glioma) is a benign or malignant tumor that can also occur in children with NF1[13-15]. Moreover, malignant peripheral schwannomas and pheochromocytomas can complicate NF1[16,17]. Because of those tumors some patients (and their parents) must sacrifice time and quality of life for continuing surgery and chemotherapy.

Unfortunately, there are currently few keys to the prognosis, especially in regard to tumorigenesis, of young children with only mCaLs who are suspected of having NF1. The gene associated with the disease is *NF1*[18,19], the phenotype-genotype relationship in NF1 in regard to prognosis and malignant tumorigenesis has not yet been defined[20,21].

Because there have been few reports of the etiology and genetic analysis of NF1 in Japanese children[22], we considered it important to explore these features in regard to the various complications of NF1—especially neurological complications. Here, with a focus on the key neurological signs in pediatric patients, we retrospectively examined the clinical aspects of all NF1 patients who visited, and were followed up by, our Department. We also performed genetic analyses of patients with NF1 and multiple complications.

Materials and Methods

Subjects

Eighty-one patients were evaluated between April 2007 and June 2018. All of them had been referred to outpatient clinic of Pediatrics, Osaka City University Hospital, for the purpose of diagnosis or further examination of NF1. The patients were aged from 0 to 44 years (average 11.3, median 10.3 years) at the time of the latest visit, and there were 39 males (48.1%) and 42 females (51.9%). The average follow-up period was 6.0 years (median, 5.5 years).

Evaluation of patient histories and neurological complications

All clinical information was obtained from the electronic medical record system of our hospital. We investigated family history and the characteristic physical findings of NF1, and we assessed physical and neurological development and brain and spine MRIs. The MRIs were evaluated by a neuropediatrician[23,24] and neuroradiologists. Clinical diagnosis was performed by using the NIH Consensus Development Conference diagnostic criteria (1988 version) (Table 1). "Neurological complications" were defined here referring to previous reports[6,25] as abnormal neuroradiological findings (UBOs, optic glioma, pilocytic astrocytoma, plexiform neurofibroma, pheochromocytoma, schwannoma); epilepsy; intellectual disability (ID); or neurodevelopmental disorder (NDD), including autism spectrum disorder (ASD), attention-deficit hyperactivity disorder (ADHD) and learning disorder (LD). Here, we further show the clinical courses of six patients with NF1 who manifested moderate to severe neurological complications (NDD, optic glioma, severe plexiform neurofibroma); we also analyzed the *NF1* genotypes of these patients and related family members.

Genetic analysis

In the six patients in five families who had multiple complications we also analyzed *NF1*. DNAs were purified from blood samples; the target region was enriched by using a TruSight One Sequencing Panel (Illumina®, San Diego, CA)[26] that included *NF1*, and it was sequenced on a Miseq platform (Illumina®, San Diego, CA). Also, we used the ClinVar (https://www.ncbi.nlm.nih.gov/clinvar/) and the

Human Gene Mutation Database (http://www.hgmd.cf.ac.uk/ac/index.php) to search for the pathological significance of mutations reported in the past. Chromosomal microarray testing using the Agilent 180K microarray (Agilent Technologies®, Santa Clara, CA) was performed as described previously[27].

Statistical analysis

Statistical analysis was performed by using analysis of variance (ANOVA) and Tukey's test for multiple pairwise comparisons. Welch's *t*-test and JMP (version 12) statistical software (SAS Institute Inc.®, Cary, NC).

This study was approved by the institutional review boards of Osaka City University Graduate School of Medicine (No. 3325 and No. 3326) and Keio University School of Medicine (No. 20110262). Written informed consent was obtained from all patients. In the case of patients with intellectual disability, or children, parents or other legally authorized representatives supplied informed consent.

Results

Figure 1 is a flowchart of all subjects included in the study. MCaLs were found in all patients. They were thus often the chief presenting complain and the catalyst for further examination. A total of 69 patients were evaluated as having definite (45 patients) or suspected (24 patients) NF1 according to NIH criteria in Table 1. The clinical signs of all patients are summarized in Table 2. Comparison of the definite and suspected groups revealed that the average age of the definite group was significantly higher than that of the suspected one. The average ages of the definite and suspected NF groups were much higher than those of the mCaLs-only group. The sex ratio did not differ significantly among groups, although in the definite NF1 group there were twice as many females as males with no neurological complications. In the definite NF1 group, 33 patients had neurological complications. In the definite NF1 group, 10 of the patients with neurological

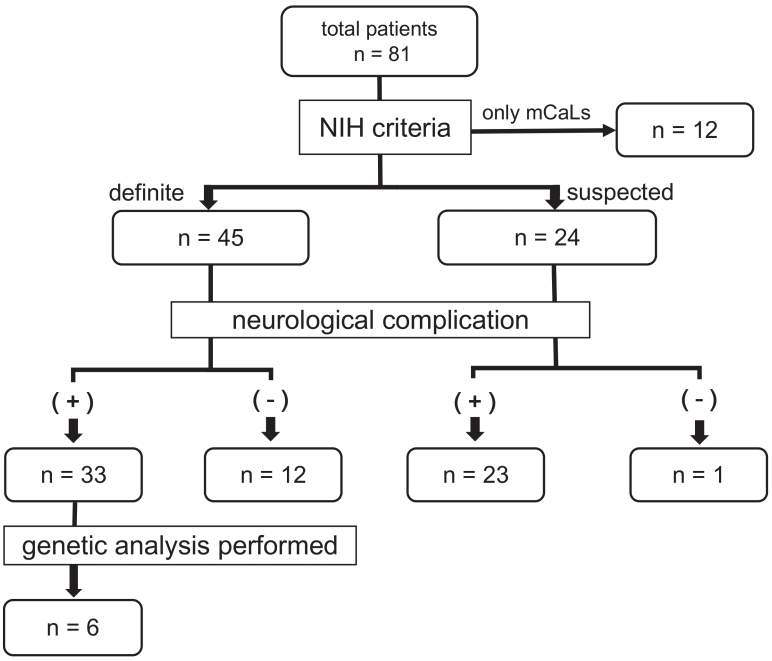

Figure 1. Flowchart of subjects included in this study. NIH, National Institutes of Health.

Table 2. Clinical profiles of all patients

		Definite NF1 n=45		Suspected NF1 n=24		mCals only n=12
Age (years, average±SD)		13.9±8.7		10.2±6.7		4.0±2.9
Neurological complications		+ n=33 (73)	− n=12 (27)	+ n=23 (96)	− n=1 (4)	
Age (years, average±SD)		14.1±8.7	13.1±9.1	9.8±6.5	19.5	
Sex	male	17 (38)	4 (9)	12 (50)	1 (4)	5
	female	16 (36)	8 (18)	11 (46)	0 (0)	7
Positive family history		17 (38)	6 (13)	-	-	-
mCaLs		33 (73)	12 (27)	23 (96)	1 (4)	12
Freckling		2 (4)	0 (0)	0 (0)	0 (0)	-
Neurofibroma		13 (29)	5 (11)	-	-	-
Plexiform neurofibroma (severe)		2 (4)	2 (4)	-	-	-
UBO		26 (58) †	-	23 (96)	-	-
Brain tumor		8 (18) †	-	0 (0)	-	-
optic glioma		7 (16)	-	-	-	-
pilocytic astrocytoma		1 (2)	-	0 (0)	-	-
schwannoma		1 (2)	-	0 (0)	-	-
Intellectual disability		4 (9)	-	-	-	-
Neurodevelopmental disorder		13 (29) †	-	1 (4)	-	-
Epilepsy		0 (0) †	-	2 (8)	-	-
Electroencephalogram abnormality		1 (2)	-	2 (8)	-	-
Ophthalmologic lesions		16 (36)	4 (9)	0 (0)	0 (0)	-
Lisch nodule		11 (24)	4 (9)	-	-	-
ocular fundus abnormality		5 (11)	3 (7)	0 (0)	0 (0)	-
Scoliosis		7 (16)	3 (7)	-	-	-
Short stature (< −2SD)		6 (13)	3 (7)	0 (0)	1 (4)	-
Macrocephaly (> +2SD)		3 (7)	1 (2)	4 (16)	0	-

Numbers in parentheses are percentages: the denominator is the number of patients with defined NF1 (n=45) or suspected NF1 (n=24). About ages, data were analyzed using ANOVA. Significant difference. And, multiple comparisons are performed using wilcoxon's test. $^{*}p<0.05$. For the neurological complications with defined NF1 and suspected NF1, we compaired with χ^2-test. †$p<0.05$. mCaLs, multiple café-au-lait spots ; and UBO, unidentified bright object.

complications had optic glioma, pilocytic astrocytoma, schwannoma, or severe plexiform neurofibroma. Pilocytic astrocytoma were found accidentally while following UBO in patient with ID. We found neurological complications in 81% of the 69 (73% of definite and 96% of suspected NF1 patients). And we found UBOs in 71.3% of our 69 definite and suspected NF1 patients combined. Exact evaluation of development and intelligence by using the Wechsler Intelligence Scale for Children or using the Kyoto scale of psychological development was not performed in all of our subjects. However, 29% of patients with definite NF1 were diagnosed as having as NDD, including ASD, ADHD, and LD. There were two patients with definite or suspected NF1 and epilepsy (West syndrome or juvenile absence epilepsy) (2.9%). The percentage of patients with neurological complications was smaller in the definite group than in the suspected group.

Six patients were found to have pathogenic mutations in *NF1* (Table 3). In the suspected NF1 group, all patients except one had UBO as a neurological complication; the remaining patient had short stature. Two patients in this group had epilepsy.

Presentations of six patients in the definite NF1 group who had tumors

1. Patient (P) 1

Her birth was normal. However, she gradually began to show developmental delay (DD) and was followed up at a local health center. She was referred to our hospital because of DD and mCaLs at age 3 years. We diagnosed her as having ID, ASD, and NF1. Optic glioma was found at the age of 4 years, but at the time of writing it had not progressed (Fig. 2a).

2. P2

He was referred to our hospital by a local hospital because of NF1 at age 13 years. His mother, grandmother, and uncle had mCaLs. He had undergone surgical procedures because of recurrent cutaneous neurofibroma, and he had abdominal plexiform neurofibroma (Fig. 2b). He did not have ID and reported having a normal social life.

3. P3

He was born normally but was followed up initially at a local hospital because of mCaLs. At the age of 9 years, he was referred to our hospital because of NDD and NF1. His brain MRI revealed multiple UBOs. He was diagnosed at 13 years as having LD. He had systemic cutaneous neurofibroma and received plastic surgery at 29 years.

4. P4

He was referred to our hospital at age 4 months because of mCaLs. He was of short stature and developed increased numbers and size of mCaLs at age 4 years. He was diagnosed as having ADHD at age 6 years because of hyperactivity and was treated with atomoxetine. The medication was not very effective, and he is now controlled with osmotic-release oral system (OROS) methylphenidate. His brain MRI revealed multiple UBOs (Fig. 2c). He has short stature (<-2SD). His mother was also diagnosed as having NF1.

5. P5 and P6

P5 and P6 (her younger brother) were referred to our hospital at the age of 3 years and 8 months, respectively. P5 had mCaLs and mild ID. Her mother had noticed a subcutaneous mass upon her (breech) birth. Her MRI revealed a large plexiform neurofibroma (Fig. 2d). P6' s brain MRI revealed multiple UBOs and an optic glioma (Fig. 2e). It developed further over a few months (Fig. 2f), so we performed treatment with chemotherapy. Details of all five patients with mutations are summarized in Table 3.

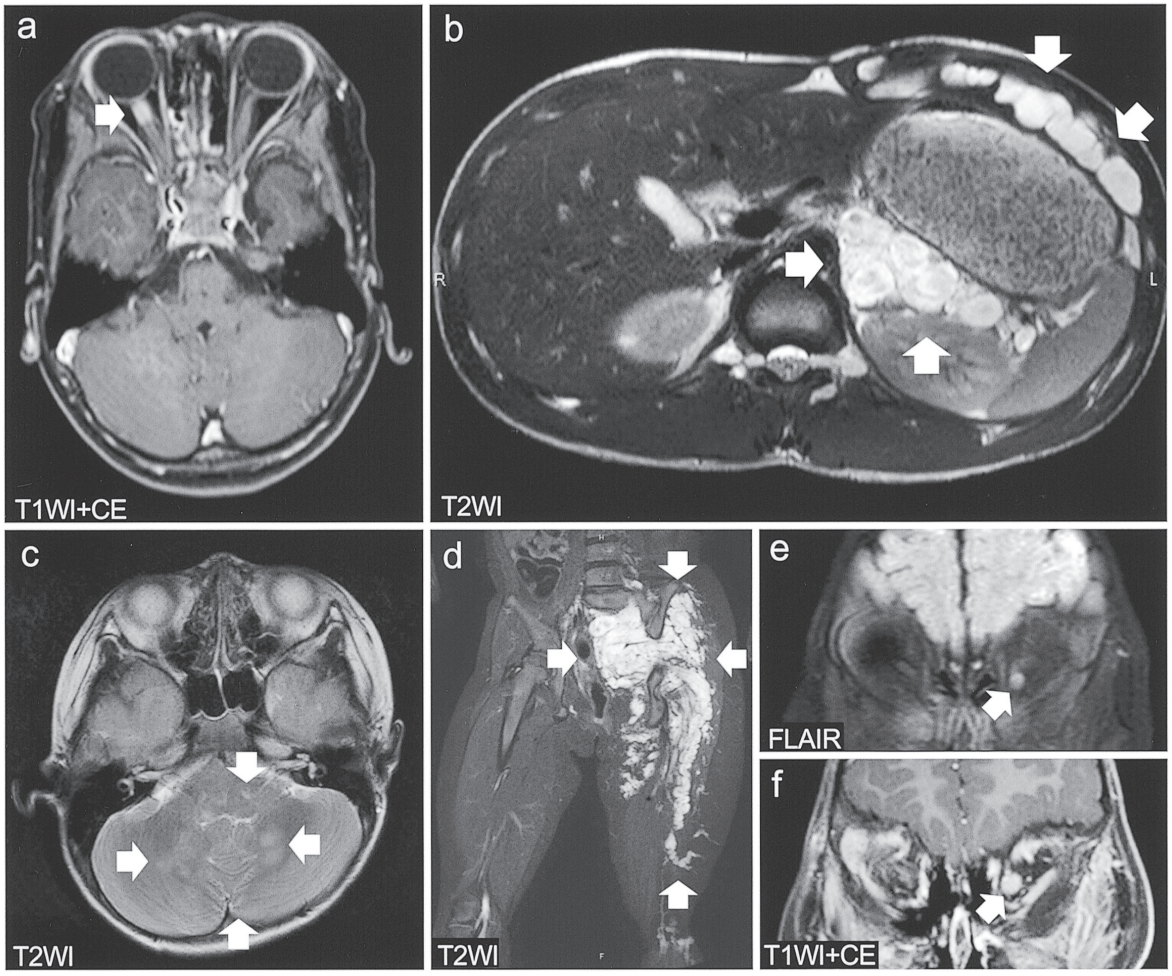

Figure 2. MRI findings in selected NF1 patients.
a, Optic glioma in patient 1 (white arrow). She had an optic glioma on the right optic nerve at age 4 years.
b, Abdominal plexiform neurofibroma in patient 2 (white arrows). He was aware of a subcutaneous mass in the right upper abdomen, and it gradually enlarged.
c, Multiple unidentified bright objects in patient 4 (white arrows). He had no malignant tumors.
d, Large plexiform neurofibroma in patient 5, from the sacrum to the distal femur (white arrows). Her parents had noticed her subcutaneous mass at the time of breech birth.
e, Optic glioma in the patient 6. An optic glioma (white arrow) was found by follow-up MRI study of unidentified bright objects.
f, MRI of the same patient 6 months later since Figure 2e revealed the optic glioma developed obviously (white arrow).
T1WI, T1-weighted image; T2WI, T2-weighted image; CE, contrast enhanced; and FLAIR, fluid-attenuated inversion recovery.

Determination of genotype

Genetic analysis was performed in all of the patients described above. The pathogenic mutation was defined in all except for P2. P1 had a *de novo* missense mutation, c.2350T >C (p.Trp784Arg). Although P2 had neither pathogenic mutation in the exons nor microdeletion/duplication upon array comparative genomic hybridization analysis, an intron mutation was found. Its pathogenic meaning remains unknown. P3 had a frameshift mutation, c.3527delG (p.Arg1176Lys fs*8). P4 and his mother had a nonsense mutation, c.1603C >T (p.Gln535*). P5 and P6 and mother had a splicing mutation, c.888+2T >A. The mutations in P3, P4, and P5 (P6) were novel. All results are summarized in Table 3.

Table 3. Relationships between neurological complications and NF1 genotype in five patients and their family members

Patient	Age (years)	Sex	Family history	Neurological complications												Results of genetic analysis			
				ID	NDD	UBO	Optic glioma	Malignant brain tumor	Plexiform Nf	Other	Lisch nodules	mCaLs	Cutaneous and/or subcutaneous Nf	Short stature	Scoliosis	Identified mutation	Exon location	Type	Related past reports
P1	5	F	−	moderate 48*	ASD	+	+	−	NE	funnel chest macrocephaly	+	+	−	−	−	c.2350T >C	20	missense	+ (no clinical information)
P2	23	M	+	NE	NE	−	−	−	+		+	+	+	−	+	(no pathogenic mutation determined)			
P3	32	M	−	borderline	LD	+	−	−	NE	HL, vertigo headache	+	+	+	−	+	c.3527delG	27	frameshift	− (novel)
P4	12	M	+	normal	ADHD	+	−	−	+		+	+	+	+	−	c.1603C >T	14	termination	− (novel)
P4's mother	34	F		NE	NE	NE	NE	NE	NE	NE	NE	+	+	+	NE				
P5	6	F	+	mild	ASD	+	−	−	+		−	+	+	−	−	c.888+2T >A	8	splicing abnormality	− (novel)
P6 (P5's brother)	3	M		mild	ASD	+	+	−	NE		−	+	−	−	−				
P5 and 6's mother	34	F		borderline	NE	NE					NE	+	+	−	NE				

In this table, the patient's age is as of june 2018. NF1, neurofibromatosis type 1; ID, intellectual disability. It evaluated by using the Kyoto scale of psychological development or the Wechsler Intelligence Scale for Children; NDD, neurodevelopmental disorder; UBO, unidentified bright object; Nf, neurofibroma; mCaLs, café-au-lait spots; P, patient; ASD, autism spectrum disorder; NE, not examined; LD, learning disorder; HL, hearing loss; and ADHD, attention-deficit hyperactivity disorder.

Discussion

We retrospectively elucidated the clinical features of all patients presenting to our department with definite or suspected NF1 during the study period. In this literature, we present two new findings. First, examining their follow-up MRIs, optic gliomas and pilocytic astrocytoma were incidentally detected in young children having ID. Second, we identified novel mutations in four patients with NF1.

In our study, 12 patients (15% of all subjects) were judged clinically in childhood by pediatricians as having only mCaLs (Table 2). This is because mCaLs are generally the initial chief complaint prompting referral to our pediatrics or dermatology departments from domestic public health centers or clinics. These patients' general condition was good and they showed no more clinical signs during their follow-up periods. They included children with tiny and mild mCaLs. We needed to decide whether to diagnose these patients as having suspected NF1 and to follow them up and examine them for various complications, or to stop our observations and label the mCaLs as mere macules or nevus syndromes. Distinction between NF1 and Legius syndrome (in which there are mCaLs with or without freckling, but never the typical NF1-associated tumors[28]) is possible by genetic analysis. However, in Japan such analyses are not common. Some doctors in charge of the children with only mCaLs planned to examine them by MRI, possibly because of certain aspects of their behavior or an impression that their mCaLs were severe. As our study was not prospective, further reasons for the lost to follow-up were unknown. Most of the doctors in charge of patients with suspected NF1 are child neurologists in our department. If they were to notice even a tiny objective finding—such as behavior suggestive of motor or developmental delay—they would suggest to a child's parents that the child receive further examinations or be observed at an outpatient clinic for a while. NF1 is a wide-spectrum disorder ranging from very mild to very severe. Moreover, children are often hard to evaluate in some examinations (e.g. MRI) without deep sedation, and some signs tend to appear after puberty. This is a reason to have no choice to postpone clarifying in childhood whether or not the patient definitely has NF1.

Next, we discussed neurological complications among 69 NF1 patients—24 with suspected NF1 and 45 with definite disease—by retrospective electronic records analysis. In our study, We found neurological complications in many NF1 patients. One Japanese report found neurological complications (except for brain tumor) in 38.1% of patients[29]. UBO is a characteristic major finding in the brains of NF1 patients. The reason for this higher percentage compared with the previous study is because it is child neurologists who mostly see and follow patients with NF1, and young children suspected of having NF1 commonly have only UBOs plus mCaLs before their diagnoses are confirmed. The average age of patients with suspected NF1 was lower than that of patients with definite NF1. It is regarded as one possibility that the percentage of patients with neurological complications was smaller in the definite group than in the suspected group because that growing patients with suspected NF1 likely move into the definite group as they age and begin developing signs other than UBO.

When examined across several studies, the frequency of LD as an NDD in children with NF1 is estimated to be between 30% and 65%[25,30]. This value is not significantly different from our study. The complication rate of epilepsy is also much higher than the percentage of the general population of Japanese children with epilepsy (0.3% to 0.5%)[31]. Another patient showed obvious abnormal epileptic discharges in her electroencephalograph. Seizures are reported elsewhere to occur in 4% to

9% of patients with NF1[32]. Relative to those in the general population, seizures in people with NF1 are more often focal and related to the presence of brain tumors. Moreover, individuals with NF1 and seizures frequently require more aggressive therapy than those without NF1, and some patients with NF1-related epilepsy should be considered for surgery when appropriate[25]. NDD and epilepsy often go together in NF1, and we need to pay close attention to them—in the same way as for brain tumors—during follow-up, as indicated in previous reports[25].

Once NF1 is diagnosed by a dermatologist, pediatrician, or medical geneticist, there is a need to start surveying for the occurrence of brain tumors and other complications. Therefore, early diagnosis is important, and we expect that patient genotyping will make it possible to determine each patient's prognosis, especially in terms of tumorigenesis. *NF1* encodes neurofibromin and is located on chromosome 17q11.2. It is 350 kb long and has 60 exons[6,19,33,34]. There are some reports in which gene mutations have been associated with phenotypes. First, patients with *NF1* microdeletion usually have more severe complications and are at increased risk of malignant peripheral sheath tumors[35]. Second, a specific single *NF1* amino-acid deletion [e.g. c.2970_2972del (p.Met992del)] could result in mild complications[36]. Third, a missense mutation (p.Arg1809Cys substitution) in neurofibromin could be a cause of NDD, ID, and optic glioma[37,38]. Recently, it was reported that the neighboring codons 844 to 848 are involved in severe NF1 phenotypes such as bone abnormalities, plexiform or symptomatic spinal neurofibroma (or both), symptomatic optic glioma, and other malignant neoplasms[21]. Other reports have suggested that NF1 patients with mutations located in the cysteine- and serine-rich domain (CSRD) were at higher risk of optic glioma than patients with mutations in other regions[39]. In mice, NF1-patient-derived germline NF1 mutations (c.2542G >C and C.2041C >T) are reportedly associated with optic glioma formation[40]. It is also known that, generally, microdeletion, truncation, or frameshift mutations tend to be phenotypically severe[41]. However, according to previous reports, an obvious genotype-phenotype relationship has not yet been elucidated[6,21].

We presented details of six patients with NF1. All patients had both NDD and UBO except for P2, with or without moderate to severe plexiform neurofibroma or optic glioma. We performed a next-generation sequencing analysis of these patients with NF1 and relatively severe neurological complications after genetic counseling of the children and their parents by a medical geneticist. Eventually, we identified four kinds of pathogenic mutations in NF1, including three novel mutations. P1 had optic glioma, moderate ID, and ASD. The mutation identified in P1 was previously reported as pathogenic[42], but there was no clinical information in that previous report. This mutation is located in the CSRD domain reported of relation with optic glioma[39]. A mutation was found in an intron of NF1 in P2, but its pathogenic significance could not be determined. P3 had LD, chronic headache, and severe systemic subcutaneous neurofibroma; a frameshift was identified in exon 27 between the tubulin-binding domains (TBD) and GAP-related domains (GRD), which interact with Ras protein (Fig. 3). The novel termination mutation identified in P4 and his mother resulted in short stature in both. P4 has severe UBO and ADHD, but his mother has not been examined. The mutation identified in P5's family shows interfamilial phenotypic variability. This may have been due to clinical variability or to differences in transcripts in terms of splicing mutations, differences in penetration rates or epigenetic factors, or other reasons.

We have compared our identified mutations with those described in reports mentioned above (Fig. 3). Neurofibromin encoded by NF1 regulates the activity of Ras protein by inactivating it through

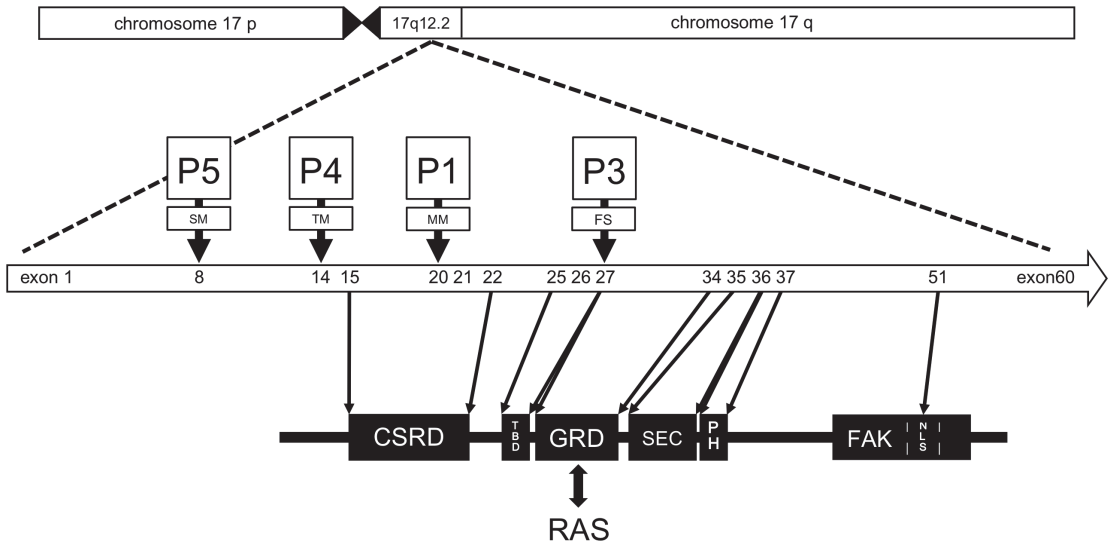

Figure 3. Scheme of NF1 gene and neurofibromin protein. This scheme is based on the figure in references 39 and 44. *NF1* contains 60 exons, including three alternatively spliced exons. Mutation in the CSRD domain, which interacts with RAS protein, carries a higher risk of optic glioma than mutations in other regions. SM, splicing mutation; TM, termination mutation; MM, missense mutation; FS, frameshift mutation; CSRD, cysteine- and serine-rich domain; TBD, tubulin binding domain; GRD, domain responsible for interaction with and GTP hydrolysis; SEC-PH, bipartite lipid-binding domain; FAK, focal adhesion kinase-interacting domain; and NLS, nuclear localization sequence.

dephosphorylation[43]. In other words, it negatively regulates the activity of Ras protein; neurofibromin is a GTP-ase activating protein that accelerates the hydrolysis of Ras-bound GTP[43,44]. Mutations in the CSRD domain interacting with Ras protein carry a high risk of optic glioma[39]. Optic glioma is the most common brain tumor associated with NF1, with as many as 15% or 20% of children with NF1 harboring an optic pathway tumor[15,45]. The lifetime incidence of brainstem gliomas in NF1 is 4%, with presentation typically before the age of 10 years[46].

NF1 carries a high risk of tumorigenesis because it is a RASopathy. Therefore, we recommend examination by MRI, avoiding radiological CT scans, especially in childhood. CT is too low resolution to evaluate UBOs and other small tumors, and repeated follow-up examination by this method is not recommended because of the need to minimize radiation exposure in children that are already at risk of tumorigenesis. However, it is still controversial to examine routine screening of MRI for early identification of optic glioma in patients with NF1 in recent reports[6,18,30,47,48]. We need to perform semiological and behavioral observations in NDD, examine electroencephalograms in epilepsy, and perform careful systemic physical examinations—especially by palpation around the abdomen and back. Along with these evaluations of the various complications of NF1, we can consider genetic analysis of the patients in cooperation with medical geneticists and genetic counselors. To elucidate phenotype-genotype relationships in NF1, we need to accumulate gene analysis data and conduct further studies with appropriate and accurate genetic counseling. In this study our research was limited by its retrospective nature.

A larger study in Japan is required in the future to predict accurately the prognosis of these patients, especially regarding the development of malignant optic glioma and other tumors. We conclude that NF1 patients should be examined by MRI and genetic analysis during follow-up; this is especially true for those with suspected moderate to severe neurological complications. We need to

accumulate more genotypic information on Japanese patients with NF1 to elucidate the genotype-phenotype relationship.

Acknowledgments

All authors have no COI to declare regarding the present study.

We thank Emeritus Prof. Haruo Shintaku, Dr. Satoru Sakuma, Dr. Tomoyuki Kawamura, and Dr. Sadao Tokimasa from our Department of Pediatrics; Clinical Prof. Hiroaki Sakamoto and Dr. Takehiro Uda from our Department of Neurosurgery, who followed up some of the patients with NF1.

We also thank Ms. Yukiko Okayama, clinical technologist in the Clinical Laboratory at Osaka City University Hospital; Ms. Tomoko Sakaguchi and Ms. Noriko Nakano, technical assistants in the Department of Pediatrics; and members of the research support platform at Osaka City University Graduate School of Medicine.

This study was supported by research funds of program for integrated database of clinical and genomic information from the Japan Agency for Medical Research and Development (JP18kk0205002).

Kanako Yamashita, and Toshiyuki Seto mainly followed the patients and wrote the first draft of this manuscript. No honorarium, grant, or other form of payment was received to produce this paper. Takao Hoshina and Norikatsu Hikita performed various examinations of NF1 and helped with the study. Takashi Hamazaki helped with the study and gave advice. Taro Shimono mainly evaluated MRI studies of the patients as a neuroradiologist. Kazuyoshi Fukai mainly followed the patients as a dermatologist. Toshiki Takenouchi, Tomoko Uehara, and Kenjiro Kosaki performed genetic analyses and gave advice on the study. Hideyuki Saya gave us the opportunity to start the study. Toshiyuki Seto designed and supervised all the research.

Part of this report was presented by K. Yamashita et al at the 7th annual meeting of the Japanese Society of Recklinghausen Disease, Tokyo, Japan, on 29 November 2015. Another part of this study was presented by K. Fujita et al at the annual meeting of the American Society of Human Genetics, Orlando, FL, USA, from 17 to 21 October 2017.

References

1. Sahin M. Neurofibromatosis. In: Kliegman R, Stanton BF, St Geme JW, Schor NF, Behrman RE, Nelson WE, editors. Nelson textbook of pediatrics.20 ed. Philadelphia: Elsevier/Saunders; 2016. pp. 2874-2877.
2. Thiele EA, Korf BR. Phakomatoses and Allied Conditions. In: Swaiman KF, Ashwal S, Ferrieo DM et al, editors. Pediatric neurology. 5 ed. Philadelphia: Elsevier/Saunders; 2012. pp. 497-502.
3. Maria BL, Menkes JH. Neurocutaneous syndromes. In: Menkes JH, Sarnat HB, Maria BL, editors. Child Neurology. 7 ed.: Lippincott Williams & Willkins; 2005. pp. 803-809.
4. Hamosh A, McInnes RR, Nussbaum RL, et al. Clinical Case Studies Illustrating Genetic Principle. In : Nussbaum RL, McInnes RR, Willard HF. editors. Thompson & Thompson Genetics in Medicine E-Book. 8 ed: Elsevier Health Sciences; 2015. pp. 993-996.
5. Lammert M, Friedman JM, Kluwe L, et al. Prevalence of neurofibromatosis 1 in German children at elementary school enrollment. Arch Dermatol 2005;141:71-74.
6. Gutmann DH, Ferner RE, Listernick RH, et al. Neurofibromatosis type 1. Nat Rev Dis Primers 2017;3:17004.
7. Neurofibromatosis. Conference statement. National Institutes of Health Consensus Development Conference. Arch Neurol 1988;45:575-578.
8. Ars E, Kruyer H, Morell M, et al. Recurrent mutations in the NF1 gene are common among neurofibromatosis type 1 patients. J Med Genet 2003;40:e82.
9. Zhang J, Tong H, Fu X, et al. Molecular characterization of NF1 and neurofibromatosis type 1 genotype-phenotype correlations in a Chinese population. Sci Rep 2015;5:11291.
10. Vezina G, Barkovich AJ. The Phakomatoses. In:Barkovich AJ, Raybaud C. editors. Pediatric Neuroimaging. 5

ed. Lippincott Williams & Willkins; 2012. pp. 569-588.
11. Sellmer L, Farschtschi S, Marangoni M, et al. Non-optic glioma in adults and children with neurofibromatosis 1. Orphanet J Rare Dis 2017;12:34.
12. Rodriguez FJ, Perry A, Gutmann DH, et al. Gliomas in neurofibromatosis type 1: a clinicopathologic study of 100 patients. J Neuropathol Exp Neurol 2008;67:240-249.
13. Listernick R, Charrow J, Greenwald MJ, et al. Optic gliomas in children with neurofibromatosis type 1. J pediatr 1989;114:788-792.
14. Listernick R, Louis DN, Packer RJ, et al. Optic pathway gliomas in children with neurofibromatosis 1: consensus statement from the NF1 Optic Pathway Glioma Task Force. Ann Neurol 1997;41:143-149.
15. Lewis RA, Gerson LP, Axelson KA, et al. von Recklinghausen Neurofibromatosis: Ⅱ. Incidence of optic gliomata. Ophthalmology 1984;91:929-935.
16. Evans DG, Baser ME, McGaughran J, et al. Malignant peripheral nerve sheath tumours in neurofibromatosis 1. J Med Genet 2002;39:311-314.
17. Opocher G, Conton P, Schiavi F, et al. Pheochromocytoma in von Hippel-Lindau disease and neurofibromatosis type 1. Fam Cancer 2005;4:13-16.
18. Ferner RE, Huson SM, Thomas N, et al. Guidelines for the diagnosis and management of individuals with neurofibromatosis 1. J Med Genet 2007;44:81-88.
19. Wallace MR, Marchuk DA, Andersen LB, et al. Type 1 neurofibromatosis gene: identification of a large transcript disrupted in three NF1 patients. Science 1990;249:181-186.
20. Bianchessi D, Morosini S, Saletti V, et al. 126 novel mutations in Italian patients with neurofibromatosis type 1. Mol Genet Genomic Med 2015;3:513-525.
21. Koczkowska M, Chen Y, Callens T, et al. Genotype-phenotype correlation in NF1: evidence for a more severe phenotype associated with missense mutations affecting NF1 codons 844-848. Am J Hum Genet 2018;102:69-87.
22. Hirabaru K, Matsuo M. Neurological comorbidity in children with neurofibromatosis type 1. Pediatr Int 2018; 60:70-75.
23. Seto T, Kono K, Morimoto K, et al. Brain magnetic resonance imaging in 23 patients with mucopolysaccharidoses and the effect of bone marrow transplantation. Ann Neurol 2001;50:79-92.
24. Seto T, Takesada H, Matsushita N, et al. Twelve-year-old girl with intracranial epidural abscess and sphenoiditis. Brain Dev 2014;36:359-361.
25. Anderson JL, Gutmann DH. Chapter 4 - Neurofibromatosis type 1. In: Islam MP, Roach ES, editors. Handbook of Clinical Neurology: Elsevier; 2015. pp. 75-86.
26. Maruoka R, Takenouchi T, Torii C, et al. The use of next-generation sequencing in molecular diagnosis of neurofibromatosis type 1: a validation study. Genet Test Mol Biomarkers 2014;18:722-735.
27. Yagihashi T, Torii C, Takahashi R, et al. Clinical utility of an array comparative genomic hybridization analysis for Williams syndrome. Congenit Anom (Kyoto) 2014;54:225-227.
28. Messiaen L, Yao S, Brems H, et al. Clinical and mutational spectrum of neurofibromatosis type 1–like syndrome. JAMA 2009;302:2111-2118.
29. Yoshida Y, Ehara Y, Koga M, et al. Epidemiological analysis of major complications requiring medical intervention in patients with neurofibromatosis 1. Acta Derm Venereol 2018;98:753-756.
30. North K, Riccardi V, Samango-Sprouse C, et al. Cognitive function and academic performance in neurofibromatosis. 1: consensus statement from the NF1 Cognitive Disorders Task Force. Neurology 1997; 48:1121-1127.
31. Kulkantrakorn K, Geller TJ. Seizures in neurofibromatosis 1. Pediatr Neurol 1998;19:347-350.
32. Camfield P, Camfield C. Incidence, prevalence and aetiology of seizures and epilepsy in children. Epileptic Disord 2015;17:117-123.
33. Ballester R, Marchuk D, Boguski M, et al. The NF1 locus encodes a protein functionally related to mammalian GAP and yeast IRA proteins. Cell 1990;63:851-859.
34. Cawthon RM, Weiss R, Xu G, et al. A major segment of the neurofibromatosis type 1 gene: cDNA sequence, genomic structure, and point mutations. Cell 1990;62:193-201.
35. Kehrer-Sawatzki H, Mautner VF, Cooper DN. Emerging genotype-phenotype relationships in patients with large NF1 deletions. Hum Genet 2017;136:349-376.
36. Upadhyaya M, Huson SM, Davies M, et al. An absence of cutaneous neurofibromas associated with a 3-bp inframe deletion in exon 17 of the NF1 gene (c.2970-2972 delAAT): evidence of a clinically significant NF1 genotype-phenotype correlation. Am J Hum Genet 2007;80:140-151.
37. Pinna V, Lanari V, Daniele P, et al. p.Arg1809Cys substitution in neurofibromin is associated with a distinctive NF1 phenotype without neurofibromas. Eur J Hum Genet 2015;23:1068-1071.

38. Rojnueangnit K, Xie J, Gomes A, et al. High incidence of noonan syndrome features including short stature and pulmonic stenosis in patients carrying NF1 missense mutations affecting p.Arg1809: genotype-phenotype correlation. Hum Mutat 2015;36:1052-1063.
39. Xu M, Xiong H, Han Y, et al. Identification of mutation regions on *NF1* responsible for high- and low-risk development of optic pathway glioma in neurofibromatosis type I. Front Genet 2018;9:270.
40. Toonen JA, Anastasaki C, Smithson LJ, et al. NF1 germline mutation differentially dictates optic glioma formation and growth in neurofibromatosis-1. Hum Mol Genet 2016;25:1703-1713.
41. Hamosh A, McInnes RR, Nussbaum RL, et al. Types of mutations and their consequences. In : Nussbaum RL, McInnes RR, Willard HF. editors. Thompson & Thompson Genetics in Medicine E-Book. 8 ed: Elsevier Health Sciences; 2015. pp. 125-128.
42. Kluwe L, Friedrich RE, Korf B, et al. NF1 mutations in neurofibromatosis 1 patients with plexiform neurofibromas. Hum Mutat 2002;19:309.
43. Ratner N, Miller SJ. A RASopathy gene commonly mutated in cancer: the neurofibromatosis type 1 tumour suppressor. Nat Rev Cancer 2015;15:290-301.
44. Abramowicz A, Gos M. Neurofibromin in neurofibromatosis type 1 - mutations in NF1 gene as a cause of disease. Dev Period Med 2014;18:297-306.
45. Listernick R, Charrow J, Greenwald MJ, et al. Optic gliomas in children with neurofibromatosis type 1. J Pediatr 1989;114:788-792.
46. Molloy PT, Bilaniuk LT, Vaughan SN, et al. Brainstem tumors in patients with neurofibromatosis type 1. a distinct clinical entity. Neurology 1995;45:1897-1902.
47. Listernick R, Charrow J, Greenwald M. Emergence of optic pathway gliomas in children with neurofibromatosis type 1 after normal neuroimaging results. J pediatr 1992;121:584-587.
48. King A, Listernick R, Charrow J, et al. Optic pathway gliomas in neurofibromatosis type 1: the effect of presenting symptoms on outcome. Am J Med Genet A. 2003;122A:95-99.

Osaka City Med. J. Vol. 65, 55-63, 2019

Change in the Thickness of Retinal Layers after Selective Retina Therapy (SRT) in Patients with Central Serous Chorioretinopathy

Kumiko Hirayama[1)], Manabu Yamamoto[1)], Takeya Kohno[1)], Dirk Theisen-Kunde[2)], Ralf Brinkmann[2,3)], Yoko Miura[2-4)], and Shigeru Honda[1)]

Department of Ophthalmology and Visual Science[1)], Osaka City University Graduate School of Medicine; Medical Laser Center Luebeck[2)]; and Institute of Biomedical Optics[3)] and Department of Ophthalmology[4)], University of Luebeck

Abstract

Background

To investigate retinal thickness after selective retina therapy (SRT) for central serous chorioretinopathy (CSC) and the factors related to visual prognosis.

Methods

This retrospective study examined 23 eyes of 21 consecutive patients (17 males, 4 females) with CSC and followed-up for >6 months. A SRT (Q-switched Nd:YLF laser, 527 μm, pulse duration 1.7 μs, 30 pulses per irradiation spot with a frequency of 100 Hz) was used for the treatment. The need for re-treatment was judged every three months after the initial treatment. The best corrected visual acuity (BCVA) and central macular thickness (CMT) were compared among pre-treatment, at the time of resolution, and at final follow-up examination. Furthermore, the inner retinal thickness (IRT) and outer retinal thickness (ORT) at the time of resolution and at final follow-up, and their rates of change were also investigated.

Results

Final BCVA improved (logMAR: from 0.01±0.22 to −0.10±0.15) and the CMT decreased (from 336±78 μm to 185±28 μm) significantly after SRT compared with pre-treatment. The IRT did not change from the time at resolution to the final examination, while the ORT increased significantly during this time period (from 77±11 μm to 86±10 μm). A stepwise regression analysis identified that the pre-treatment BCVA and the rate of ORT increase have a significant positive correlation with the final BCVA.

Conclusions

SRT may improve final visual acuity of the patient of CSC, which is accompanied by the increase in the thickness of the outer retinal layer shortly after the resolution of subretinal fluid.

Received September 12, 2018; accepted November 27, 2018.
Correspondence to: Manabu Yamamoto, MD.
Department of Ophthalmology and Visual Sciences, Osaka City University Graduate School of Medicine, 1-4-3 Asahimachi, Abeno-ku, Osaka 545-8585, Japan
Tel: +81-6-6645-3867; Fax: +81-6-6645-3873
E-mail: manabun@msic.med.osaka-cu.ac.jp

Key Words: Laser therapy; Central serous chorioretinopathy; Retina; Subretinal fluid

Introduction

Central serous chorioretinopathy (CSC) is accompanied by subretinal fluid (SRF) of the macular region, and can lead to reduced visual acuity, metamorphopsia, micropsia, central scotoma, and decreased contrast sensitivity, etc[1,2]. It is a disease that can be expected to resolve spontaneously within a few months, with a good prognosis for visual acuity. However, there are some cases in which SRF is long-standing, which often develop irreversible damage to the neurosensory retina and retinal pigment epithelium (RPE), sometimes with permanent sequelae[3-5].

Selective retina therapy (SRT) was developed as a laser procedure in which the RPE cells are selectively disrupted without affecting the neural retina or choroid[6-8]. In this procedure, a microsecond pulsed laser is used to induce an instantaneous increase in the temperature of just at the melanosomes in the RPE. When exceeding the vaporization temperature microbubbles around the melanosomes occur, resulting in a temporary expansion of the volume of the cells that causes mechanical disruption of the RPE cells. Due to the spatial and temporal thermal confinement through the laser pulse shorter than the thermal relaxation time of the RPE, there is no significant temperature increase in the surrounding tissues which might cause thermal damage[9,10].

SRT is known to be effective for CSC, diabetic macular edema (DME), and prolonged SRF after retinal detachment[11-17]. The therapeutic mechanism of SRT is to disrupt diseased RPE cells and promote the regrowth of the surrounding healthy ones. We previously reported the safety of SRT for CSC using microperimetry up to 3 months after treatment[17]. Although it is known that SRT is effective in the short term to resolve subretinal fluid for CSC, there has been no study on the factors related to visual acuity after SRT. The current study aimed to observe the retinal thickness after SRT in detail and to investigate factors related to visual prognosis.

Methods

This retrospective study examined 23 eyes of 21 consecutive patients (17 males, 4 females) diagnosed with CSC and followed-up for more than 6 months at Osaka City University Hospital during the study period from July 2011 to July 2013. The average patient age was 48.1 years (range, 29 to 67 years). The basic clinical data of all patients are shown in Table 1.

The inclusion criteria were as follows: (1) minimum age of 20 years; (2) subjective symptoms of central scotoma, metamorphopsia, or decline of visual acuity; (3) history of more than 3 months with no sign of improvement of CSC [diagnosed with optical coherence tomography (OCT)]; (4) presence of SRF on OCT; (5) presence of active leakage on fluorescence angiography (FA); and (6) SRF disappeared within 1 year after the last SRT, and no recurrence occurred for more than 3 months after resolution of SRF.

The exclusion criteria were as follows: (1) having another retinal disease; (2) having a condition associated with choroidal neovascularization; (3) prior history of another therapy such as PDT or local retinal photocoagulation within the past 6 months; (4) having a systemic inflammatory disease; (5) haemorrhagic diathesis or taking anticoagulants; (6) having a systemic disease such as untreated hypertension or diabetes mellitus; or (7) pregnant or possibly pregnant.

SRT laser

This study was approved by the Institutional Review Board (IRB) of the University hospital (No.

Table 1. Patient characteristics before treatment

Characteristics	
Number of patients	21 Cases (23 eyes)
Sex (Cases; eyes)	Male 17; 19, Female 4; 4
Age; Mean (Range)	48.1 (29-67)
Number of episodes (%)	
First	13 (56.5)
Second or more	10 (43.5)
Characteristics of leakage in FA (%)	
Focal leakage	18 (78.3)
Diffuse leakage	5 (21.7)
Duration of symptom (months); Median (Range)	6 (3-24)
Pretreatment BCVA (logMAR); Mean (Range)	0.03 (−0.30-0.70)
Pretreatment CMT (μm); Mean (Range)	336.0 (226-475)

FA, fluorescein angiography; BCVA, best corrected visual acuity; logMAR, logarithm of the minimum angle of resolution; and CMT, central macular thickness.

2009 and 2421), based on the Declaration of Helsinki, and was registered with University Hospital Medical Information Network (UMIN) (No. 000005396). Written informed consent was acquired from all patients. The SRT laser system used was developed by the Medical Laser Center Lübeck (Lübeck, Germany). The laser itself is a Q-switched Nd:YLF-laser (wavelength 527 nm) with a pulse duration of 1.7 μs, which applies 30 pulses per irradiation spot with a frequency of 100 Hz. A Mainster central field contact lens with a magnifying power of 1.05 was used and adjusted so that the spot size on the retina is 200 μm.

The induced thermomechanical cell damage is not ophthalmoscopically visible during SRT, therefore the generation of microbubbles in the RPE cells and the subsequent RPE cell destruction were inferred from the ultrasonic wave being induced from the microbubble expansion. These ultrasonic waves were measured with a transducer embedded in the contact lens. This signal was processed by a software algorithm to compute an optoacoustic value (OA value) as reported earlier by Yasui et al[17], which serves as an indicator for microbubble formation and thus cell disruption.

After performing visual acuity testing, slit-lamp microscopy, OCT, and fundus autofluorescence, test irradiations were conducted around vascular arcades upper or lower part of the macula in order to decide the range of treatment laser energy. The test irradiation was performed with the energy started at 60 μJ, followed by increases with 20-μJ increments, until the OA value reached several hundred. After test irradiations, FA and Indocyanine Green Angiography (IA) were performed, and leakage from the test irradiation sites was confirmed. The main laser treatment was initiated with the lowest energy level at which leakage was observed in test irradiation. If the OA value is low during treatment, the treatment energy was adjusted such that the OA value might be around several hundred. Following the main treatment, FA was repeated, and after confirming the increase of fluorescein leaks from the treated region, the treatment was concluded.

The need for re-treatment was judged every three months after the initial treatment. If OCT showed residual SRF in the macular region, FA was conducted, and the presence or absence of

fluorescein leaks was confirmed. If fluorescein leaks were present, the leakage site was irradiated with intervals of 2 to 3 spots' diameter, whereas the SRF region was diffusely irradiated in the same manner if no clear leakage points were observed.

Clinical examinations

Best corrected visual acuity (BCVA) and central macular thickness (CMT) were compared among three points in time; before treatment, at the time of resolution, and at the final follow-up examination. The resolution time was defined as the complete disappearance of the SRF on OCT. The time point of the final follow-up examination was at least 3 months after SRF resolution. As for BCVA, decimal visual acuity was measured and converted to logarithm of the minimum angle of resolution (logMAR) for analysis. CMT, defined as the thickness of the retina in the central area, was measured by OCT using a Heidelberg SPECTRALIS® (Heidelberg Engineering GmbH, Heidelberg, Germany). On the OCT images from the time of resolution and final follow-up, the installed image processing software was used to carry out intraretinal segmentation by dividing the retina into two layers, an inner layer and an outer layer, with the external limiting membrane as the dividing line, and their thickness were then compared. The associations between final BCVA and sex, age, recurrent or de novo CSC, time period of subjective symptoms, time required for resolution, visual acuity, and CMT as pretreatment factors, and with inner retinal thickness (IRT) and outer retinal thickness (ORT) at the time of resolution and at final follow-up and their rates of change as post-treatment factors were investigated (Fig. 1). Factors for which $p<0.20$ on single correlation analysis were entered into multivariate analysis by stepwise regression analysis.

Statistical analysis

Differences in BCVA were tested using Wilcoxon's signed-rank test for significance, and differences

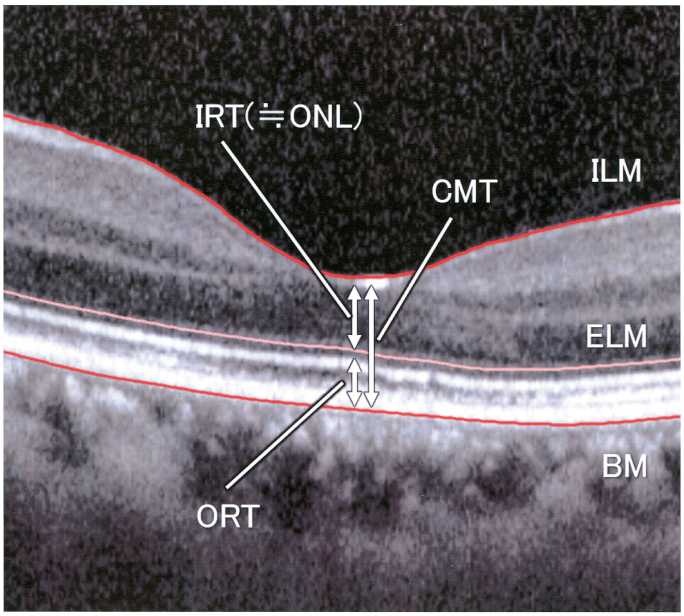

Figure 1. A horizontal scan of spectral domain optic coherence tomography (SD-OCT) through the central fovea. Central macular thickness (CMT) is defined as the distance between the surface of the inner limiting membrane (ILM) and the inner border of the Bruch's membrane (BM) at the central fovea. Inner retinal thickness (IRT) is measured as the distance between the outer border of the ILM and the inner border of the external limiting membrane (ELM). IRT is almost the same as outer nuclear layer (ONL) at fovea. Outer retinal thickness (ORT) is measured as the distance between the outer border of the ELM and the inner border of the BM.

in CMT, IRT, and ORT were tested using a paired t-test. Correlations were investigated using Pearson's correlation coefficient for pairs of normally distributed variables and Spearman's rank correlation coefficient for non-normally distributed variables. Associations with sex and recurrence status were tested using the Mann-Whitney U test. When comparing three groups, a paired t-test was performed for every pair of group, and the p values were adjusted using the False Discovery Rate method. The statistical software used was IBM® SPSS® Statistics 24.0 (IBM Japan, Ltd., Tokyo, Japan), and $p<0.05$ was regarded as significant.

Results

The number of test irradiations required for initial treatment ranged from 4-12 (mean 7.8), and the number of irradiations required for the main laser treatment ranged from 2-17 (mean 7.0). The irradiation energy used in initial treatment ranged from 62-184 μJ (median 116 μJ), and the OA value was 54-6455 (median 225). The number of SRT sessions required until SRF resolution was 1-3 (mean 1.3). The time from initial treatment to resolution was 1-12 months (median 1 month), and the time from resolution to final follow-up was 3-6 months (median 4 months). A representative case of CSC is shown in Figure 2.

Mean BCVA (logMAR) was 0.01±0.22 pre-treatment, −0.04±0.20 at the time of resolution, and −0.10±0.15 at final follow-up, with significant differences between the values at final follow-up and

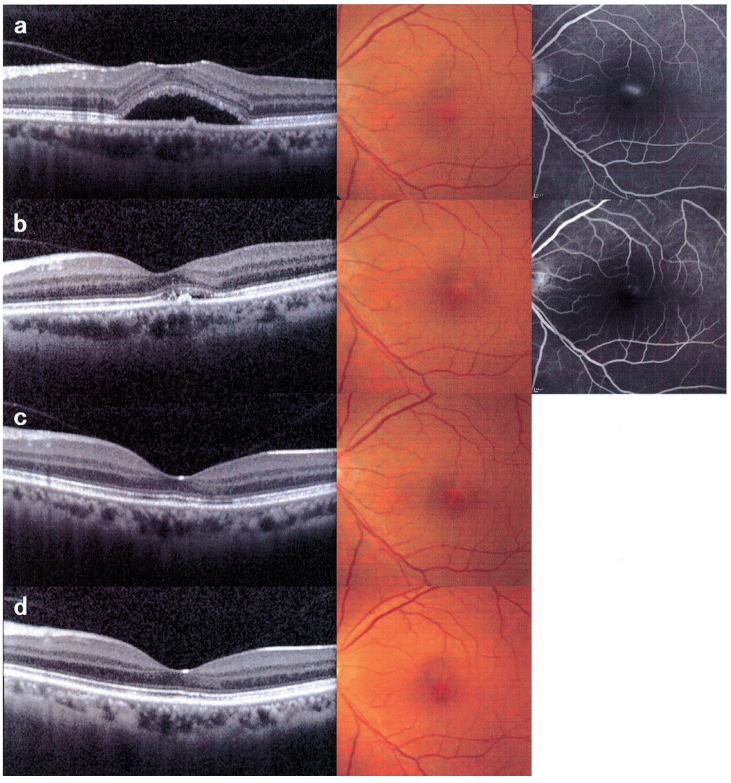

Figure 2. A representative case of central serous chorioretinopathy (CSC). Horizontal scan of optic coherence tomography (OCT) (left), color fundus image (center) and fluorescein angiography (FA) (right) of pretreatment (a), 3 months after SRT (b), resolution of SRF at 6 month (c), and final follow-up (at 12 month) (d). Subretinal fluid (SRF) decreased and the leakage on FA disappeared at 3 months follow-up after SRT (b), followed by the SRF disappearance at 6 months (c). At 12 months follow-up after SRT, there is no recurrence, and the outer retinal thickness was increased from 77 μm to 86 μm (d).

those both pre-treatment and at the time of resolution (pre-treatment vs final follow-up $p<0.01$, resolution vs final follow-up $p<0.01$) (Fig. 3).

Mean CMT was 336±78 μm pre-treatment, 175±25 μm at resolution, and 185±28 μm at final follow-up, with significant differences between all three time points (pretreatment vs resolution, $p<0.001$; pretreatment vs final follow-up, $p<0.001$; resolution vs final follow-up, $p<0.001$) (Fig. 4). There was no significant difference between IRT during at resolution (97±21 μm) and at final follow-up (98±24 μm; $p=0.45$), whereas ORT showed a significant increase, where it was 77±11 μm at resolution and 86±10 μm at final follow-up ($p<0.001$) (Fig. 5).

Single correlation analysis identified pre-treatment BCVA, IRT at resolution, and the rates of change of IRT and ORT between at resolution and at final examination as significant factors

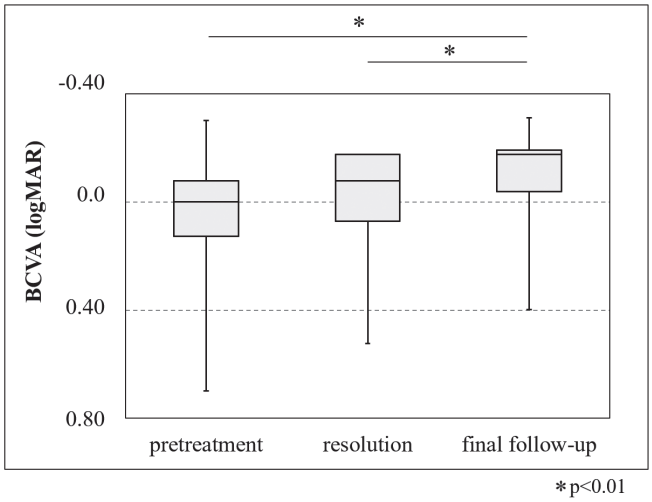

Figure 3. Box plots for the time course of best corrected visual acuity (BCVA) (logMAR). Mean BCVA was 0.01±0.22 pre-treatment, −0.04±0.20 at the time of resolution, and −0.10±0.15 at final follow-up, with significant improvement between each time point toward the final follow-up.

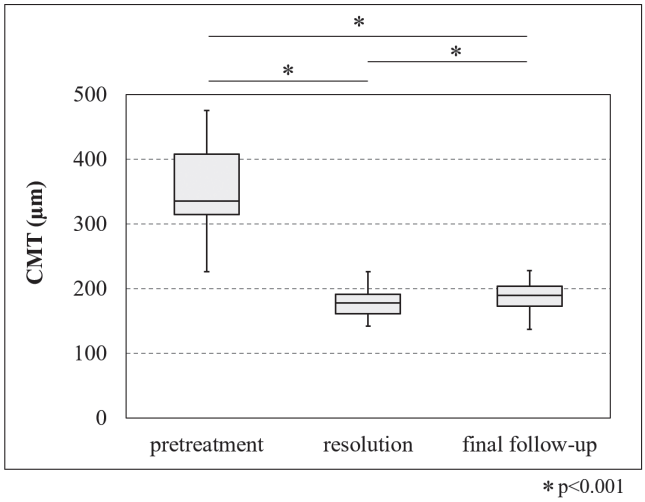

Figure 4. Box plots for the time course of central macular thickness (CMT). Mean CMT was 336±78 μm pre-treatment, 175±25 μm at resolution, and 185±28 μm at final follow-up, with significant differences between all three time points.

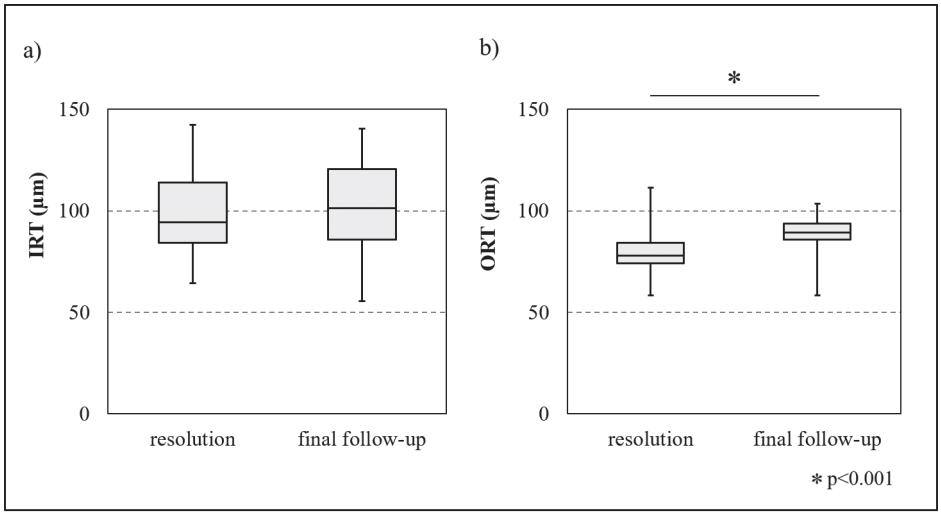

Figure 5. Box plots for the time course of inner retinal thickness (IRT) (a) and outer retinal thickness (ORT) (b). There was no significant difference of IRT between at the time of resolution (97±21 μm) and at final follow-up (98±24 μm), whereas ORT showed a significant difference, where it was 77±11 μm at the time of resolution and 86±10 μm at final follow-up.

Table 2. Univariate analysis of factors associated with final BCVA

variables	r, ρ	p value
Pretreatment		
Sex*1	-	0.50
Age*2	0.07	0.75
Recurrence*1	-	0.87
Duration of symptom*2	0.09	0.69
Pretreatment BCVA*3	0.84	<0.001
Pretreatment CMT*3	−0.283	0.19
Resolution		
Disappearance time of SRF*2	0.23	0.30
Inner retinal thickness*3	−0.45	0.03
Outer retinal thickness*3	−0.39	0.07
Final follow-up		
Δ Inner retinal thickness*3	−0.44	0.03
Δ Outer retinal thickness*3	−0.63	<0.001

*1: Mann-Whitney U test. *2: Spearman's rank correlation coefficient. *3: Pearson's correlation coefficient. BCVA, best corrected visual acuity; CMT, central macular thickness; and SRF, subretinal fluid.

Table 3. Multivariate analysis of factors associated with final BCVA

variables	B	SE B	β	p value
BCVA	0.49	0.12	0.66	0.01
Δ Outer retinal thickness	−0.75	0.31	−0.37	0.03
R^2 0.78				

SE, standard error; and BCVA, best corrected visual acuity.

associated with final BCVA (Table 2). Stepwise regression analysis of factors for which $p<0.20$ identified significant associations with pre-treatment BCVA and the rate of change of ORT (Table 3).

Discussion

The persistence of SRF is known to cause structural changes in the neuroretina and RPE that undoubtedly affect the prognosis for visual acuity. Atrophy of the subfoveal RPE and cystoid macular degeneration have been implicated in causing the serious loss of vision that occurs in chronic CSC[1,2]. However, more than that, the thickness of the outer nuclear layer (ONL) after resolution of SRF is also considered to be one of the important determining factors for visual prognosis[18,19]. When SRF persists long-term, extension of the photoreceptor outer segment and thinning of the ONL are known to occur[20,21]. Regarding the retina of the patients with resolved CSC, Nakamura et al reported that the cone density (cell density in the ONL) measured with adaptive optics fundus camera is significantly decreased, which is associated with the decrease of the ORT and visual acuity[22]. In cases of protracted SRF treated by photo dynamic therapy (PDT), the thickening of the ONL after treatment is reportedly positively associated with the better visual prognosis after SRF resolution[18,19,23,24]. These changes after SRF resolution following PDT include the improvement of the visibility of the ellipsoid zone and the ONL increasing in thickness. In the present study, IRT, which is almost the same as the range of the ONL at fovea, did not change significantly during post-resolution follow-up, but the ORT increased significantly. In the detailed correlation analysis it was also shown that the thickness increase of the ORT after treatment is positively correlated to the visual prognosis, not of the IRT, which is not consistent with the previous reports. As the reason of it, some possibility can be discussed; First, it might be just because the short observation period in this study. Secondly, it may lie on the difference in the therapeutic mechanism between PDT and SRT. Namely, it would be hypothesized that SRT might promote the restoration of photoreceptors outer segment (the main component of the ORT), better or at least earlier, than after PDT. However, as there are still no comparison studies, further investigation is necessary to evaluate the changes in retinal thickness after different therapies.

The limitations of this study include its nature as a retrospective study, its small sample size, the comparatively short follow-up period of 3-6 months after SRF resolution, and the fact that patients with recurrent or persistent SRF were excluded. If patients can be maintained long-term without SRF recurrence, further changes in retinal structure might occur. The effect of recurrent or persistent SRF must also be taken into account in the case of long-term follow-up.

In conclusion, SRT may improve final visual acuity significantly, and this improvement was associated with two factors: pretreatment visual acuity and the rate of change in ORT. Although CSC is a disease with a high tendency to heal spontaneously, the persistent SRF can cause the morphological changes in the neuroretina as well as of the RPE, which has been shown to associate with the decreasing visual acuity. Therefore, its earlier resolution needs to be prioritized to preserve the retinal structure and the long-term visual acuity of patients with CSC.

Acknowledgments

All authors have no COI to declare regarding the present study.

References

1. Yannuzzi LA, Shakin JL, Fisher YL, et al. Peripheral retinal detachments and retinal pigment epithelial atrophic tracts secondary to central serous pigment epitheliopathy. Ophthalmology 1984;91:1554-1572.
2. Spaide RF, Campeas L, Haas A, et al. Central serous chorioretinopathy in younger and older adults. Ophthalmology 1996;103:2070-2080.
3. Loo RH, Scott IU, Flynn HW Jr, et al. Factors associated with reduced visual acuity during long-term follow-up of patients with idiopathic central serous chorioretinopathy. Retina 2002;22:19-24.
4. Piccolino FC, de la Longrais RR, Ravera G, et al. The foveal photoreceptor layer and visual acuity loss in central serous chorioretinopathy. Am J Ophthalmol 2005;139:87-99.
5. Imamura Y, Fujiwara T, Spaide RF. Fundus autofluorescence and visual acuity in central serous chorioretinopathy. Ophthalmology 2011;118:700-705.
6. Roider J, Liew SH, Klatt C, et al. Selective retina therapy (SRT) for clinically significant diabetic macular edema. Graefes Arch Clin Exp Ophthalmol 2010;248:1263-1272.
7. Brinkmann R, Roider J, Birngruber R. Selective retina therapy (SRT): a review on methods, techniques, preclinical and first clinical results. Bull Soc Belge Ophtalmol 2006;(302):51-69.
8. Roider J, Brinkmann R, Wirbelauer C, et al. Retinal sparing by selective retinal pigment epithelial photocoagulation. Arch Ophthalmol 1999;117:1028-1034.
9. Schuele G, Elsner H, Framme C, et al. Optoacoustic real-time dosimetry for selective retina treatment. J Biomed Opt 2005;10:064022.
10. Neumann J, Brinkmann R. Boiling nucleation on melanosomes and microbeads transiently heated by nanosecond and microsecond laser pulses. J Biomed Opt 2005;10:024001.
11. Park YG, Kim JR, Kang S, et al. Safety and efficacy of selective retina therapy (SRT) for the treatment of diabetic macular edema in Korean patients. Graefes Arch Clin Exp Ophthalmol 2016;254:1703-1713.
12. Roider J, Liew SH, Klatt C, et al. Selective retina therapy (SRT) for clinically significant diabetic macular edema. Graefes Arch Clin Exp Ophthalmol 2010;248:1263-1272.
13. Koinzer S, Elsner H, Klatt C, et al. Selective retina therapy (SRT) of chronic subfoveal fluid after surgery of rhegmatogenous retinal detachment: three case reports. Graefes Arch Clin Exp Ophthalmol 2008;246:1373-1378.
14. Kang S, Park YG, Kim JR, et al. Selective retina therapy in patients with chronic central serous chorioretinopathy: a pilot study. Medicine (Baltimore) 2016;95:e2524.
15. Elsner H, Pörksen E, Klatt C, et al. Selective retina therapy in patients with central serous chorioretinopathy. Graefes Arch Clin Exp Ophthalmol 2006;244:1638-1645.
16. Framme C, Walter A, Berger L, et al. Selective retina therapy in acute and chronic-recurrent central serous chorioretinopathy. Ophthalmologica 2015;234:177-188.
17. Yasui A, Yamamoto M, Hirayama K, et al. Retinal sensitivity after selective retina therapy (SRT) on patients with central serous chorioretinopathy. Graefes Arch Clin Exp Ophthalmol 2017;255:243-254.
18. Matsumoto H, Sato T, Kishi S. Outer nuclear layer thickness at the fovea determines visual outcomes in resolved central serous chorioretinopathy. Am J Ophthalmol 2009;148:105-110.
19. Van Rijssen TJ, Mohabati D, Dijkman G, et al. Correlation between redefined optical coherence tomography parameters and best-corrected visual acuity in non-resolving central serous chorioretinopathy treated with half-dose photodynamic therapy. PLoS One 2018;13:e0202549.
20. Matsumoto H, Kishi S, Otani T, et al. Elongation of photoreceptor outer segment in central serous chorioretinopathy. Am J Ophthalmol 2008;145:162-168.
21. Ozdemir I, Eren A, Ersöz G. Outer nuclear layer thickness at the central fovea relation with symptom duration in central serous chorioretinopathy. Int Ophthalmol 2018;18:doi:10.1007/s10792-018-0950-y.
22. Nakamura T, Ueda-Consolvo T, Oiwake T, et al. Correlation between outer retinal layer thickness and cone density in patients with resolved central serous chorioretinopathy. Graefes Arch Clin Exp Ophthalmol 2016; 254:2347-2354.
23. Hua L, Lin B, Hong J, et al. Clinical research on one-third dose verteporfin photodynamic therapy in the treatment of chronic central serous chorioretinopathy. Eur Rev Med Pharmacol Sci 2018;22:278-284.
24. Ohkuma Y, Hayashi T, Sakai T, et al. One-year results of reduced fluence photodynamic therapy for central serous chorioretinopathy: the outer nuclear layer thickness is associated with visual prognosis. Graefes Arch Clin Exp Ophthalmol 2013;251:1909-1917.

Osaka City Med. J. Vol. 65, 65-76, 2019

Assessment of Dual-time-point ^{18}F-fluorodeoxyglucose-Positron Emission Tomography/Computed Tomography Imaging of Malignant Tumors Using Visually and Semiquantitatively: What Kind of Tumors is Useful?

Hirotaka Seura[1)], Terue Okamura[1)], Koichi Koyama[2)], and Yutaka Masuoka[3)]

PET center[1)], Osaka Saiseikai Nakatsu Hospital;
Department of Diagnostic and Interventional Radiology[2)], Osaka City University Graduate School of Medicine; and Department of Radiology[3)], Osaka Prefectural Medical Center for Respiratory and Allergic Diseases

Abstract

Background

To retrospectively evaluate the effectiveness of dual-time-point imaging ^{18}F-fluorodeoxyglucose-positron emission tomography/computed tomography in assessing various malignant tumors at our hospital.

Methods

This study included 1153 patients who underwent dual-time-point imaging from November 2009 to October 2011 (702 males, 451 females), including 1211 histopathologically diagnosed malignant lesions. Early and delayed images were acquired at 1 and 2 h after intravenous injection, respectively. Fluorodeoxyglucose-positron emission tomography/computed tomography images were evaluated visually and semiquantitatively.

Results

According to visual analysis, abnormal uptake was detected in 1032 and 1096 lesions among all tumors, and 362 and 416 among 526 small tumors (diameter <3 cm) in early and delayed images, respectively. On delayed images, abnormal uptake was detected in all lesions showing abnormal uptake in early images, and 64 additional lesions among all tumors and 54 additional lesions among small tumors that had not been detected in early images. Tumors detected in delayed images and not in early images included laryngeal, bile duct, pancreatic, uterine cervical and uterine corpus cancers. In semiquantitative analysis, maximum standardized uptake values differed significantly between early and delayed images in both all tumors and small tumors. Retention index, grouped as $>10\%$, $\geqq -10\%$ but $\leqq 10\%$, and $<-10\%$ were 942, 135 and 14 in all tumors, and 320, 86 and 13 in small tumors, respectively.

Received May 25, 2018; accepted January 15, 2019.
Correspondence to: Hirotaka Seura, MD.
PET center, Osaka Saiseikai Nakatsu Hospital,
2-10-39, Shibata, Kita-ku, Osaka 530-0012, Japan
Tel: +81-6-6372-0712; Fax: +81-6-6372-0732
E-mail: hirotakaseura@yahoo.co.jp

Conclusions

Dual-time-point imaging could be effective when fluorodeoxyglucose uptake is not detected in early images, particularly in tumors with diameter <3 cm.

Key Words: Dual-time-point imaging; FDG-PET/CT; Malignancy; Standardized uptake value (SUV)

Introduction

In recent years, ^{18}F-fluorodeoxyglucose (FDG)-positron emission tomography (PET)/computed tomography (CT) has been widely used as a common diagnostic tool for assessing tumor malignancy, determining the clinical stage of tumors, judging therapeutic effects, and detecting recurrence. FDG-PET/CT has been recognized as a useful diagnostic tool for various malignant tumors, but is known to show some limitations. Differentiation between malignant tumors and benign lesions by FDG accumulation alone is known to be difficult, because FDG accumulates in not only malignant tumors, but also benign lesions including benign tumors and inflammatory lesions.

Dual-time-point imaging (DTPI) FDG-PET/CT has recently been recognized as an excellent and simple tool for improving the diagnostic impact of FDG-PET/CT[1-4]. For this method, PET is usually performed twice, at 1 h (as an early image) and approximately 2 h (as a delayed image) after intravenous injection of FDG. Most malignant tumors show gradually increasing FDG uptake as time advances, whereas benign lesions usually show decreased or unchanged FDG uptake[1,4,5]. Using this difference, DTPI offers higher diagnostic utility than standard FDG-PET/CT.

Previous reports, including meta-analyses, have assessed the usefulness of DTPI[1,2,6]. However, no detailed assessments appear to have investigated DTPI for different malignant tumors using the same PET system. Early and delayed images have usually been compared using standard uptake values (SUV)[1,3,6-8], but no investigations have compared visual analyses.

The purpose of this single-institution study was to retrospectively evaluate the effectiveness of DTPI in visually and semiquantitatively assessing malignant tumors, and to investigate what kind of tumor DTPI is best suited to.

Methods

Patients

A total of 1153 consecutive patients on whom DTPI had been performed from November 2009 to October 2011 were investigated (702 males, 451 females; age range, 17-90 years; median, 68 years). Patients were diagnosed histopathologically, and in total were shown to have 1211 malignant lesions. Numbers of malignant lesions found per location are shown in Table 1.

The software of PET reconstruction for our PET/CT scanners was updated in 2012. There were the obvious differences between before and after software updated images in not only visual analysis but also semi-quantitative analysis, therefore the cases after software updated were not included in this study.

This study was approved by the ethics review board of our hospital (institutional review board number: #H28-051) and was performed in accordance with the ethical standards of the 1964 Declaration of Helsinki and its later amendments.

FDG-PET/CT scanning

Images were acquired with a PET/CT single helical scanner (SET-3000BCT/L; Shimadzu, Kyoto,

Table 1. The number of each malignant lesion

	All tumors	Tumors of less than 3 cm
Head and neck	**303**	**176**
Tongue	42	26
Gingiva	23	8
Oral floor	9	7
Nasal and paranasal sinus	9	1
Epipharynx	14	5
Oropharynx	51	20
Hypopharynx	37	17
Larynx	62	50
Thyroid gland	37	31
Ear canal	7	6
Others	12	5
Chest	**314**	**152**
Lung	286	137
Breast	19	14
Others	9	1
Abdomen	**82**	**52**
Liver	11	7
Bile duct	17	10
Gallbladder	5	3
Pancreas	45	28
Others	4	4
Digestive tract	**348**	**90**
Esophagus	87	21
Stomach	83	27
Duodenum	5	2
Colon	172	40
Others	1	0
Hematology	**90**	**31**
Malignant lymphoma	84	29
Multiple myeloma	6	2
Gynecology	**55**	**16**
Uterine cervix	14	6
Uterine corpus	28	10
Ovary	11	0
Others	2	0
Others	**19**	**9**
Prostate	5	2
Others	14	7

Japan) after the patient had fasted for a minimum of 5 h. Patients were administered FDG at 2.7 MBq/kg body weight and scanned at both 60 and 120 min after injection. Both early and delayed emission images covered the body of the patient from the orbits to the upper thighs and were obtained by three-dimensional acquisition using a z-axis 20-cm field of view. Transmission scans were simultaneously obtained using an external source (Cs-137). Table speed was 1 mm/s. Raw emission images were reconstructed using the Fourier rebinning-dynamic row-action maximum likelihood algorithm, and attenuation was corrected by the measured attenuation correction method. FDG was produced by a cyclotron (CYPRIS-HM12; Sumitomo Heavy Industries, Tokyo, Japan). CT was performed after completion of the delayed PET, using the same field of view to reconstruct PET/CT images. CT parameters used were: peak energy, 120 kV; electric current, 60-180 mA according to patient body shape with appropriate radiation exposure; helical pitch, 7 mm; collimation, 7 mm;

thickness, 7 mm. During CT, patients were requested to perform shallow breathing.

Image analysis

1. Image evaluation

All images were retrospectively reviewed by 2 radiologists, both with more than 10 years of experience. Consensus was reached by discussion.

2. Visual analysis

For all malignant tumor lesions visually detected in either early or delayed images, the observed change in FDG uptake was assigned one of three possible labels: increasing; unchanged; or decreasing. This study defined small malignant tumors as lesions ≦3 cm in diameter, because Ohtaka et al reported that using maximum SUV (SUVmax) corrected by a recovery coefficient curve calculated by measuring sphere activity and dividing that activity by true sphere activity was useful in diagnosing lung cancer lesions ≦3 cm in diameter[9]. Referring to the recovery coefficient curve described in the FDG-PET/CT imaging procedure guidelines for cancers (2nd edition)[10], SUV is underestimated in lesions ≦3 cm because the recovery coefficient is <1.0. On the other hand, if the tumor is >3 cm, the recovery coefficient value approaches 1.0 and SUV is considered to be evaluated accurately. We examined the observed changes in FDG uptake not only for all malignant lesions, but also for small malignant lesions alone.

3. Semiquantitative analysis

Semiquantitative analysis was performed using the SUVmax of malignant tumors. All malignant tumors detected in either early or delayed images and with SUVmax that did not exceed the measurable upper limit were analyzed.

The retention index (RI) compares FDG uptake in the early image to FDG uptake in the delayed image and was calculated for each lesion. RI was calculated using the following formula: RI (%) = (SUVmax of delayed image−SUVmax of early image)/SUVmax of early image×100%.

Suitable RI thresholds have been previously reported as −10% and 10%[11,12]. Malignant tumors were therefore divided into 3 groups using the calculated RI: RI <−10%; RI between −10% and 10%; and RI >10%. The same three categories were applied to the small malignant lesions group.

Statistical analysis

Wilcoxon signed-rank test was used to compare SUVmax between early and delayed images. For all analyses, values of $p<0.05$ were considered statistically significant.

Results

Visual analysis

The results of visual analyses for all 1211 malignant lesions, including details of the locations in the early or delayed images, are shown in Table 2.

1. Lesion detection

A total of 1032 lesions (85.2%) and 1096 lesions (90.5%) were detected in early and delayed images, respectively. All lesions detected on early images were also detected on delayed images. Of the 179 lesions (14.8%) not detected on early images, 64 lesions (35.8%) were detected on delayed images. Typical cases with malignant tumors >3 cm in which delayed images were useful for detecting tumors compared to the early image are shown in Figure 1.

Among all lesions, 526 lesions showed a diameter <3 cm. Of these, 362 lesions (68.8%) and 420 lesions (79.8 %) were detected on early and delayed images, respectively. All lesions detected on early

Table 2. The detectability of malignant lesions in the early image and the delayed image on the visual analysis

	All tumors						Tumors of less than 3 cm					
	early(-)			early(+)			early(-)			early(+)		
	delayed(-)		delayed(+)				delayed(-)		delayed(+)			
Malignant lesions	**115**	**(9.5%)**	**64**	**(5.3%)**	**1032**	**(85.2%)**	**106**	**(20.2%)**	**58**	**(11.0%)**	**362**	**(68.8%)**
Head and neck	**49**	**(16.2%)**	**14**	**(4.6%)**	**240**	**(79.2%)**	**47**	**(26.7%)**	**13**	**(7.4%)**	**116**	**(65.9%)**
Tongue	8	(19.0%)	3	(7.1%)	31	(73.8%)	6	(23.1%)	2	(7.7%)	18	(69.2%)
Gingiva	0	(0.0%)	0	(0.0%)	23	(100.0%)	0	(0.0%)	0	(0.0%)	8	(100.0%)
Oral floor	2	(22.2%)	0	(0.0%)	7	(77.8%)	2	(28.6%)	0	(0.0%)	5	(71.4%)
Nasal and paranasal sinus	0	(0.0%)	0	(0.0%)	9	(100.0%)	0	(0.0%)	0	(0.0%)	1	(100.0%)
Epipharynx	0	(0.0%)	0	(0.0%)	14	(100.0%)	0	(0.0%)	0	(0.0%)	5	(100.0%)
Oropharynx	2	(3.9%)	3	(5.9%)	46	(90.2%)	2	(10.0%)	3	(15.0%)	15	(75.0%)
Hypopharynx	4	(10.8%)	1	(2.7%)	32	(86.5%)	4	(23.5%)	1	(5.9%)	12	(70.6%)
Larynx	24	(38.7%)	6	(9.7%)	32	(51.6%)	24	(48.0%)	6	(12.0%)	20	(40.0%)
Thyroid gland	8	(21.6%)	1	(2.7%)	28	(75.7%)	8	(25.8%)	1	(3.2%)	22	(71.0%)
Ear canal	1	(14.3%)	0	(0.0%)	6	(85.7%)	1	(16.7%)	0	(0.0%)	5	(83.3%)
Others	0	(0.0%)	0	(0.0%)	12	(100.0%)	0	(0.0%)	0	(0.0%)	5	(100.0%)
Chest	**9**	**(2.9%)**	**17**	**(5.4%)**	**288**	**(91.7%)**	**9**	**(5.9%)**	**16**	**(10.5%)**	**127**	**(83.6%)**
Lung	6	(2.1%)	17	(5.9%)	263	(92.0%)	6	(4.4%)	16	(11.7%)	115	(83.9%)
Breast	3	(15.8%)	0	(0.0%)	16	(84.2%)	3	(21.4%)	0	(0.0%)	11	(78.6%)
Others	0	(0.0%)	0	(0.0%)	9	(100.0%)	0	(0.0%)	0	(0.0%)	1	(100.0%)
Abdomen	**17**	**(20.7%)**	**11**	**(13.4%)**	**54**	**(65.9%)**	**15**	**(28.8%)**	**9**	**(17.3%)**	**28**	**(53.8%)**
Liver	8	(72.7%)	1	(9.1%)	2	(18.2%)	7	(100.0%)	0	(0.0%)	0	(0.0%)
Bile duct	5	(29.4%)	4	(23.5%)	8	(47.1%)	4	(40.0%)	3	(30.0%)	3	(30.0%)
Gallbladder	2	(40.0%)	0	(0.0%)	3	(60.0%)	2	(66.7%)	0	(0.0%)	1	(33.3%)
Pancreas	1	(2.2%)	4	(8.9%)	40	(88.9%)	1	(3.6%)	4	(14.3%)	23	(82.1%)
Others	1	(25.0%)	2	(50.0%)	1	(25.0%)	1	(25.0%)	2	(50.0%)	1	(25.0%)
Digestive tract	**27**	**(7.8%)**	**9**	**(2.6%)**	**312**	**(89.7%)**	**23**	**(25.6%)**	**9**	**(10.0%)**	**58**	**(64.4%)**
Esophagus	11	(12.6%)	1	(1.1%)	75	(86.2%)	9	(42.9%)	1	(4.8%)	11	(52.4%)
Stomach	12	(14.5%)	6	(7.2%)	65	(78.3%)	10	(37.0%)	6	(22.2%)	11	(40.7%)
Duodenum	1	(20.0%)	0	(0.0%)	4	(80.0%)	1	(50.0%)	0	(0.0%)	1	(50.0%)
Colon	3	(1.7%)	2	(1.2%)	167	(97.1%)	3	(7.5%)	2	(5.0%)	35	(87.5%)
Others	0	(0.0%)	0	(0.0%)	1	(100.0%)	0		0		0	
Hematology	**7**	**(7.8%)**	**5**	**(5.6%)**	**78**	**(86.7%)**	**7**	**(22.6%)**	**4**	**(12.9%)**	**20**	**(64.5%)**
Malignant lymphoma	6	(7.1%)	4	(4.8%)	74	(88.1%)	6	(20.7%)	4	(13.8%)	19	(65.5%)
Multiple myeloma	1	(16.7%)	1	(16.7%)	4	(66.7%)	1	(50.0%)	0	(0.0%)	1	(50.0%)
Gynecology	**3**	**(5.5%)**	**7**	**(12.7%)**	**45**	**(81.8%)**	**2**	**(12.5%)**	**6**	**(37.5%)**	**8**	**(50.0%)**
Uterine cervix	2	(14.3%)	3	(21.4%)	9	(64.3%)	2	(33.3%)	3	(50.0%)	1	(16.7%)
Uterine corpus	0	(0.0%)	3	(10.7%)	25	(89.3%)	0	(0.0%)	3	(30.0%)	7	(70.0%)
Ovary	1	(9.1%)	1	(9.1%)	9	(81.8%)	0		0		0	
Others	0	(0.0%)	0	(0.0%)	2	(100.0%)	0		0		0	
Others	**3**	**(15.8%)**	**1**	**(5.3%)**	**15**	**(78.9%)**	**3**	**(33.3%)**	**1**	**(11.1%)**	**5**	**(55.6%)**
Prostate	0	(0.0%)	0	(0.0%)	5	(100.0%)	0	(0.0%)	0	(0.0%)	2	(100.0%)
Others	3	(21.4%)	1	(7.1%)	10	(71.4%)	3	(42.9%)	1	(14.3%)	3	(42.9%)

early(–), not detected on early image; early(+), detected on early image; delayed(–), not detected on delayed image; and delayed(+), detected on delayed image.

images were also detected on delayed images. Of the 164 lesions (10.2%) not detected on early images, 58 lesions (35.4%) were detected on delayed images.

Most lesions not detected on early images but detected on delayed images showed diameter <3 cm. Typical cases with malignant tumors ≦3 cm in which delayed images were useful for detecting tumors compared to the early image are shown in Figure 2.

2. Lesion detection per location

Lesions detected on neither early nor delayed images were most frequently head and neck cancers (such as laryngeal, oral floor, thyroid, or tongue cancer), abdominal cancers (such as hepatic or gallbladder cancer), breast cancers, and gastric cancers.

Lesions not detected on early images but detected on delayed images were frequently laryngeal cancer, abdominal cancers (such as bile duct or pancreatic cancer), and gynecological cancers (such as uterine cervical or uterine corpus cancer). On very few occasions, these lesions were from a cancer of a digestive organ.

All lesions of gingival, nasal cavity and paranasal sinus cancer, epipharyngeal cancer, and more than 90% of oropharyngeal, lung and colon cancer were detected on both early and delayed images.

Six lesions larger than 3 cm in diameter were not detected on early images, but all these lesions were detected on delayed images. These lesions were tongue, hepatic, bile duct, ovarian, and lung

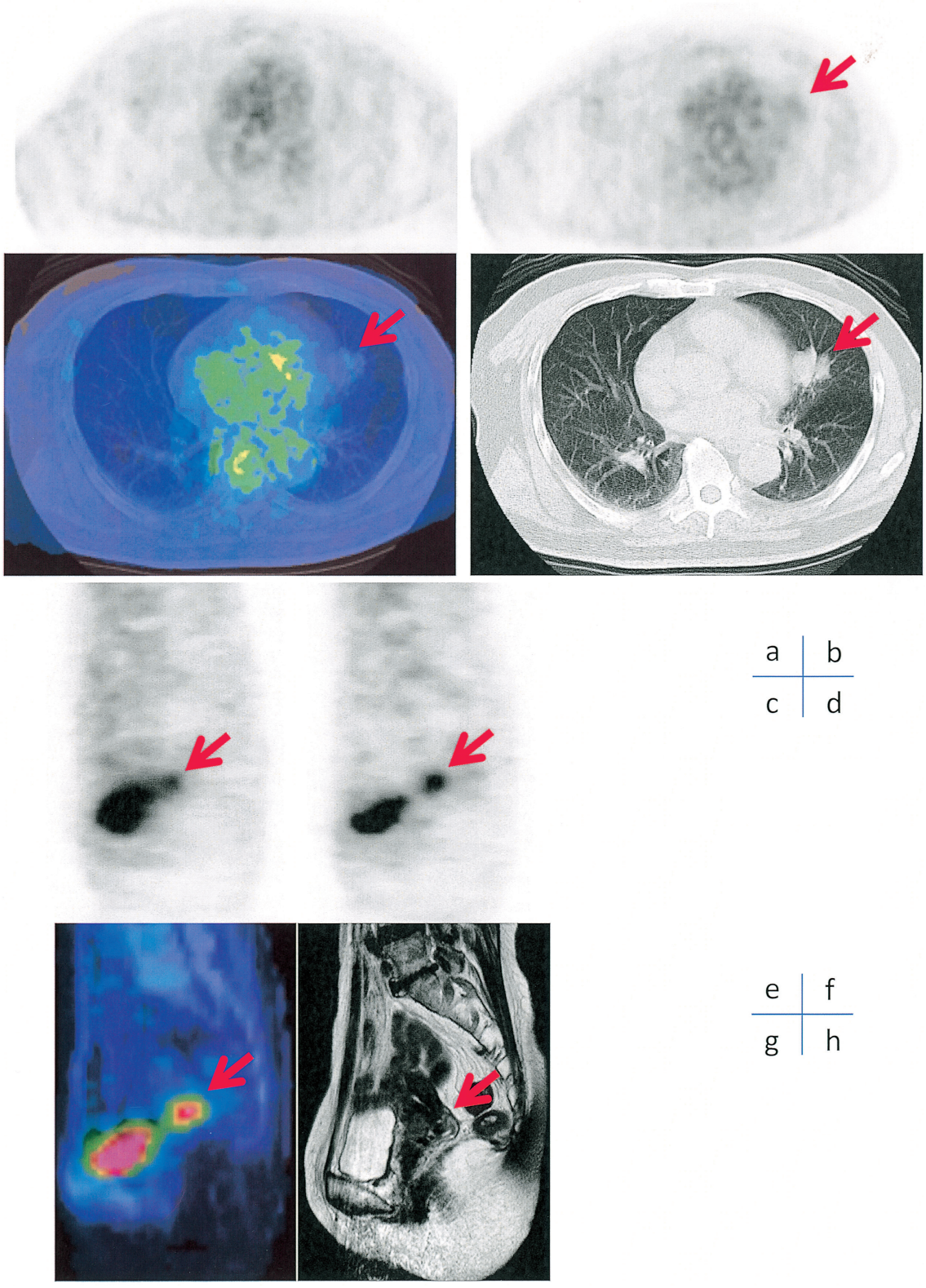

Figure 1. Cancer lesions with diameter ≧3 cm.

a-d) A 67-year-old man with lung cancer (3 cm). The lesion could not be detected on the early image but was detected on the delayed image. a, Early image from FDG-PET (SUVmax 1.2); b, Delayed image from FDG-PET (SUVmax 1.8); c, Delayed image from FDG-PET/CT; and d, CT image.

e-h) A 62-year-old woman with uterine cervical cancer (3.7 cm). The lesion could be detected on both early and delayed images, showing increased FDG uptake on the delayed image. e, Early image from FDG-PET, SUVmax 3.5; f, Delayed image from FDG-PET, SUVmax 4.6; g, Delayed image from FDG-PET/CT; and h, MR image.

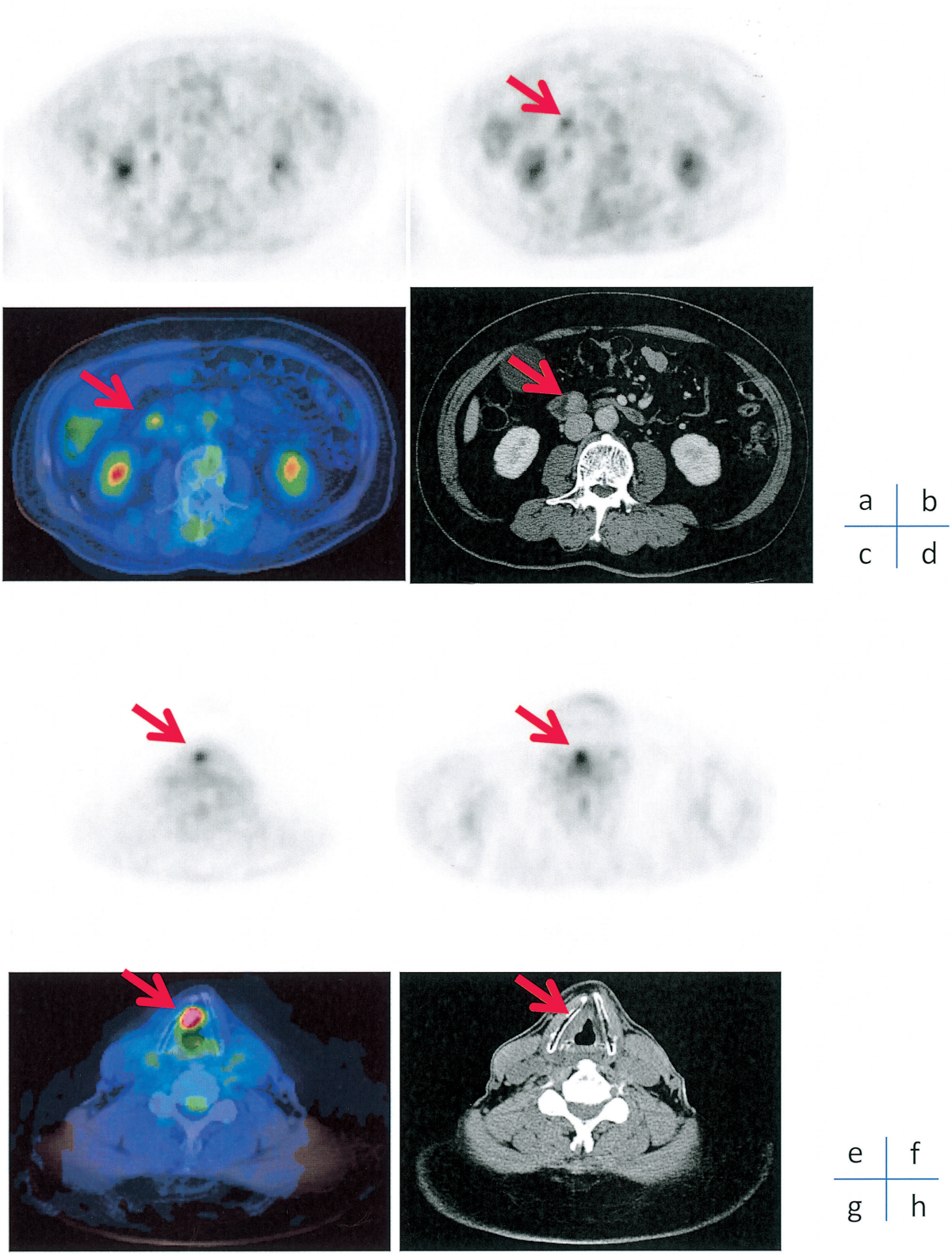

Figure 2. Cancer lesions with diameter <3 cm.

a-d) A 66-year-old man with bile duct cancer. This lesion could not be detected on the early image, but was detectable on the delayed image. a, Early image from FDG-PET (SUVmax 1.8); b, Delayed image from FDG-PET (SUVmax 3.2); c, Delayed image from FDG-PET/CT; and d, CT image.

e-h) A 70-year-old man with laryngeal cancer (1.5 cm), this lesion was detected of both early and delayed images, and showed increasing FDG uptake on delayed image; e, Early image (SUVmax 3.3); f, Delayed image (SUVmax 4.5); g, Delayed image of FDG-PET/CT image; and h, CT image.

cancers, and multiple myeloma.

3. Changes in FDG uptake between early and delayed images

Within head and neck cancers, gingival, epipharyngeal, and oropharyngeal cancers displayed the lowest percentage of lesions that showed increasing FDG uptake. Hypopharyngeal and laryngeal cancers tended to show both increasing and decreasing changes. Other cancers (except hepatic cancer) tended to show increasing FDG uptake. Increasing FDG uptake was observed more frequently in lesions with diameter <3 cm than in all lesions (Table 3).

Semiquantitative analysis

1. SUVmax of all malignant lesions

A total of 1091 lesions were included in this part of the analysis. Because the remaining 120 lesions showed faint or no abnormal uptake, SUVmax of these lesions was too difficult to measure. Mean (±standard deviation) SUVmax was 7.0±5.2 in early images and 8.8±6.4 in delayed images, representing a significant difference ($p<0.0001$).

Among these 1091 lesions, 420 lesions showed diameter <3 cm. For these lesions, SUVmax was 3.8±3.4 in early images and 4.7±4.1 in delayed images, again representing a significant difference ($p<0.0001$).

2. RI of all malignant lesions

Table 3. The changes between FDG uptake in the early images and that in delayed image on the visual analysis

	All tumors				Tumors of less than 3 cm			
	increasing	no change	decreasing	N/A	increasing	no change	decreasing	N/A
Malignant lesions	**751 (68.5%)**	**332 (30.3%)**	**13 (1.2%)**	**115**	**314 (74.8%)**	**94 (22.4%)**	**12 (2.9%)**	**106**
Head and neck	**109 (42.9%)**	**135 (53.1%)**	**10 (3.9%)**	**49**	**67 (51.9%)**	**53 (41.1%)**	**9 (7.0%)**	**47**
Tongue	15 (44.1%)	17 (50.0%)	2 (5.9%)	8	9 (45.0%)	9 (45.0%)	2 (10.0%)	6
Gingiva	5 (21.7%)	18 (78.3%)	0 (0.0%)	0	3 (37.5%)	5 (62.5%)	0 (0.0%)	0
Oral floor	3 (42.9%)	3 (42.9%)	1 (14.3%)	2	2 (40.0%)	2 (40.0%)	1 (20.0%)	2
Nasal and paranasal sinus	7 (77.8%)	2 (22.2%)	0 (0.0%)	0	1 (100.0%)	0 (0.0%)	0 (0.0%)	0
Epipharynx	4 (28.6%)	10 (71.4%)	0 (0.0%)	0	2 (40.0%)	3 (60.0%)	0 (0.0%)	0
Oropharynx	10 (20.4%)	39 (79.6%)	0 (0.0%)	2	5 (27.8%)	13 (72.2%)	0 (0.0%)	2
Hypopharynx	16 (48.5%)	13 (39.4%)	4 (12.1%)	4	8 (61.5%)	2 (15.4%)	3 (23.1%)	4
Larynx	26 (68.4%)	9 (23.7%)	3 (7.9%)	24	19 (73.1%)	4 (15.4%)	3 (11.5%)	24
Thyroid gland	17 (58.6%)	12 (41.4%)	0 (0.0%)	8	14 (60.9%)	9 (39.1%)	0 (0.0%)	8
Ear canal	2 (33.3%)	4 (66.7%)	0 (0.0%)	1	2 (40.0%)	3 (60.0%)	0 (0.0%)	1
Others	4 (33.3%)	8 (66.7%)	0 (0.0%)	0	2 (40.0%)	3 (60.0%)	0 (0.0%)	0
Chest	**266 (87.2%)**	**38 (12.5%)**	**1 (0.3%)**	**9**	**133 (93.0%)**	**9 (6.3%)**	**1 (0.7%)**	**9**
Lung	244 (87.1%)	36 (12.9%)	0 (0.0%)	6	123 (93.9%)	8 (6.1%)	0 (0.0%)	6
Breast	14 (87.5%)	1 (6.3%)	1 (6.3%)	3	9 (81.8%)	1 (9.1%)	1 (9.1%)	3
Others	8 (88.9%)	1 (11.1%)	0 (0.0%)	0	1 (100.0%)	0 (0.0%)	0 (0.0%)	0
Abdomen	**54 (83.1%)**	**11 (16.9%)**	**0 (0.0%)**	**17**	**33 (89.2%)**	**4 (10.8%)**	**0 (0.0%)**	**15**
Liver	1 (33.3%)	2 (66.7%)	0 (0.0%)	8	0	0	0	7
Bile duct	10 (83.3%)	2 (16.7%)	0 (0.0%)	5	6 (100.0%)	0 (0.0%)	0 (0.0%)	4
Gallbladder	2 (66.7%)	1 (33.3%)	0 (0.0%)	2	0 (0.0%)	1 (100.0%)	0 (0.0%)	2
Pancreas	38 (86.4%)	6 (13.6%)	0 (0.0%)	1	24 (88.9%)	3 (11.1%)	0 (0.0%)	1
Others	3 (100.0%)	0 (0.0%)	0 (0.0%)	1	3 (100.0%)	0 (0.0%)	0 (0.0%)	1
Digestive tract	**232 (72.3%)**	**87 (27.1%)**	**2 (0.6%)**	**27**	**50 (74.6%)**	**15 (22.4%)**	**2 (3.0%)**	**23**
Esophagus	48 (63.2%)	27 (35.5%)	1 (1.3%)	11	9 (75.0%)	2 (16.7%)	1 (8.3%)	9
Stomach	53 (74.6%)	17 (23.9%)	1 (1.4%)	12	12 (70.6%)	4 (23.5%)	1 (5.9%)	10
Duodenum	3 (75.0%)	1 (25.0%)	0 (0.0%)	1	1 (100.0%)	0 (0.0%)	0 (0.0%)	1
Colon	127 (75.1%)	42 (24.9%)	0 (0.0%)	3	28 (75.7%)	9 (24.3%)	0 (0.0%)	3
Others	1 (100.0%)	0 (0.0%)	0 (0.0%)	0	0	0	0	0
Hematology	**42 (50.6%)**	**41 (49.4%)**	**0 (0.0%)**	**7**	**14 (58.3%)**	**10 (41.7%)**	**0 (0.0%)**	**7**
Malignant lymphoma	39 (50.0%)	39 (50.0%)	0 (0.0%)	6	13 (56.5%)	10 (43.5%)	0 (0.0%)	6
Multiple myeloma	3 (60.0%)	2 (40.0%)	0 (0.0%)	1	1 (100.0%)	0 (0.0%)	0 (0.0%)	1
Gynecology	**36 (69.2%)**	**16 (30.8%)**	**0 (0.0%)**	**3**	**12 (85.7%)**	**2 (14.3%)**	**0 (0.0%)**	**2**
Uterine cervix	8 (66.7%)	4 (33.3%)	0 (0.0%)	2	3 (75.0%)	1 (25.0%)	0 (0.0%)	2
Uterine corpus	21 (75.0%)	7 (25.0%)	0 (0.0%)	0	9 (90.0%)	1 (10.0%)	0 (0.0%)	0
Ovary	6 (60.0%)	4 (40.0%)	0 (0.0%)	1	0	0	0	0
Others	1 (50.0%)	1 (50.0%)	0 (0.0%)	0	0	0	0	0
Others	**12 (75.0%)**	**4 (25.0%)**	**0 (0.0%)**	**3**	**5 (83.3%)**	**1 (16.7%)**	**0 (0.0%)**	**3**
Prostate	4 (80.0%)	1 (20.0%)	0 (0.0%)	0	1 (50.0%)	1 (50.0%)	0 (0.0%)	0
Others	8 (72.7%)	3 (27.3%)	0 (0.0%)	3	4 (100.0%)	0 (0.0%)	0 (0.0%)	3

Increasing, higher FDG uptake on delayed image than early Image; no change, no significant change between early and delayed image; decreasing, lower FDG uptake on delayed image than on early image; and N/A, not applicable.

A total of 942 lesions (86.3%) showed RI >10%, 135 lesions (12.4%) showed RI between −10% and 10%, and 14 lesions (1.3%) showed RI <−10% (Table 4). Of the 420 lesions with diameter <3 cm, 321 lesions (76.4%) showed RI >10%, 86 lesions (20.5%) showed RI between −10% and 10%, and 13 lesions (3.1%) showed RI <−10% (Table 4).

3. RI per location

Most sites of all tumor lesions and small lesions showed RI >10%, including all nasal cavity and paranasal sinus cancers, hepatic cancers, multiple myelomas, and prostatic cancers. Among cancer lesions with RI between −10% and 10%, the ear canal cancer was the most frequent site (4/6, 66.7%). Fourteen lesions showed RI <−10% in all tumor lesions. These lesions comprised 2 hypopharyngeal cancers, 2 laryngeal cancers, 2 breast cancers, 1 tongue cancer, 1 oropharyngeal cancer, 1 thyroid cancer, 1 lung cancer, 1 esophageal cancer, 1 gastric cancer, 1 colon cancer and 1 malignant lymphoma. Of the 14 lesions above, 13 lesions (excluding 1 case of colon cancer) showed diameter <3 cm (Table 4).

In cases where lesions showed diameter <3 cm, hypopharyngeal and breast cancers frequently showed RI <−10% (Table 4).

Discussion

The utility of DTPI as a diagnostic tool has been reported previously, with most studies focusing

Table 4. Retention index of malignant lesions on the semiquantitative analysis

	All tumors			Tumors of less than 3cm		
	10% < RI	-10% ≤ RI ≤ 10%	RI < -10%	10% < RI	-10% ≤ RI ≤ 10%	RI < -10%
Malignant tumor	**942 (86.3%)**	**135 (12.4%)**	**14 (1.3%)**	**321 (76.4%)**	**86 (20.5%)**	**13 (3.1%)**
Head and neck	**189 (74.4%)**	**58 (22.8%)**	**7 (2.8%)**	**84 (65.1%)**	**38 (29.5%)**	**7 (5.4%)**
Tongue	25 (73.5%)	8 (23.5%)	1 (2.9%)	14 (70.0%)	5 (25.0%)	1 (5.0%)
Gingiva	17 (73.9%)	6 (26.1%)	0 (0.0%)	4 (50.0%)	4 (50.0%)	0 (0.0%)
Oral floor	4 (57.1%)	3 (42.9%)	0 (0.0%)	3 (60.0%)	2 (40.0%)	0 (0.0%)
Nasal and paranasal sinus	9 (100.0%)	0 (0.0%)	0 (0.0%)	1 (100.0%)	0 (0.0%)	0 (0.0%)
Epipharynx	10 (71.4%)	4 (28.6%)	0 (0.0%)	3 (60.0%)	2 (40.0%)	0 (0.0%)
Oropharynx	35 (71.4%)	13 (26.5%)	1 (2.0%)	10 (55.6%)	7 (38.9%)	1 (5.6%)
Hypopharynx	25 (75.8%)	6 (18.2%)	2 (6.1%)	8 (61.5%)	3 (23.1%)	2 (15.4%)
Larynx	31 (81.6%)	5 (13.2%)	2 (5.3%)	20 (76.9%)	4 (15.4%)	2 (7.7%)
Thyroid gland	21 (72.4%)	7 (24.1%)	1 (3.4%)	15 (65.2%)	7 (30.4%)	1 (4.3%)
Ear canal	2 (33.3%)	4 (66.7%)	0 (0.0%)	2 (40.0%)	3 (60.0%)	0 (0.0%)
Others	10 (83.3%)	2 (16.7%)	0 (0.0%)	4 (80.0%)	1 (20.0%)	0 (0.0%)
Chest	**280 (91.8%)**	**22 (7.2%)**	**3 (1.0%)**	**122 (85.3%)**	**18 (12.6%)**	**3 (2.1%)**
Lung	258 (92.1%)	21 (7.5%)	1 (0.4%)	112 (85.5%)	18 (13.7%)	1 (0.8%)
Breast	14 (87.5%)	0 (0.0%)	2 (12.5%)	9 (81.8%)	0 (0.0%)	2 (18.2%)
Others	8 (88.9%)	1 (11.1%)	0 (0.0%)	1 (100.0%)	0 (0.0%)	0 (0.0%)
Abdomen	**53 (81.5%)**	**12 (18.5%)**	**0 (0.0%)**	**27 (73.0%)**	**10 (27.0%)**	**0 (0.0%)**
Liver	3 (100.0%)	0 (0.0%)	0 (0.0%)	0	0	0
Bile duct	10 (83.3%)	2 (16.7%)	0 (0.0%)	4 (66.7%)	2 (33.3%)	0 (0.0%)
Gallbladder	2 (66.7%)	1 (33.3%)	0 (0.0%)	1 (100.0%)	0 (0.0%)	0 (0.0%)
Pancreas	36 (81.8%)	8 (18.2%)	0 (0.0%)	20 (74.1%)	7 (25.9%)	0 (0.0%)
Others	2 (66.7%)	1 (33.3%)	0 (0.0%)	2 (66.7%)	1 (33.3%)	0 (0.0%)
Digestive tract	**294 (91.6%)**	**24 (7.5%)**	**3 (0.9%)**	**56 (83.6%)**	**9 (13.4%)**	**2 (3.0%)**
Esophagus	72 (94.7%)	3 (3.9%)	1 (1.3%)	10 (83.3%)	1 (8.3%)	1 (8.3%)
Stomach	59 (83.1%)	11 (15.5%)	1 (1.4%)	11 (64.7%)	5 (29.4%)	1 (5.9%)
Duodenum	3 (75.0%)	1 (25.0%)	0 (0.0%)	1 (100.0%)	0 (0.0%)	0 (0.0%)
Colon	159 (94.1%)	9 (5.3%)	1 (0.6%)	34 (91.9%)	3 (8.1%)	0 (0.0%)
Others	1 (100.0%)	0 (0.0%)	0 (0.0%)	0	0	0
Hematology	**67 (85.9%)**	**10 (12.8%)**	**1 (1.3%)**	**17 (70.8%)**	**6 (25.0%)**	**1 (4.2%)**
Malignant lymphoma	62 (84.9%)	10 (13.7%)	1 (1.4%)	16 (69.6%)	6 (26.1%)	1 (4.3%)
Multiple myeloma	5 (100.0%)	0 (0.0%)	0 (0.0%)	1 (100.0%)	0 (0.0%)	0 (0.0%)
Gynecology	**44 (84.6%)**	**8 (15.4%)**	**0 (0.0%)**	**9 (64.3%)**	**5 (35.7%)**	**0 (0.0%)**
Uterine cervix	9 (75.0%)	3 (25.0%)	0 (0.0%)	1 (25.0%)	3 (75.0%)	0 (0.0%)
Uterine corpus	24 (85.7%)	4 (14.3%)	0 (0.0%)	8 (80.0%)	2 (20.0%)	0 (0.0%)
Ovary	9 (90.0%)	1 (10.0%)	0 (0.0%)	0	0	0
Others	2 (100.0%)	0 (0.0%)	0 (0.0%)	0	0	0
Others	**15 (93.8%)**	**1 (6.3%)**	**0 (0.0%)**	**6 (100.0%)**	**0 (0.0%)**	**0 (0.0%)**
Prostate	5 (100.0%)	0 (0.0%)	0 (0.0%)	2 (100.0%)	0 (0.0%)	0 (0.0%)
Others	10 (90.9%)	1 (9.1%)	0 (0.0%)	4 (100.0%)	0 (0.0%)	0 (0.0%)

RI, retention index(%).

on the differentiation of malignant and benign tumors[1,4,6,11]. No reports have investigated which malignant tumors benefit most from DTPI, as in the present study. Routine performance of DTPI in all patients has recently been reported as inappropriate[13], as dose exposure is increased for every CT acquisition on the PET/CT scanner. Imaging of the target organ alone is thus becoming more common with DTPI. With the particular PET/CT scanner used in the present study, acquisition of images without unnecessarily increasing the exposure is possible while comparing early and delayed images on an equal basis. We therefore visually and semiquantitatively investigated the kinds of malignant tumor for which DTPI is most useful using only patients scanned at our hospital.

In this study, the detection rate by visual analysis of all malignant tumor lesions was 85.2% on early images and 90.5% on delayed images. This result revealed that delayed images were better than early images for detecting malignant lesions. The detectability of malignant tumor lesions has been reported as 77%-78% on early images and 94% on delayed images, comparable to our results[1,2]. In small lesions <3 cm in diameter, detection rate was 68.8% on early images and 79.8% on delayed images. These detection rates were lower than those corresponding to rates for the group encompassing all lesions. Most lesions not detected on early images showed diameter <3 cm. Only 15 of 685 lesions (2%) with a diameter ≧3 cm were not detected on early images. Of the lesions with diameter <3 cm not detected on early images, approximately one-third were detected on delayed images. DTPI has been reported as useful for small pancreatic cancers, with an average diameter of 2.5 cm[14]. We suppose that DTPI would be useful for lesions with diameters <3 cm.

With regard to the utility of DTPI for different types of tumor, tumor lesions that were difficult to detect on both early and delayed images were more frequently head and neck cancers, abdominal malignant tumors and gastric cancers than other types of tumor lesions. Lesions that could not be detected on early images but were detected on delayed images were only infrequently digestive tract cancers, but were commonly laryngeal cancers, bile duct cancers, pancreatic cancers, uterine cervical cancers, and cancers of the uterine corpus. Most of these tumors showed diameter <3 cm. The utility of DTPI for head and neck cancers has been reported previously[1,15]. However, Yen et al reported that detection rates of epipharyngeal cancer were higher with FDG-PET than with MRI, and no useful additional information was obtained from delayed imaging[16]. Various reports have examined DTPI in thyroid cancer[1,17,18], with limited success, and no reports have examined DTPI for laryngeal cancer. In the present study, while DTPI seemed useful, some laryngeal cancer lesions failed to be detected by FDG accumulation in both early and delayed images, possibly due to tumor disappearance or shrinkage after biopsy. DTPI has already proven useful in detecting bile duct cancer[1,19], and reports have been conflicting regarding differentiation of benign lesions from malignant pancreatic cancers using delayed imaging[20,21]. SUVmax of the pancreatic adenocarcinoma was reported to increase statistically from early to delayed time[22]. In the present study, detecting abnormal FDG uptake on early images was difficult to these lesions due to the nature of the tumors and the small size. DTPI proved useful in detecting both uterine cervical cancer lesions and lesions of the uterine corpus cancer in the present study, but reports are conflicting on the usefulness of DTPI for uterine cervical cancer[23,24] and no reports have examined the situation for cancer of the uterine corpus. In the present study, presence or absence of tumor FDG uptake was determined not only using SUVmax, but also by visually analyzing tumor contrast compared to uptake by surrounding tissue FDG. To the best of our knowledge, no other reports discussing the usefulness of DTPI have investigated tumor FDG uptake in such a manner. Most tumor lesions showed visually increased uptake of FDG. This was attributed

to increased tumor FDG uptake in delayed images and decreased uptake in the surrounding tissue over time. In head and neck cancers, the proportion of lesions showing increasing FDG uptake was small in cases of gingival cancer, epipharyngeal cancer and oropharyngeal cancer among small tumor lesions. In these tumors, the utility of DTPI has been considered limited. Based on the above results, we strongly recommend DTPI as a useful tool for detecting laryngeal cancer, bile duct cancer, pancreatic cancer, uterine cervical cancer, and cancer of the uterine corpus, particularly for small tumors.

In semiquantitative analysis, SUVmax was significantly increased on delayed images compared to early images for both all lesions and lesions smaller than 3 cm. This finding is consistent with results from previous reports[1,2,4].

Concerning RI, 86.3% of all lesions showed RI >10%. For tumors with diameter <3 cm, the three groups of RI >10%, −10%< RI <10% and RI <−10% were almost equivalent to the three groups of increasing, unchanged and decreasing uptake on visual analysis. For all tumors, the group with RI <−10% (1.3%) was almost equivalent to the group with decreasing FDG uptake on visual analysis (1.2%), but the group with RI >10% (86.9%) was larger than the group with increasing FDG uptake on visual analysis (68.9%). This suggests that visually assessing the increase in delayed images is difficult because of the high uptake in large tumors seen even on early images.

Of the only 1.3% of total tumor lesions showing a reduction of >10% in SUVmax, most showed a diameter <3 cm. The hypopharyngeal and breast cancers were included among these lesions. No reports have discussed RI for hypopharyngeal cancer. Our results for the RI of breast cancer were similar to those from other published reports[1].

Within the head and neck cancer group, the proportion of tumor lesions showing increased RI was high among laryngeal, nasal and paranasal cavity cancers. All lesions of the bile duct, pancreatic, uterine cervix and uterine corpus showed increased RI.

The findings of the present study must be considered in light of various limitations. First, this study only analyzed malignant lesions, and benign tumors and inflammatory lesions were not included. Second, since this study was retrospective in design, various biases may have been present despite the inclusion of consecutive patients.

In conclusion, additional delayed imaging appears warranted if tumor FDG uptake cannot be detected on early images, particularly for tumor lesions with diameter <3 cm. Regarding head and neck cancers, DTPI is not thought to be necessary for hypopharyngeal cancer or oral floor cancer, but additional delayed imaging is recommended to be performed for laryngeal cancer. For tumors other than head and neck tumors, additional delayed imaging is recommended to be performed for cancers of the bile duct, pancreas, uterine cervix, and uterine corpus.

Acknowledgments

All authors have no COI to declare regarding the present study.

References

1. Schillaci O. Use of dual-point fluorodeoxyglucose imaging to enhance sensitivity and specificity. Semin Nucl Med 2012;42:267-280.
2. Chan WL, Ramsay SC, Szeto ER, et al. Dual-time-point ^{18}F-FDG-PET/CT imaging in the assessment of suspected malignancy. J Med Imaging Radiat Oncol 2011;55:379-390.
3. Cui J, Zhao P, Ren Z, et al. Evaluation of dual time point imaging 18F-FDG PET/CT in differentiating

malignancy from benign gastric disease. Medicine (Baltimore) 2015;94:e1356.
4. Cheng G, Torigian DA, Zhuang H, et al. When should we recommend use of dual time-point and delayed time-point imaging techniques in FDG PET? Eur J Nucl Med Mol Imaging 2013;40:779-787.
5. Cheng G, Alavi A, Lim E, et al. Dynamic changes of FDG uptake and clearance in normal tissues. Mol Imaging Biol 2013;15:345-352.
6. Saleh Farghaly HR, Mohamed Sayed MH, Nasr HA, et al. Dual time point fluorodeoxyglucose positron emission tomography/computed tomography in differentiation between malignant and benign lesions in cancer patients. Does it always work? Indian J Nucl Med 2015;30:314-319.
7. García Vicente AM, Soriano Castrejón Á, León Martín A, et al. Molecular subtypes of breast cancer: metabolic correlation with ^{18}F-FDG PET/CT. Eur J Nucl Med Mol Imaging 2013;40:1304-1311.
8. Lin WY, Tsai SC, Hung GU. Value of delayed 18F-FDG-PET imaging in the detection of hepatocellular carcinoma. Nucl Med Commun 2005;26:315-321.
9. Ohtaka K, Hida Y, Kaga K, et al. Outcome analysis of (18)F-fluorodeoxyglucose positron-emission tomography in patients with lung cancer after partial volume correction. Anticancer Res 2013;33:5193-5198.
10. Hiroyoshi H, Keiichi O, Takahiro S, et al. Gan FDG-PET/CT satsueihou gaidolain dai2han, Kakuigaku Gijutsu 2013;33:377-420. (In Japanese)
11. Lan XL, Zhang YX, Wu ZJ, et al. The value of dual time point (18)F-FDG PET imaging for the differentiation between malignant and benign lesions. Clin Radiol 2008;63:756-764.
12. Sanz-Viedma S, Torigian DA, Parsons M, et al. Potential clinical utility of dual time point FDG-PET for distinguishing benign from malignant lesions: implications for oncological imaging. Rev Esp Med Nucl 2009; 28:159-166.
13. Lee ST, Scott AM. Are we ready for dual-time point FDG PET imaging? J Med Imaging Radiat Oncol 2011; 55:351-352.
14. Kawada N, Uehara H, Hosoki T, et al. Usefulness of dual-phase 18F-FDG PET/CT for diagnosing small pancreatic tumors. Pancreas 2015;44:655-659.
15. Hustinx R, Smith RJ, Benard F, et al. Dual time point fluorine-18 fluorodeoxyglucose positron emission tomography: a potential method to differentiate malignancy from inflammation and normal tissue in the head and neck. Eur J Nucl Med 1999;26:1345-1348.
16. Yen TC, Chang YC, Chan SC, et al. Are dual-phase ^{18}F-FDG PET scans necessary in nasopharyngeal carcinoma to assess the primary tumour and loco-regional nodes? Eur J Nucl Med Mol Imaging 2005;32:541-548.
17. Lee S, Park T, Park S, et al. The clinical role of dual-time-point ^{18}F-FDG PET/CT in differential diagnosis of the thyroid incidentaloma. Nucl Med Mol Imaging 2014;48:121-129.
18. D'Souza MM, Marwaha RK, Sharma R, et al. Prospective evaluation of solitary thyroid nodule on 18F-FDG PET/CT and high-resolution ultrasonography. Ann Nucl Med 2010;24:345-355.
19. Nishiyama Y, Yamamoto Y, Kimura N, et al. Comparison of early and delayed FDG PET for evaluation of biliary stricture. Nucl Med Commun 2007;28:914-919.
20. Nakamoto Y, Higashi T, Sakahara H, et al. Delayed (18)F-fluoro-2-deoxy-D-glucose positron emission tomography scan for differentiation between malignant and benign lesions in the pancreas. Cancer 2000; 89:2547-2554.
21. Santhosh S, Mittal BR, Bhasin D, et al. Dual-phase 18F-FDG PET/CT imaging in the characterization of pancreatic lesions: does it offer prognostic information? Nucl Med Commun 2014;35:1018-1025.
22. Mena E, Sheikhbahaei S, Taghipour M, et al. 18F-FDG PET/CT metabolic tumor volume and intratumoral heterogeneity in pancreatic adenocarcinomas: impact of dual-time point and segmentation methods. Clin Nucl Med 2017;42:e16-e21.
23. Yen TC, Ng KK, Ma SY, et al. Value of dual-phase 2-fluoro-2-deoxy-d-glucose positron emission tomography in cervical cancer. J Clin Oncol 2003;21:3651-3658.
24. Yu L, Jia C, Wang X, et al. Evaluation of ^{18}F-FDG PET/CT in early-stage cervical carcinoma. Am J Med Sci 2011;341:96-100.

Instructions for Authors

The Osaka City Medical Journal will consider the publication of any original manuscript, review, case report, or short communication. Articles should be in English.

Manuscript submission. Manuscripts should be sent to the Editor, Osaka City Medical Journal, Osaka City Medical Association, Osaka City University Medical School, 1-4-3 Asahimachi, Abeno-ku, Osaka 545-8585, Japan; phone and fax 06-6645-3782; e-mail shiigakukai@med.osaka-cu.ac.jp

The Journal accepts only manuscripts that contain material that has not been and will not be published elsewhere. Duplicate publication of scientific data is not permitted. If closely related papers might be considered to be duplicate publications, the possible duplicate should be submitted with the manuscript and the authors should explain in their covering letter what is original in the submitted paper. Submit three copies of the manuscript (two of which may be photocopies) together with CD-R or DVD-R containing the body text, tables and figures. The manuscript should be prepared by Microsoft Word or its compatible software (doc or docx). Acceptable formats for figures are JPG or TIF. Use only 12-point font size and a standard serif font. Double-space throughout the manuscript and use standard-sized (ISO A4, 212×297 mm) white bond paper. Make margins at least 25 mm wide on all sides. Number pages consecutively starting with the title page and ending with the reference list. Begin each of these sections on a separate page: title page, abstract, text, acknowledgments, references, tables (each one separate), and figure legends. Do not use abbreviations in the title or abstract and limit their use in the text, defining each when it first appears. Manuscripts should meet the requirements outlined below to avoid delay in review and publication. Authors whose native language is not English must seek the assistance of a native English speaker who is familiar with medical sciences. Please attach the certificate from the person(s) who edit the manuscript. Some minor editorial revision of the manuscript will be made when the editorial committee considers it necessary.

Title page. All submissions must include a title page. The full title of the paper, should be concise, specific, and informative, and should contain the message of the paper without being in sentence form. Next, include the full names and academic affiliations of all authors, and indicate the corresponding author, address, phone, fax, and e-mail address. Give a running title (not to exceed 50 characters including spaces), and three to five key words. Last, give the word count for text only, exclusive of title, abstract, references, tables, and figure legends.

Structured abstract. The abstract of 250 words or less should consist of four paragraphs headed **Background, Methods, Results,** and **Conclusions.**

Text. Full papers about experiments or observations may be divided into sections headed **Introduction, Methods, Results,** and **Discussion.**

Tables. Each table should be typed on a separate sheet in characters of ordinary size, double-spaced (with at least 6 mm of white space between lines). Each table must have a title and should be assigned an Arabic numeral ('Table 3'). Vertical rules should not be used.

Figures. For black-and-white figures, submit three original glossy prints or laser-quality proofs and three photocopies of each. One transparency and three color prints should be submitted of each color figure. Label the front of figures with the figure number. Indicate on the back of each figure the first author, the first few words of the manuscript title, and the direction of the top of the figure (if needed). Photomicrographs should have scale markers that indicate the magnification. Provide figure legends on a separate page, double-spaced, immediately after the tables. All illustrations and graphs, to be referred to as figures, should be numbered in Arabic numerals ('Fig. 2' etc.). The approximate position of each figure in the text should be indicated in the right margin of the manuscript. Illustrations in full color are accepted for publication if the editors judge that color is necessary, with the cost paid by the author.

References. Reference must be double-spaced and numbered consecutively in the order cited in the text. When listing references, follow the style of the Uniform Requirements (http://www.icmje.org/) and abbreviate names of journals according to PubMed (http://www.ncbi.nlm.nih.gov/sites/netrez). List all authors up to three; when there are four or more, list the first three and use et al.

Examples of reference style

1. Priori SG, Schwartz PJ, Napolitano C, et al. Risk stratification in the long-QT syndrome. N Engl J Med 2003;348:1866-1874.
2. Schwartz PJ, Priori SG, Napolitano C. The long-QT syndrome. In: Zipes DP, Jalife J, editors. Cardiac electrophysiology: from cell to bedside. 3rd ed. Philadelphia: W.B. Saunders; 2000. pp. 597-615.

Proofs. One set of proofs together with the original manuscript will be sent to the author, to be carefully checked for any essential changes or printer's errors. The author is requested to return the corrected proofs within 48 h of their receipt.

Short communications and case reports.

1. A short communication should have between 1500 and 2000 words, including the abstract. This word count is equivalent to about four double-spaced manuscript pages.
2. The original and two copies including three sets of figures and tables should be sent to the Editorial Office.

Manuscript submission fee. A nonrefundable fee of 10,000 JPY is due on submission of original manuscripts, case reports, and short communications. A manuscript returned beyond six months of the date of the initial decision will be considered a new submission.

Page charges and reprints. Authors are required to pay page charges of 10,000 JPY per printed page to share in the high costs of publication. Authors receive with the proofs a reprint order form that must be filled out and returned with the proofs to the Editorial Office. Later orders cannot be filled because reprints are made at the time the journal is printed.

Studies of human subjects. It is the responsibility of the authors to ensure that any clinical investigation they did and report in manuscripts submitted to the Osaka City Medical Journal are in accordance with the Declaration of Helsinki (http://www.wma.net).

Animal studies. It is the responsibility of the authors to ensure that their experimental procedures are in compliance with the "Guiding Principles in the Care and Use of Animals" (http://www.the-aps.org/pub_affairs/humane/pa_aps_guiding.htm) published each month in the information for authors of the American Journal of Physiology.

Conflict of Interest (COI) Disclosure.

1. It is the responsibility of the authors to disclose any COI by signing the form.
2. If the authors have no conflicts, please state "All authors have no COI to declare regarding the present study" in the Acknowledgments.

   Authors are required to disclose any relationships with company or organization (such as funds, consultancy fee, grant, fee for speaking, stock or shares). At the time of initial submission, the corresponding author is responsible for obtaining conflict of interest information from all authors.

[Reviced: April 2019]

COPYRIGHT TRANSFER AND STATEMENT OF ORIGINALITY

We approve the submission of this paper to the Osaka City Medical Association for publication and have taken to ensure the integrity of this work. We confirm that the manuscript is original and does not in whole or part infringe any copyright, violate any right of privacy or other personal or priority right whatever, or falsely designate the source of authorship, and that it has not been published in whole or in part and is not being submitted or considered for publication in whole or in part elsewhere (abstracts excluded).
We agree to transfer copyright the manuscript entitled

_____

_____

to the Osaka City Medical Association upon its acceptance for publication.

Write clearly and signature

(Author: print or type)	(Signature)	(Date)
(Author: print or type)	(Signature)	(Date)
(Author: print or type)	(Signature)	(Date)
(Author: print or type)	(Signature)	(Date)
(Author: print or type)	(Signature)	(Date)
(Author: print or type)	(Signature)	(Date)
(Author: print or type)	(Signature)	(Date)
(Author: print or type)	(Signature)	(Date)
(Author: print or type)	(Signature)	(Date)
(Author: print or type)	(Signature)	(Date)

OCMJ for Conflict of Interest (COI) Disclosure Statement

The purpose of this form is to provide readers of your manuscript with information about your other interests that could influence how they receive and understand your work. The form is designed to be completed and stored electronically. Each author should submit this form and is responsible for the accuracy and completeness of the submitted information.

1. 1) Have you accepted from a sponsor or any company or organization (More than 1,000,000 JPY per year from a specific organization) ? (Please circle below)
   (1) Funds ? ..... Yes / No
   (2) Consultancy fee ? ..... Yes / No
   (3) Any grant ? ..... Yes / No
   (4) Fee for speaking ? ..... Yes / No

   2) Do you hold any stock or shares related to the manuscript ?
   (1) Directly ? ..... Yes / No
   (2) Indirectly, via family members or relatives ? ..... Yes / No

   3) If any of above items are “yes”, please provide detailed information below.

2. If none of the above apply and there is no COI please clearly state “All authors have no COI to declare regarding the present study”.

Manuscript Title:

Name / Signature_____ **Date**_____

Manuscript Identifying Number (if you know it):

Editorial Committee

The volumes and issues published in 1954-2018 were as follows: Vol 1 (one issue), Vols 2-5 (2 issues, each), Vols 6-7 (one issue, each), Vols 8-9 (2 issues, each), Vol 10 (one issue), Vol 11 (2 issues), Vol 12 (one issue), Vol 13 (2 issues), Vols 14-20 (one issue, each), Vol 21 (2 issues), Vol 22 (one issue), Vols 23-64 (2 issues, each)

Publisher : Osaka City Medical Association,
Osaka City University Medical School,
1-4-3 Asahimachi, Abeno-ku, Osaka 545-8585, Japan